UNIVERSITÉ DE SHERBROOKE
Faculté de génie
Département de génie civil

STRUCTURAL BEHAVIOR OF GFRP-RC BRIDGE-DECK SLABS CONNECTED WITH UHPFRC CLOSURE JOINTS IN ACCELERATED BRIDGE CONSTRUCTION

ESSAIS STRUCTURAUX SUR DES DALLES DE PONTS PRÉFABRIQUÉES EN BÉTON ARMÉ D'ARMATURE EN PRFV JOINTÉES AVEC DU BÉTON AUX FIBRES À HAUTE PERFORMANCE UTILISÉES EN CONSTRUCTION ACCÉLÉRÉE DE PONTS

Thèse de doctorat
Spécialité : génie civil

Mohamed Hassan YOUSSEF

Sherbrooke (Québec) Canada

Mars 2019

MEMBRES DU JURY

Professeur Brahim BENMOKRANE
Directeur de thèse

Professeur Sébastien LANGLOIS
Rapporteur et examinateur

Professeur Adel EL-SAFTY
Examinateur

Hany TOBBI, ing., Ph.D.
Examinateur

ABSTRACT

Accelerated bridge construction (ABC) techniques have become increasingly commonplace alternatives to conventional construction techniques over the recent years. This thesis investigates the structural behavior of one common technique of ABC, using ultra-high-performance fiber-reinforced concrete (UHPFRC) closure joints between precast deck slabs. Glass fiber-reinforced polymer (GFRP) bars are used as alternative reinforcement in bridge-deck slabs to avoid steel corrosion problems, especially in harsh weather conditions. The experimental program consisted of two phases. Phase I included investigation of the UHPFRC closure joint located at the zone of maximum negative moment and subjected to flexural and shear stresses. In Phase II, however, the closure joints were positioned at the constant positive moment region and subjected to pure flexural stresses. A total of 14 full-scale slab specimens measuring 3,000 mm long × 1,000 mm wide × 225 mm thick were fabricated and tested to failure; Two specimens were cast monolithically without closure joints to serve as reference specimens, and 12 jointed specimens. The jointed specimen consisted of two GFRP-RC precast slabs connected with UHPFRC closure joint. Three splice lengths were developed, namely: 100, 150, and 200 mm, with a corresponding joint width of 120, 170, and 220 mm, respectively. Two reinforcement ratios were investigated using No. 15 and No. 20 GFRP bars with the same spacing. The test specimens were tested under monotonic line loading in two different schemes; cantilever-panel setup for Phase I and four-point bending for Phase II. The test results were discussed and analyzed in terms of crack pattern, load–deflection response, crack width, and GFRP-reinforcement and concrete strains. The load-carrying capacities of the specimens were predicted using the available bridge-codes and compared to the experimental capacities.

The findings of the current study demonstrated the feasibility of producing a short GFRP splice length embedded in UHPFRC closure joint to maintain the continuity between the precast slabs. The UHPFRC closure joints yielded adequate strength and performance until failure and remained intact without visible cracks.

Keywords: Accelerated bridge construction (ABC); ultra-high-performance fiber-reinforced concrete (UHPFRC); precast concrete slabs; bridge deck; glass-fiber-reinforced-polymer (GFRP); joint; longitudinal joint; transverse joint; connection; deflection, shear strength, bridge design code; splice length; joint width.

RÉSUMÉ

Les techniques de construction accélérée de ponts (*Accelerated bridge construction - ABC*) sont devenues des solutions alternatives de plus en plus courantes aux techniques de construction conventionnelles au cours des dernières années. Cette thèse étudie le comportement structural d'une technique courante d'ABC, utilisant des joints de clavage en béton fibré à ultra-hautes performances (BFUP) entre des dalles de tablier préfabriquées. Les barres en polymère renforcé de fibres de verre (PRFV) ont été utilisées comme renforcement alternatif dans les dalles de tablier de pont afin d'éviter les problèmes de corrosion de l'acier, en particulier dans des environnements difficiles. Le programme expérimental comportait deux phases. La phase I comprenait le développement et l'étude de joints de clavage en BFUP situés dans la zone de moment négatif maximal et soumis à des contraintes de flexion et de cisaillement. Dans la phase II, les joints de clavage étaient positionnés dans la région du moment positif constant et soumis à des contraintes de flexion simple. Un total de 14 dalles pleine grandeur mesurant 3 000 mm de long, 1 000 mm de large et 225 mm d'épaisseur ont été fabriquées et testées jusqu'à la rupture. Deux spécimens ont été fabriqués sans joint de clavage pour servir de référence, tandis que 12 spécimens comportaient des joints de clavage. Le spécimen avec joint était composé de deux dalles préfabriquées avec des armatures de PRFV reliées à l'aide d'un joint de clavage en BFUP. Trois longueurs de recouvrement ont été considérées, à savoir : 100 mm, 150 mm et 200 mm, avec une largeur de joint correspondante de 120 mm, 170 mm et 220 mm, respectivement. Deux taux d'armature ont été étudiés en utilisant des barres n° 15 et n° 20 en PRFV avec le même espacement. Les dalles ont été testées sous charge linéaire monotone selon deux montages différents : un montage en porte-à-faux pour la phase I et un autre montage pour un essai de flexion quatre points pour la phase II. Les résultats des essais sont discutés et analysés en termes de patron de fissuration, de courbes charge-flèche, de largeur de fissures, et de déformations dans le béton et dans les armatures de

PRFV. Les capacités portantes des spécimens ont été prédites à l'aide des codes de pont existants et ont été comparées aux capacités portantes obtenues expérimentalement.

Les résultats de la présente étude ont démontré la possibilité de produire de courtes longueurs de recouvrement pour les barres de PRFV intégrées dans un joint clavage en BFUP afin d'assurer la continuité entre les dalles préfabriquées. Les joints clavage en BFUP ont démontré une résistance et une performance adéquates jusqu'à la rupture et sont restés intacts sans fissures apparentes.

Mots clés: Construction accélérée de ponts (ABC), béton fibré à ultra-hautes performances (BFUP), dalles de béton préfabriquées, tablier de pont, polymère renforcé de fibres de verre (PRFV), joint, joint longitudinal, joint transversal, connexion, flèche, résistance au cisaillement, code de conception de pont, longueur de recouvrement, largeur de joint.

ACKNOWLEDGMENT

I would like to sincerely thank my supervisor, Dr. Brahim BENMOKRANE for initially believing in me and giving me the opportunity to perform this Ph.D. His constant availability and guidance have been invaluable. His dedication has certainly been an inspiration and I have learnt a lot from him throughout the Ph.D.

I am also very grateful to Dr. Ehab AHMED for his constant support, continuous encouragement, consulting, and guidance throughout the Ph.D.

I wish to acknowledge the financial support to this research from the Natural Sciences and Engineering Research Council of Canada (NSERC). I would like to thank the following companies for supplying materials for this research: Pultrall Inc. for providing the GFRP reinforcement and Lafarge-Holcim Canada Inc. for providing the Ductal® materials.

I would also like to thank all my colleagues and friends at the University of Sherbrooke for their support friendliness streamlined during the period of Ph.D. I wish to express my gratitude to the technical staff of the new Canadian Foundation for Innovation (CFI) structural lab in the Department of Civil Engineering at the University of Sherbrooke for their help during the experimental work.

Last but certainly not least, I would like to say a special thank you to all my family members, who were patient and helped me to complete this research work.

Mohamed Youssef

TABLE OF CONTENTS

LIST OF TABLES

LIST OF FIGURES

CHAPTER 1 INTRODUCTION

1.1. General Background

Accelerated Bridge Construction (ABC) is a technique that uses innovative planning, design, materials, and construction methods in a safe and cost-effective manner to reduce the onsite construction time that occurs when building new bridges or replacing and rehabilitating existing bridges (Culmo, 2011). The use of prefabricated elements such as full-depth precast concrete deck panels has become more commonplace for over twenty years. The prefabricated full-depth bridge deck panels are connected by field-cast closure joints. The closure joints are cast using ultra-high-performance fiber-reinforced concrete (UHPFRC). The high early concrete strength and high bond strength of UHPFRC allow transferring the forces between the prefabricated deck panels through short splice lengths. This type of construction eliminates the need for cast in place formwork and reduces cost, construction time, and environmental impact. In addition, precast panels are constructed in a controlled environment which leads to a more durable and high quality product.

Ultra-high-performance fiber-reinforced concrete (UHPFRC) is a relatively new structural material composed of Portland cement, fine sand, silica fume, ground quartz, steel fibers, water and high range of water reducer (Graybeal, 2006a). UHPFRC has approximately four to eight times higher compressive strength and eight times higher abrasion resistance than Normal Strength Concrete (NSC). UHPFRC has compressive strength over 150 MPa, and its tensile strength ranges from 6.2 – 11.7 MPa (Graybeal, 2007).

The use of glass fiber-reinforced polymer reinforcement (GFRP) as alternative reinforcement has become of interest to overcome the problems of steel corrosion and associated deteriorations (Ahmed and Benmokrane, 2014). In deicing salts and aggressive environments, corrosion of steel reinforcement is a major factor affecting the structural

durability of precast panels and overall serviceability of a bridge deck. To prevent such corrosion problems, fiber-reinforced polymer (FRP) reinforcement has been proposed as a substitute for conventional steel reinforcement due to its high corrosion resistance and high strength to weight ratio.

The closure joints in concrete bridge-decks may be subjected to either pure flexural stresses or combined flexural and shear stresses, depending on the type and location of the joints. The two common cases for the closure joints are longitudinal and transverse joints. Figure 1.1 shows a typical orientation of the closure joints indicating the corresponding test specimens. To determine the controlling load case of the longitudinal joint, the longitudinal joint should be located at the mid-span between longitudinal girders carrying the largest positive or negative moments. The transverse joint should be positioned over an interior support in a continuous span bridge system resisting moment and shear forces (French et al. 2011).

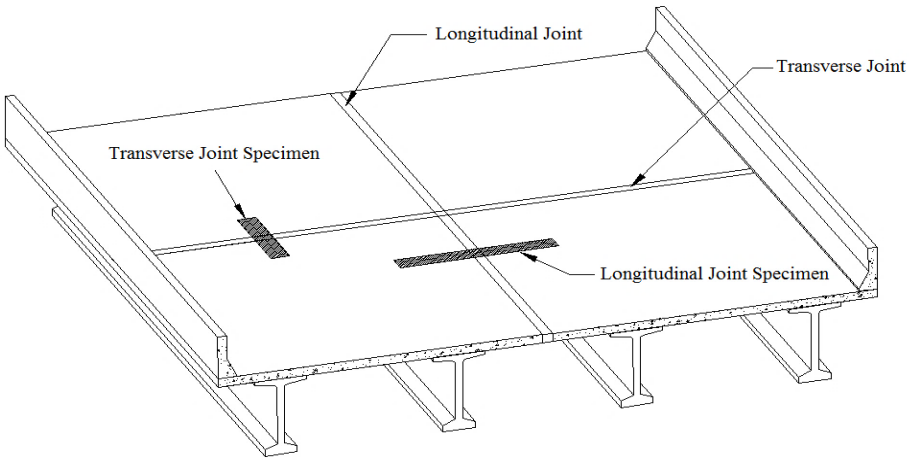

Figure 1.1 -Typical orientation of the closure joints and their corresponding test specimens

This research project aims at investigating the structural behavior of innovative UHPFRC closure joints between precast GFRP-RC bridge deck panels. The experimental program included the two common cases of closure joints. The specimens were designed to satisfy

requirements of the Canadian Highway Bridge Design Code CHBDC (CAN/CSA S6, 2014). The outputs of this research will contribute to extend the use of precast GFRP-RC bridge-deck panels with UHPFRC closure joints, which is an innovative solution to overcome the corrosion problems, eliminate the delay in construction, and improve the product durability. The findings of this study are expected to support the work of the North American technical committees engaged in developing standards and design provisions for GFRP-RC bridge-deck slabs connected with UHPFRC closure joints.

1.2. Motivation of the Research

The use of GFRP reinforcement, which is corrosion resistant, eliminates the corrosion and related deterioration. Thus, it extends the service life of the RC structures especially in harsh exposure conditions.

The aging highway bridge infrastructure in North America is subjected to increasing traffic volumes and must be continuously renewed while accommodating traffic flow. Speed of construction, especially for the case of bridge replacement and repair projects, is an important factor. The use of prefabricated bridge systems can minimize traffic disruption, improve work-zone safety, minimize impact to the environment, improve constructability, increase quality, and lower the life-cycle costs. This technology is applicable and needed for both existing bridge replacement and new bridge construction (French et al. 2011).

The need for more experimental data for the behavior of UHPFRC closure joints between prefabricated GFRP-RC deck panels under shear and flexural stresses is the primarily motivation for this study. In particular, considerable research in recent years has been undertaken to investigate the structural behavior of closure joints between prefabricated elements. However, there is still a need for solid recommendations for UHPFRC closure joints when GFRP is used as the primary reinforcement in concrete bridge-deck slabs

The design specifications for RC highway bridges, such as the Canadian Highway Bridge Design Code CHBDC (CAN/CSA S6, 2014) and AASHTO LRFD (2009), do not provide guidelines or empirical equations for designing the UHPFRC closure joints for precast

deck systems. Therefore, this research project aims at providing design recommendations for such cases.

1.3. Objectives and Scope

The main objective of this research project is to investigate and gain a better understanding of the structural behavior of UHPFRC closure joint connecting GFRP-RC bridge-deck panels under quasi-static loading. The specific objectives of the current study can be summarized as follows:

- Evaluate the structural performance of the GFRP-RC precast bridge deck panels jointed by UHPFRC closure joints.
- Compare the structural performance of the GFRP precast panels jointed by UHPFRC closure joints against the reference panels without a closure joint.
- Investigate the flexural behavior and serviceability performance of the GFRP-RC jointed slabs under quasi-static loads.
- Investigate the effect of different parameters on the structural behavior and serviceability performance of the jointed panels, such as the splice length (joint width) and longitudinal reinforcement ratio.
- Prediction of the specimens' load carrying capacities using the available bridge code provisions and compare these predicted capacities against experimental values.
- Provide new design recommendations for UHPFRC closure joints between GFRP-RC deck slabs considering the joints in shear and flexural zones in the bridge system. These recommendations may contribute to update the current design standards such as the CHBDC (CAN/CSA S6, 2014).

1.4. Methodology

To achieve the objectives of this research project, the experimental program includes construction and testing of 14 specimens representing full-depth UHPFRC closure joints between precast deck slabs. All the specimens measured 3,000 mm long × 1,000 mm wide × 225 mm thick and were reinforced with GFRP bars. Two specimens were cast monolithically without closure joint to serve as reference specimens. 12 jointed specimens, however, each contained two precast segments connected with UHPFRC closure joint simulating a common technique of accelerated bridge construction. Geometries and reinforcement details for all the test specimens are selected so satisfy the requirements of the Canadian Highway Bridge Design Code CHBDC (CAN/CSA S6, 2014). The test specimens were fabricated and tested under quasi-static loading up to failure. The test parameters were: splice length and joint width, GFRP reinforcement ratio, and the location of the closure joint. The experimental program is divided into two phases:

- Phase I includes 7 specimens: six jointed specimen and one reference specimen without closure joint. The closure joints were located at the zone of negative moment where subjected to combined flexural and shear stresses. The specimens were tested in a cantilever-panel setup with the closure joint located over the support.

- Phase II includes 7 specimens: six jointed specimens and one reference specimen without closure joint. The closure joints were located at the middle of the specimen within the zone of constant positive moment. The specimens were tested in a four-point bending scheme, at which the closure joints were subjected to pure flexural stresses.

1.5. Outline of the Dissertation

This dissertation consists of six chapters; the following is a brief description of each chapter's content:

- Chapter 1 defines the problem, presents the main objectives, introduces the methodology, and provides an outline of the thesis with a brief description of each chapter.
- Chapter 2 presents a review of literature on relevant work related to UHPFRC closure joints. The review includes the mechanical properties of GFRP bars and UHPFRC. The recently conducted studies concerning ABC are also reviewed.
- Chapter 3 describes the conducted experimental program. It presents the geometry and reinforcement details of the test specimens including fabrication, instrumentation, and testing procedures.
- Chapter 4 presents the first paper in this dissertation entitled "Structural Behavior of GFRP-RC Bridge-Deck Slabs Connected with UHPFRC Joints under Flexure and Shear". This chapter provides an investigation of the behavior of GFRP-RC bridge-deck slabs jointed with full-depth UHPFRC closure joint. Seven full-scale one-way slab specimens were tested up to failure, considering the closure joint subjected to shear and flexural stresses. The influences of the test parameter on the structural behavior of the tested specimens were investigated.
- Chapter 5 presents the second paper in this dissertation entitled "Behavior of Field-Cast Full-Depth UHPFRC Moment Closure Joints between precast Bridge-Deck Slabs reinforced with GFRP bars". This chapter investigates the behavior of the UHPFRC closure joint between GFRP-RC bridge-deck slabs under pure flexural stresses. Seven full-scale one-way slab specimens were fabricated and loaded to collapse. The effects of the test parameter on the structural behavior and serviceability of the tested specimens were studied.
- Chapter 6 presents the summary, conclusions based on the test results, and recommendation for future research work.

CHAPTER 2 LITERATURE REVIEW

2.1. General

This chapter mainly reviews previous relevant studies into the use of ultra-high-performance fiber-reinforced concrete (UHPFRC) closure joints between GFRP-RC prefabricated elements in accelerated bridge construction (ABC). A brief investigation about the use of ABC as an alternative technique to conventional construction is reviewed. This chapter, however, includes the basic mechanical properties of fiber-reinforced polymer (FRP) reinforcement as an alternative to steel reinforcement in addition to the mechanical properties of UHPFRC. Design provisions of GFRP-RC deck slabs in bridge codes and guidelines are also presented in this chapter.

(Culmo, 2011) presented a manual giving all respects of accelerated bridge construction (ABC). The intent of this manual was to fill in the gaps left by publication of the previous manuals. The manual covered ABC techniques, project planning and scoping, implementing ABC in a Transportation Agency, and prefabricated elements.

Glass fiber-reinforced Polymer (GFRP) reinforcing bars provide a promising solution for corrosion due to their non-corrosive nature. GFRP bars are commonly available as grade I, II, and III (CAN/CSA S807, 2010). The Canadian Highway Bridge Design Code CHBDC (CAN/CSA S6, 2014) and AASHTO-LRFD Bridge Design Guide Specifications for GFRP-Reinforced Concrete Bridge-Decks and Traffic Railings (AASHTO, 2009) allow the use of GFRP as a primary reinforcement in reinforced concrete bridges.

Russell and Graybeal (2013) provided an extensive review on UHPFRC including information about materials and production, mechanical properties, structural design and structural testing, durability and durability testing, and actual and potential applications. In

the report, UHPFRC were defined as cementitious-based composite materials with discontinuous fiber reinforcement that exhibit compressive strength above 150 MPa, pre- and post-cracking tensile strength above 5 MPa, and enhanced durability via a discontinuous pore structure.

There has been a considerable amount of research and experience with full-depth closure joints between precast concrete elements, as well as precast deck panels installed on steel girders. Most of these researches studied the closure joints with steel reinforcement, while a few of them used GFRP reinforcing bars. Moreover, the closure joints reinforcement had different configurations. Review of the structural testing of such structural elements is presented in section 2.5.

2.2. Accelerated Bridge Construction (ABC)

ABC is a bridge construction technique that uses innovative planning, design, materials, and construction methods in a safe and cost-effective manner to reduce the onsite construction time that occurs when building new bridges or replacing and rehabilitating existing bridges (Culmo, 2011). Over the last 20 years, there have been progressive advancements in the use of ABC, for instance, bridge deck construction using full depth precast concrete deck panels. More recently, ABC projects have spread to all bridge elements including substructures and foundations.

On the other hand, Conventional bridge construction does not significantly reduce the onsite construction time that is needed to build, replace, or rehabilitate of bridge projects. Conventional construction methods involve onsite activities that are time consuming and weather dependent. In conventional bridge construction, only the concrete or steel girders can be prefabricated. In contrast, all bridge components can be prefabricated in case of accelerated bridge construction. Figure 2.1 shows a comparison between the two bridge construction techniques.

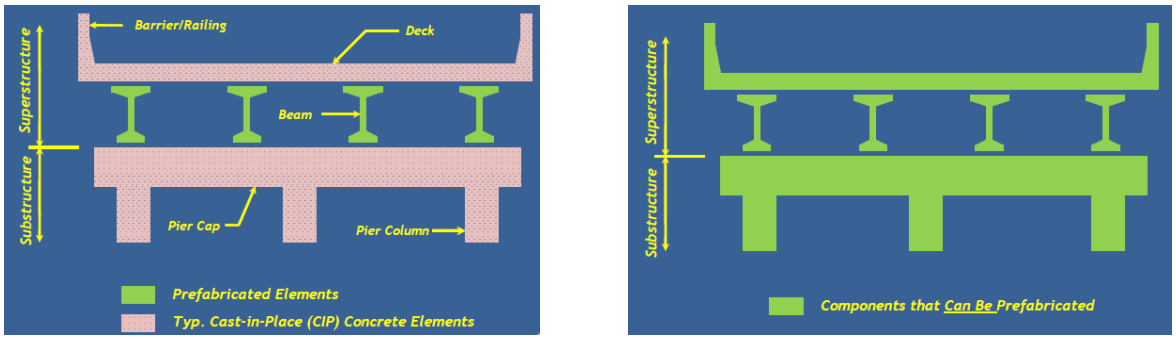

(a) Conventional bridge construction (b) Accelerated bridge construction

Figure 2.1 - Typical bridge construction

2.2.1. Why Consider ABC?

A common reason to choose ABC is to reduce traffic impacts because the safety of the traveling public and the flow of the transportation network are directly affected by onsite construction related activities. However, other common and equally viable reasons to use ABC deal with site constructability issues. In addition, long detours, costly use of temporary structures, remote site locations, and limited construction periods present opportunities where the use of ABC methods can provide more practical and economical solutions compared with the conventional construction methods (Culmo, 2011). The benefits of using UHPFRC in ABC projects can be summarized as follows:

- Improve site constructability, total project delivery time, material quality, and long-term durability. The bridge elements are prefabricated under controlled environmental conditions and jointed in site by short width field-cast closure joints.
- Increase safety for the workers and traveling public.
- Reduce traffic impacts and weather-related time delays by shortening the onsite construction time.
- Minimize environmental impacts and impacts to existing roadway alignment.
- Increases the benefit cost ratio of the project by reducing the required maintenance and extending the service life.

2.2.2. Prefabricated Bridge Elements (Culmo, 2011)

The use of prefabricated bridge elements and systems is a technique that meets the objectives of accelerated bridge construction. Prefabricated elements reduce the onsite construction time and mobility impact time compared to conventional construction systems. Bridge elements are typically built in a prefabricated and repeatable manner to offset costs. The elements are built under controlled environmental conditions, avoiding the influence of weather related impacts, to achieve better product quality and long-term durability.

The use of innovative materials such as ultra-high-performance fiber-reinforced concrete (UHPFRC) in filling the joints between prefabricated elements can significantly help to achieve the objectives of ABC. This is because of the exceptional properties of UHPFRC, especially the high early compressive strength. ABC systems include the entire superstructure (decks and girders) and substructure (abutments and piers) prefabricated components, the following contains examples of the most common prefabricated superstructure elements in ABC systems.

2.2.2.1. **Prefabricated Deck Elements**

Prefabricated deck system eliminates activities that are associated with conventional deck construction, which typically includes onsite installation of deck forms, overhang bracket and formwork installation, reinforcing bars placement, paving equipment set up, concrete placement, and concrete curing, all typically occurring in a sequential manner. Some examples of prefabricated deck element systems are listed below, Figure 2.2 shows some examples of prefabricated deck elements.

- Partial-depth precast deck panels;
- Full-depth precast deck panels;
- Light-weight precast deck panels; and
- Orthotropic deck.

(a) Partial-depth precast deck panels

(b) Full-depth precast deck panels

(c) Light-weight precast deck panels

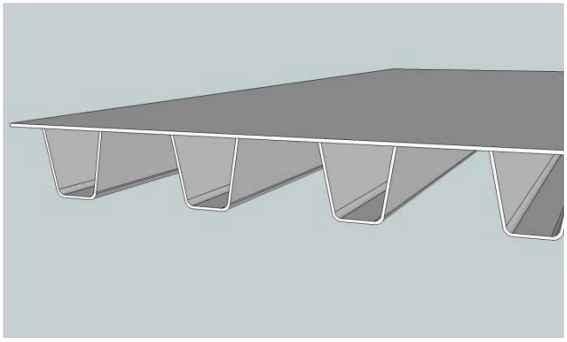

(d) Orthotropic deck

Figure 2.2 - Examples of prefabricated deck elements (Culmo, 2011)

2.2.2.2. **Prefabricated Beam Elements**

Prefabricated beam elements are composed of two types: deck beam elements and full-width beam elements. Deck beam elements eliminate conventional onsite deck forming activities, see Figure 2.3. To reduce onsite deck forming operations, deck beam elements are typically placed in an abutting manner. Examples of Deck Beam Elements include:

- Adjacent deck bulb tee beams,
- Adjacent double tee beams,
- Adjacent inverted tee beams, and
- Modular beams with decks.

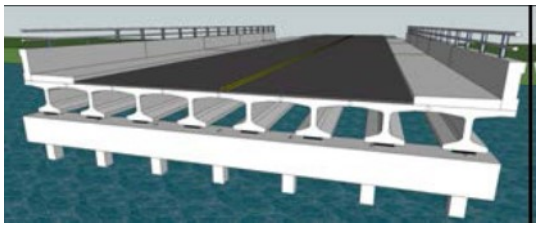

(a) Adjacent deck bulb tee beams

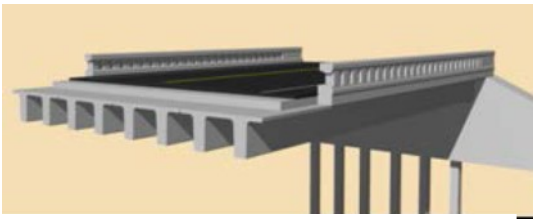

(b) Adjacent double tee beams

(c) Adjacent inverted tee beams

(d) Modular beams with decks

Figure 2. 3 - Examples of prefabricated deck beam elements (Culmo, 2011)

Full-width beam elements, shown in Figure 2.4, eliminate conventional onsite beam placement activities. They are typically rolled, slid, or lifted into place to allow deck placement operations to begin immediately after placement. Examples of Full-Width Beam Elements include:

- Truss span without deck, and
- Arch span without deck.

Truss span without deck

Arch span without deck

Figure 2.4 - Examples of prefabricated full-width beam elements (Culmo, 2011)

2.2.3. Examples of ABC Using UHPFRC Closure Joints

Recently, in North America, The use of field-cast UHPFRC closure joints between precast concrete modular components has become commonplace. UHPFRC allows for simplified joint details, rapid construction time, and more durable structure. field-cast UHPFRC closure joints between prefabricated bridge components have been implemented in many bridges in North America (Perry and Royce, 2010; Graybeal, 2011; Arafa et al. 2016). A general overview of some of these projects in Canada and the United States is provided below.

2.2.3.1. **Bridge Projects in Ontario**

The Ministry of Transportation of Ontario (MTO) has been a leader in deployment of field-cast UHPFRC connection technology (Graybeal, 2010). MTO has completed construction of many bridges in Ontario, with UHPFRC closure joints between precast concrete elements, starting from 2006 up to date. The type of UHPFRC used in all Ontario bridge projects was Ductal® developed by Lafarge-Holcim (Lafarge, 2009). In 2006, the Rainy Lake Bridge was constructed on Highway 11 between Fort Frances and Atikokan, Ontario. This project used precast bridge deck panels to rehabilitate the deck on a single span steel stringer bridge. UHPFRC (Ductal®) was used in joints between adjacent deck panels as well as in the composite joint between the panels and the girders. The joints were

200 mm in width and included straight GFRP reinforcing bars (Ductal, 2016). Figure 2.5 provides photos of the Rainy Lake Bridge showing the joints before and after casting.

Placement of Ductal® into the joint

Joints after casting of Ductal®

Figure 2.5 - The Rainy Lake Bridge on Highway 11 between Fort Frances and Atikokan, Ontario (photos by MTO)

In 2007, the Sunshine Creek Bridge was constructed on Highway 11/17 near Thunder Bay, Ontario. This project included the removal of the existing simple span superstructure and the replacement with 10 adjacent box girders of 21 m length. 9 longitudinal joints along the length of the girders were cast with a field-cast Ductal® UHPFRC joints (Ductal, 2016). The joints had diamond-shaped shear keys including hairpin-shaped GFRP details (Figure 2.6).

The Hawk Lake Bridge, owned by MTO, was constructed on Highway 17 near Hawk Lake, Ontario in 2008. The project included 12 side-by-side precast box girders connected with 11 Ductal® UHPFRC closure joints (Ductal, 2016). The joints had a diamond-shaped shear keys between the simple span precast girders of length 27.2 m, and reinforced with GFRP straight bars, as shown in Figure 2.7.

Figure 2.6 – The Sunshine Creek Bridge on Highway 11/17 near Thunder Bay, Ontario (photo by MTO)

Joints ready for casting

Casting of Ductal® into the joint

Figure 2.7 – The Hawk Lake Bridge on Highway 17 near Hawk Lake, Ontario (photos by MTO)

The longest single span bridge in Canada, the Chukuni River Bridge, was constructed on Highway 105 over the Chukuni River near Red Lake, Ontario in 2010. It has 101 m long with a clear span of 83.5 m (Ductal, 2016). This project included four 3.7 m deep steel girders and 54 half-width conventional concrete precast deck panels. The longitudinal and transverse joints were constructed with field-cast UHPFRC. The discrete reinforcement in

the joints included straight GFRP bars. The UHPFRC also completed the composite connections to the girders in the periodic shear pockets and provided the bedding under the deck panels, each 3.6 m wide panel contained two shear pockets. Figure 2.8 shows photos of the bridge construction.

GFRP straight splices

Shear pockets

Overview of the bridge

Figure 2.8 – The Chukuni River Bridge on Highway 105 over the Chukuni River near Red Lake, Ontario (photos by MTO)

The world's first cable-stayed bridge with GFRP-RC deck slabs, the Nipigon River Bridge, was completed over the Nipigon River as part of the extension of the Highway 11/17 east of Thunder Bay, Ontario in 2017. The bridge consisted of two traffic lanes and a pedestrian sidewalk in each direction, with a total width of 36.2 m and 251.8 m total length. It is divided into two spans supported on three central towers 51 m in height. The precast panels were 225 mm thick and reinforced with two No. 15 HM-GFRP bars extended inside 220-mm rectangular closure joints. Four hundred and eighty precast panels measuring 3×7 m were precast for the bridge deck (Arafa et al. 2016). Figure 2.9 shows the stacked GFRP-RC precast panels and their installation on the bridge deck.

Precast GFRP-RC panels

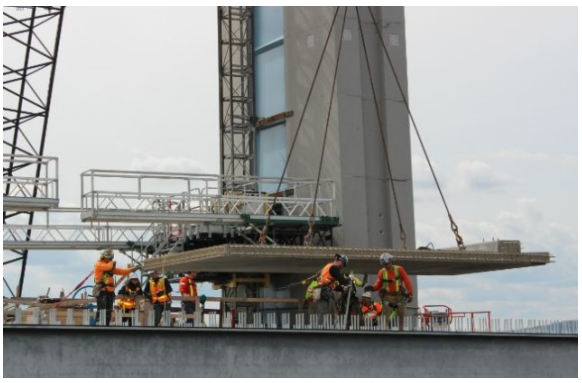

Precast GFRP-RC panels

Figure 2.9 - The Nipigon River Bridge on Highway 11/17 east of Thunder Bay, Ontario (photos by Ehab, A. Ahmed)

2.2.3.2. **Bridge Projects in New York**

The New York State Department of Transportation (NYSDOT) has played a significant role in advancing the use of field-cast UHPFRC closure joints between modular bridge components. NYSDOT has a strong interest in using full-depth precast deck panels and deck-bulb-tee prestressed girders for use in constructing and reconstructing bridges. In both bridge types, the precast concrete elements are connected together at the deck level via permanent, durable joints. The long-term performance of the bridge is dependent on acceptable performance of the joints (Graybeal, 2010). In 2009, NYSDOT constructed two bridges using field-cast UHPFRC joints between prefabricated elements. The first bridge

was the Route 31 Bridge in Lyons, New York. In this bridge superstructure replacement, newly fabricated 1.04 m deep prestressed concrete deck-bulb-tee girders were installed in the bridge over the Canandaigua Outlet. The longitudinal joint width was 152 mm with a diamond shear key, 16M straight epoxy-coated steel bars projected from precast girder decks into the joint 150 mm splice length. Figure 2.10 provides photos showing the longitudinal joints and the completed bridge.

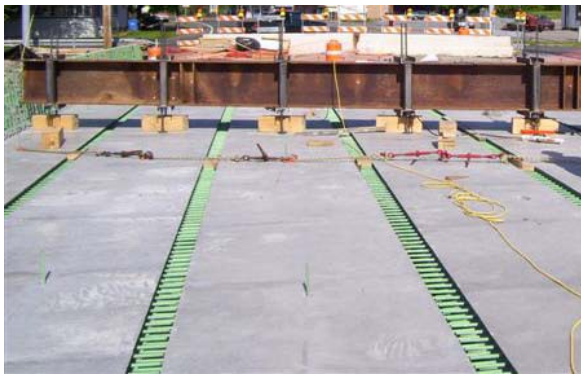

Longitudinal joints

Casting of UHPFRC

The completed bridge

Figure 2.10 - Route 31 Bridge in Lyons, New York (photos by NYSDOT)

The other project in 2009 was replacement of the Route 23 Bridge in Oneonta, New York. The bridge included the use of full-depth precast deck panels and field-cast UHPFRC transverse joints. The diamond-shaped joint reinforcement consisted of epoxy-coated hair pin 13M mild-steel reinforcement with a lap length of 100 mm. The UHPC was mixed, cast, and cured. After curing, a 40 mm thickness concrete overlay was installed so as to provide a smooth riding surface (Graybeal, 2010). Figure 2.11 shows construction of the Route 23 Bridge project.

Transverse joints

Field casting of UHPFRC

Elevation view of the bridge

Figure 2.11 - Route 23 Bridge in Oneonta, New York (photos by NYSDOT)

2.3. Fiber Reinforced Polymer (FRP) background

2.3.1. General

During the last decade, fiber reinforced polymer (FRP) materials have been extensively used as a practical alternative material for steel reinforcing bars in concrete structures. FRP reinforcing bars offer advantages over steel reinforcement in which FRP bars have an excellent corrosion resistance and high strength-to-weight ratio compared to steel. This part provides general information and properties of the FRP composite materials. It is focusing on composition, types, compressive and tensile properties, and the use of FRP as reinforcement for concrete structures.

2.3.2. FRP Constituents and Manufacturing process

FRP products are composite materials which consist of a matrix (resin) and reinforcing fibers. As shown in Figure 2.12, the fibers are stronger than the matrix. In order to provide the reinforcing function, the fiber-volume fraction should be more than 55 percent for FRP bars and rods and 35 percent for FRP grids (ISIS Canada, 2007). The matrix not only coats fibers and protects them from mechanical abrasion, but also transfers stresses between them (Figure 2.13). Moreover, it transfers inter-laminar and in-plane shear in the composite, and provides lateral support to fibers against buckling when subjected to compressive loads. Additives and fillers may be added for curing or enhancing mechanical and/or physical properties.

Pultrusion is a common technique for manufacturing continuous lengths of FRP bars that are of constant or nearly constant profile. A schematic representation of this technique is shown in Figure 2.14. Continuous strands of reinforcing material are drawn from creels, through a resin tank, where they are saturated with resin, and then through a number of wiper rings into the mouth of a heated die. The speed of pulling through the die is predetermined by the curing time needed. To ensure good bond with concrete, the surface of the bars is usually braided or sand-coated. The most common products manufactured using this process are pipes, tubes, and storage tanks (ISIS Canada, 2007).

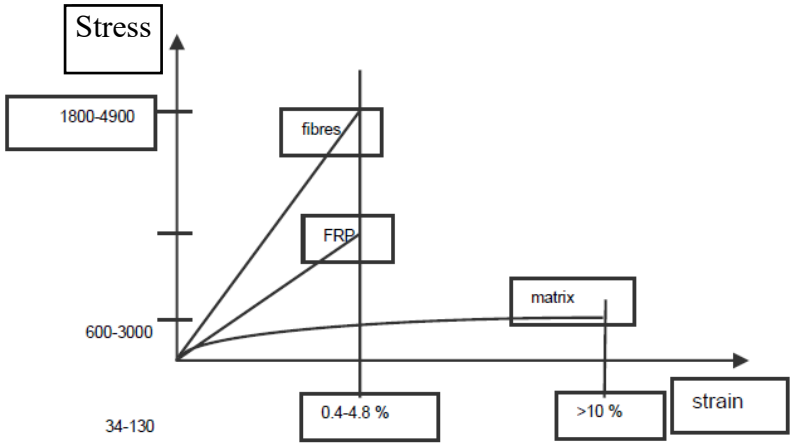

Figure 2.12 - Stress-strain relationships for fibrous reinforcement and matrix (ISIS Canada, 2007)

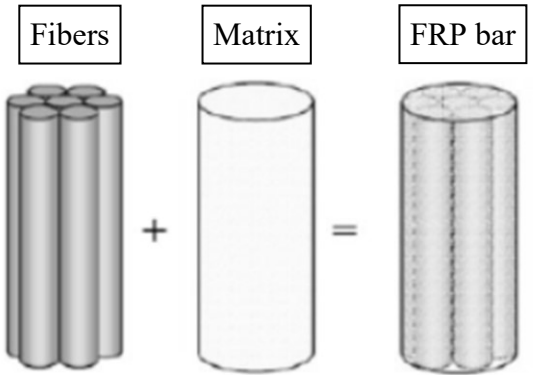

Figure 2.13- Basic material components of FRP

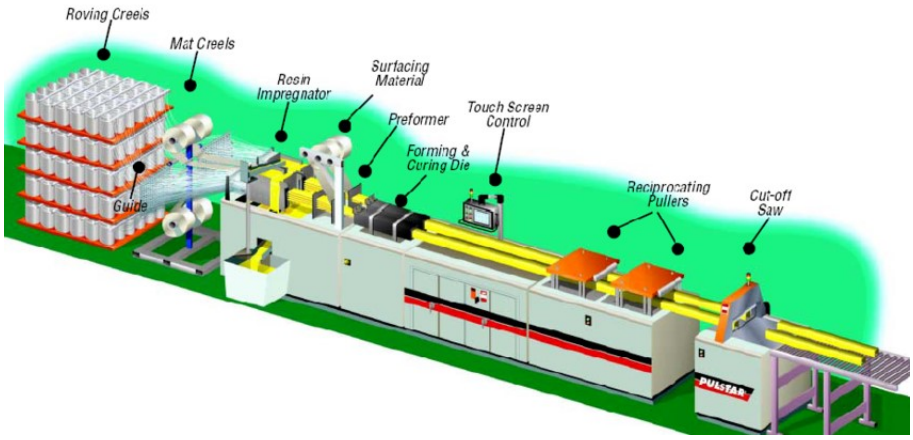

Figure 2.14 - Pultrusion process

2.3.3. Fibers

Fibers used for manufacturing composite materials must have high strength and stiffness, toughness, durability and preferably low cost. The performance of fibers is affected by their length, cross-sectional shape and chemical composition. Fibers are available in different cross-sectional shapes and sizes. The most commonly used fibers for FRPs are aramid, carbon, and glass (ISIS Canada, 2007).

2.3.3.1. **Aramid fibers**

Aramid fibers were used to produce first-generation FRP pre-stressing tendons in the 1980 in Europe and Japan; however, few manufacturers still produce aramid fiber FRP reinforcing bars or tendons.

A combination of their relatively high price, difficulty in processing, high moisture absorption (up to 6% by weight), low melting temperatures (around 425^{o}C), and relatively poor compressive properties have made them less attractive for FRP parts for structural engineering applications (Bank 2006). Their advantages include extremely high tenacity and toughness. Like carbon fibers, they have a negative coefficient of thermal expansion in the fiber longitudinal direction. They are the lightest of the high performance fibers, having a density of around 1.4 g/cm^{3}. Depending on the type of aramid fiber, the fiber longitudinal tensile strength ranges from 3400 to 4100 MPa, and its longitudinal tensile modulus ranges from 70 to 125 GPa.

2.3.3.2. **Carbon fibers**

Carbon fibers are used in FRP strengthening sheets and fabrics, in FRP strengthening strips, and in FRP pre-stressing tendons. Carbon fiber is a solid semi crystalline organic material consisting on the atomic level of planar two-dimensional arrays of carbon atoms. The two-dimensional sheet is usually known as the graphitic form; hence, the fibers are also known as graphite fibers (the three-dimensional array is well known as the diamond form). Carbon fiber is produced in grades known as standard modulus (SM), intermediate modulus (IM), high strength (HS), and ultra-high modulus (UHM).

The longitudinal axis of the fiber is parallel to the graphitic planes and gives the fiber its high longitudinal modulus and strength. Carbon fiber is produced at high temperatures (1200 to 2400^{o} C) from three possible precursor materials: a natural cellulosic rayon textile fiber, a synthetic polyacrilonitrile (PAN) textile fiber, or pitch (coal tar). The carbon fibers are very durable and perform very well in hot and moist environments and when subjected to fatigue loads (Bank 2006). They do not absorb moisture. They have a negative or very low coefficient of thermal expansion in their longitudinal direction, giving them excellent dimensional stability. They are, however, thermally and electrically conductive.

2.3.3.3. **Glass fibres**

Glass fiber is a material made from extremely fine fibers of glass, and it is the largest reinforcement measured in sales. The glass fiber was invented in 1938 by Russell Games Slayter of Owens-Corning as a material to be used as insulation. Ever since then, glass fiber has become widely used as insulation and composite reinforcement material. Based on the composition and the application, glass fibers can be classified in several types. The most commonly used glass fiber type for composite applications are E-glass (electrical glass) and S-glass (structural or high-strength glass). The E-glass has good mechanical properties and high electrical insulation. S-glass is also used in composite materials where high tensile strength is desired; however this material comes at a much higher cost. The glass fibers are excellent thermal and electrical insulators and are the most inexpensive of the high-performance fibers (Bank 2007). Table 2.1 indicates approximate properties of common grades of glass fibers.

Table 2.1 - Approximate Properties of Common Grades of Glass Fibers (Bank 2007)

Grade of Glass Fibre	Density gm/cm^3	Tensile Modulus GPa	Tensile Strength MPa	Max. Elongation (%)
E	2.57	72.5	3400	2.5
A	2.46	73	2760	2.5
C	2.46	74	2350	2.5
S	2.47	88	4600	3.0

2.3.4. Resins

Selection of the proper matrix is a very important issue in the manufacture of composites because the physical and thermal properties of the matrix significantly affect the final mechanical properties as well as the manufacturing process. In order to be able to exploit the full strength of the fibers, the matrix should be able to develop a higher ultimate strain than the fibers (Phillips, 1989). Very important roles of the matrix are transfer of inter-laminar and in-plane shear in the composite, and provision of lateral support to fibers against buckling when subjected to compressive loads. There are two types of polymeric matrices widely used for FRP composites; namely, thermosetting and thermoplastic.

Thermosetting polymers are used more often than thermoplastic. They are low molecular-weight liquids with very low viscosity (ACI 1995), and their molecules are joined together by chemical cross-links. Hence, they form a rigid three dimensional structure that once set, cannot be reshaped by applying heat or pressure. Thermosetting polymers are processed in a liquid state to obtain good wet-out of fibers. Some commonly used thermosetting polymers are polyesters, vinyl esters and epoxies. These materials have good thermal stability and chemical resistance and undergo low creep and stress relaxation. The FRP reinforcing bars should be produced and properly cured with a degree of curing above 95

percent (ISIS Canada, 2007). However, these polymers have relatively low strain to failure, resulting in low impact strength. Two major disadvantages are their short shelf life and long manufacturing time. Mechanical properties of some thermoset resins are provided in Table 2.2.

2.3.5. FRP Reinforcing Products

FRP reinforcing bars are manufactured from continuous fibers (such as aramid, carbon, and glass) embedded in matrices (thermosetting or thermoplastic). Similar to steel reinforcement, FRP bars are produced in different diameters, depending on the manufacturing process. The surface of the rods can be spiral, straight, sanded-straight, sanded-braided, and deformed. The bond of these bars to concrete is usually equal to, or better than, the bond of steel bars (ISIS Canada, 2007). Table 2.3 gives the mechanical properties of some commercially available FRP reinforcing bars. Figure 2.15 shows typical stress strain relationships for aramid, carbon, and glass FRP bars compared to steel and Figure 2.16 shows typical different shapes of FRP products. Table 2.4 presents typical mechanical properties of V-Rod GFRP bars developed by Pultrall Inc. (Pultrall, 2016).

Table 2.2 - Typical Properties of Thermosetting Resins (ISIS Canada, 2007)

Resin	Specific Gravity	Tensile Strength (MPa)	Tensile Modulus (GPa)	Cure Shrinkage (%)
Epoxy	1.20-1.30	55.00-130.00	2.75-4.10	1.00-5.00
Polyester	1.10-1.40	34.50-103.50	2.10-3.45	5.00-12.00
Vinyl Ester	1.12-1.32	73.00-81.00	3.00-3.35	5.40-10.30

Table 2.3 - Typical mechanical Properties of FRP bars (ISIS Canada, 2007)

Trade name	Tensile strength (MPa)	Modulus of elasticity (GPa)	Ultimate tensile strain
Carbon fibre			
V-ROD	1596	120.0	0.013
Aslan	2068	124.0	0.017
Leadline	2250	147.0	0.015
NEFMAC	1200	100.0	0.012
Glass fibre			
V-ROD	710	46.0	0.017
Aslan	690	40.8	0.017
NEFMAC	600	30.0	0.020

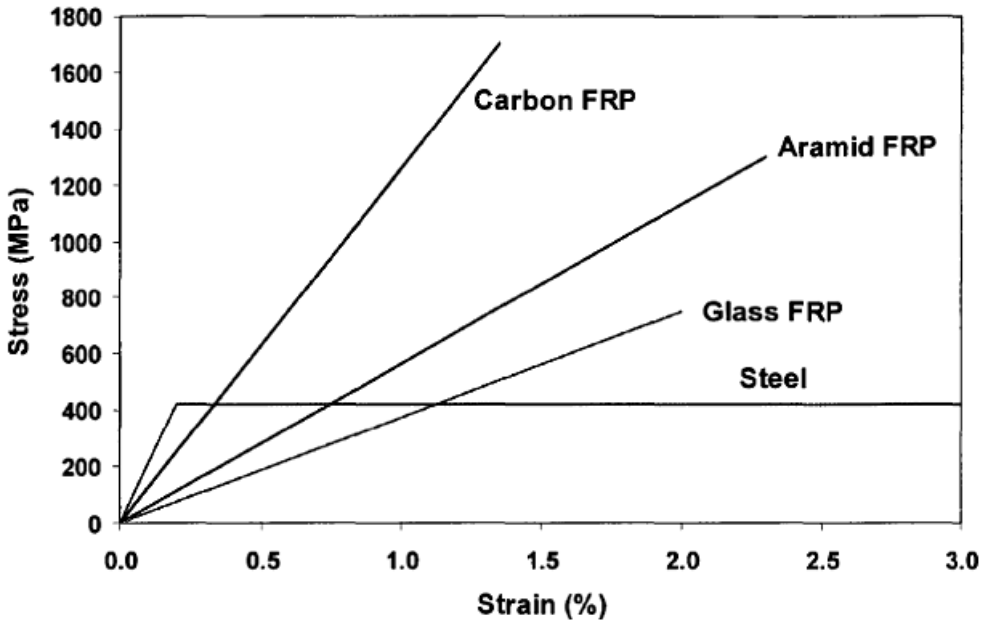

Figure 2.15 - Typical stress strain relationships for FRPs compared to steel (ISIS Canada, 2007)

Figure 2.16 - Different shapes of FRP products (fib, 2007)

Table 2.4 - Typical mechanical properties of V-Rod GFRP bars (Pultrall, 2016)

Trade name [a]	Tensile strength (MPa)	Modulus of elasticity (GPa)	Ultimate tensile strain
V-Rod LM	588 – 804	40 – 47	0.0134 – 0.0189
V-Rod SM	703 – 938	50 – 59	0.0133 – 0.0179
V-Rod HM	1000 – 1372	60 – 69	0.0151 – 0.0211

[a] LM: low modulus; SM: standard modulus; and HM: high modulus, according to the manufacturer.

2.4. MECHANICAL PROPERTIES OF UHPFRC

2.4.1. General

Ultra High Performance Concrete **(**UHPC) refers to a class of advanced cementitious composite materials. UHPC is a relatively new structural material composed of Portland cement, fine sand, silica fume, ground quartz, steel fibers, water and high range of water reducer (Graybeal 2006a).

Concrete or cementitious composites with compressive strength over 150 MPa are generally described as ultra-high-performance concrete (UHPC), if steel fibers are added in order to decrease brittleness and increase energy absorption capacity the term ultra-high-performance fiber-reinforced concrete (UHPFRC) is used (Yuguang et al. 2008). This part summarizes the current knowledge related to characterization of Ultra High Performance Concrete (UHPC). It is focusing on composition, types, compressive and tensile properties.

UHPC is used in several bridge applications, including precast, prestressed girders, precast waffle panels for bridge decks, and as a jointing material between precast concrete deck panels and girders and between the flanges of adjacent girders. In Canada, the first UHPC bridge was constructed in 1997. This pedestrian bridge consists of a precast, post-tensioned space truss. At least 26 bridges have been built in Canada using UHPC in one or more components (Russell and Graybeal, 2013).

2.4.2. Typical Composition of UHPC

UHPC formulations often consist of a combination of portland cement, fine sand, silica fume, high-range water-reducing admixture (HRWR), fibers (usually steel), and water. Small aggregates are sometimes used, as well as a variety of chemical admixtures. Different combinations of these materials may be used, depending on the application and supplier (Russell and Graybeal, 2013).

The UHPFRC used most often in North America for both research and applications is a commercial product known as Ductal® made by Lafarge Company. Table 2.5 shows a typical composition of this product (Graybeal, 2006a).

2.4.3. Compressive Strength

Compressive strength is an important property in the design of any concrete structure. It is also the property that is most frequently measured. Several studies have been conducted to investigate the compressive strength of UHPC. Cylinder and cube compression test methods used for conventional concrete are appropriate for the determination of UHPC compressive strength.

Graybeal (2006a) reported the compressive strengths of nearly 1,000 specimens subjected to the following four different curing conditions:

a) Steam curing at (90°C) and 95-percent relative humidity for 48 hours starting about 24 hours after casting.
b) Steam curing at (60°C) for 48 hours starting about 24 hours after casting.
c) Steam curing at (90°C) for 48 hours starting about 15 days after casting.
d) Curing under laboratory conditions (23°C) and ambient humidity.

Density of the UHPC ranged from 2400 to 2500 kg/m^3. The tests were conducted on (76 by 152 mm) cylinders, generally used the procedures of ASTM C39 (ASTM, 2005), except the loading rate was increased to (1 MPa/s), and a (165 mm) diameter spherical bearing plate was used. The average measured compressive strengths at 28 days for six cylinders cured using methods a, b, c, and d were (193, 171, 171, and 126 MPa), respectively.

Richard (1996) reported that compressive strengths as high as 550 MPa can be achieved at atmospheric pressure and heat treating at 250 °C. With pressure, compressive strengths as high as 810 MPa are possible. With conventional production capabilities and curing at 90 °C, strengths of 280 MPa can be achieved.

Table 2.5 - Typical composition of Ductal® (Graybeal, 2006a)

Material	Amount (kg/m^3)	Percent by weight (%)
Portland cement	712	28.5
Fine sand	1020	40.8
Silica fume	231	9.3
Ground quartz	211	8.4
Super-plasticizer	30.7	1.2
Accelerator	30	1.2
Steel fiber	156	6.2
Water	109	4.4

2.4.4. Tensile Strength

In conventional structural design for concrete structures, the tensile strength of concrete is assumed to be zero in reinforced concrete design. The tensile strength of UHPC is higher than that of conventional concrete, and UHPC can exhibit sustained tensile strength after first cracking. The results of tests for tensile strength of UHPC, therefore, often report a value of first cracking strength as well as a peak post-cracking strength. Consequently, tensile strength takes on increasing importance as a property to consider in design (Russell and Graybeal, 2013).

Graybeal et al. (2012) captured the tensile stress-strain response obtained from a readily available UHPC containing 2 percent by volume steel fiber reinforcement. The results are indicated in Figure 2.17.

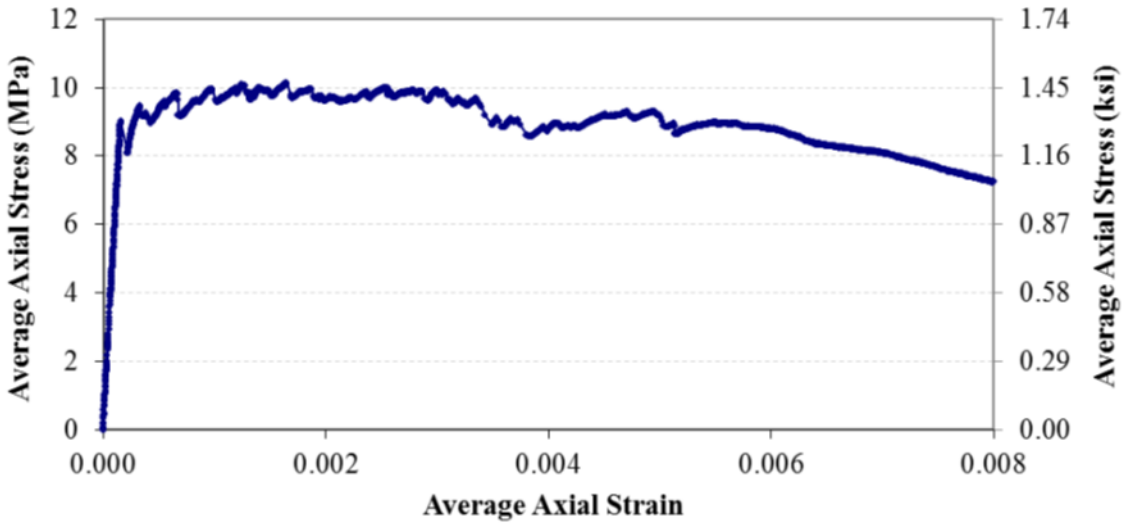

Figure 2.17 - Tensile stress-strain response of UHPC (Graybeal et al. 2012)

Graybeal (2006a) reported measurements of tensile strength using flexural prisms, split cylinders, mortar briquettes, and direct tension tests of cylinders. The combined results of these tests indicated a first tensile cracking strength of approximately (9.0 MPa) for steam-cured specimens and approximately (6.2 MPa) without any heat treatment.

Graybeal and Baby (2013) conducted a uniaxial direct tension test on UHPC. This test method is based on a standard tension test applied to metals, provides the uniaxial tensile mechanical response of UHPC and is applicable to both cast and extracted test specimens. Tests were completed on two UHPCs containing multiple steel fiber reinforcement percentages and cured through ambient laboratory and steam-treated conditions. The results demonstrated that these two UHPCs could sustain more than 9 MPa of uniaxial tensile load. In the split cylinder tests (ASTM C496, 2011), measured splitting tensile strengths at first cracking were (11.7 MPa) for steam-cured specimens and (9.0 MPa) for untreated specimens. For the steam-cured specimens, the splitting tensile strengths at first cracking varied from 3 to 5 percent of the measured compressive strength. The post-cracking peak tensile splitting stresses ranged from 12 to 16 percent of the compressive strength.

According to JSCE (2006) recommendations, when a commercially available UHPC constituent material used, the average tensile strength is found to vary between 10 to 15 MPa. The direct tensile test would be essentially the best way to obtain the tensile strength and tension softening characteristics.

2.4.5. Modulus of Elasticity

The modulus of elasticity of normal strength concrete with compressive strength values of 28 to 55 MPa is typically 25 to 35 GPa (ACI, 2014). The elastic modulus of high performance concrete (HPC) with compressive strengths of 83 to 124 MPa is approximately 33 to 44 GPa (ACI, 1992). UHPC has a high elastic modulus typically in the range of 57 to 70 GPa (Richard and Cheyrezy, 1995).

Graybeal (2006a) measured the modulus of elasticity of six cylinders in compression in accordance with ASTM C469 (ASTM, 2002) at ages from 1 to 56 days. After steam curing, the measured values were about 50 GPa. Cylinders cured under standard laboratory conditions had modulus of elasticity values of about 42.7 GPa at 28 days.

The modulus of elasticity was also measured in direct tension tests. The average measured values were 51.9 GPa for steam treated specimens and 47.6 GPa for untreated specimens. These values were slightly higher than those measured in compression (Russell and Graybeal, 2013).

2.4.6. Flexural Strength

UHPC has superior flexural strength compared to normal and HPC. The UHPC has a flexural strength around 30 - 60 MPa and had a toughness of 250 times that of normal strength concrete (Richard and Cheyrezy, 1995). Typical UHPC behavior under flexure is characterized by linear elastic behavior up to the first cracking strength of the material, a strain-hardening phase up to the maximum load, and a strain softening phase after the maximum load is reached.

Graybeal (2006a) reported the flexural cracking strength subjected to different curing conditions as explained in section 2.4.3. Tests were conducted according to ASTM C1018 (ASTM, 1997). The average measured splitting tensile strengths at first cracking at 28 days cured using methods a, b, c, and d were (11.7, 11.7, 11.7, and 9 MPa), respectively.

2.4.7. Poisson's Ratio

The Poisson's ratio is defined as the relationship of the transverse strain divided by the longitudinal strain. The value of Poisson's ratio was reported by various researchers, it ranges from 0.16 to 0.21. The average value is approximately 0.18 (Graybeal, 2011).

2.4.8. Bond Strength

Carbonell et al. (2012) investigated the bond strength between conventional concrete substrates and UHPC toppings. Primary variables were surface temperature and moisture condition of the substrate. Half the specimens were subjected to 300 freeze-thaw cycles in accordance with ASTM C666 (ASTM, 2008) Method B. The bond strength has been evaluated using an indirect splitting tensile test along the interface. Samples subjected to the freeze-thaw tests had greater bond strength than samples of the same age without freeze-thaw cycles. Samples in which the substrate was saturated before placing the UHPC achieved higher bond strengths than samples with a dry substrate.

2.4.9. Shrinkage

Two types of shrinkage may be present in UHPC. Drying shrinkage is that caused by loss of moisture from the UHPC. Autogenous shrinkage is that caused by a decrease in volume as the cementitious materials hydrate. The standard test in the United States for measuring shrinkage is ASTM C157 (ASTM, 2006), which is designed to measure drying shrinkage beginning after the concrete has hardened. Other methods are used to measure autogenous shrinkage because these measurements must begin immediately after the UHPC is placed.

Shrinkage of UHPC measured in accordance with ASTM C157 (ASTM, 2006) using (76- by 76-mm) prisms provided an ultimate shrinkage range of 620 to 766 millionths,

depending on the method of steam curing, and 555 millionths for untreated specimens (Grabeal, 2006a).

Francisco et al. (2009) reported autogenous shrinkage of about 270 millionths and drying shrinkage of about 100 millionths at 350 days on 70 mm diameter cylinders cured at 50 °C.

2.5. Design of GFRP-RC Bridge-Deck Slabs

The Canadian Highway Bridge Design Code CHBDC (CAN/CSA S6 2014) and AASHTO-LRFD Bridge Design Guide Specifications (AASHTO, 2009 and 2012) specify different design methods for bridge decks reinforced with steel and GFRP reinforcing bars. Design of bridge-deck slab based on these codes requires the presence of top and bottom mats of orthogonal reinforcing bars.

2.5.1. Design Approaches in the CHBDC (CAN/CSA S6, 2014)

The CHBDC (CAN/CSA S6, 2014) provides two methods, flexural design method and empirical design method specified in clauses 5.7.1 and 8.18.4, respectively. The following are the bridge decks design provisions for the two methods:

2.5.1.1. **Flexural Design Method**

In the flexural design method, concrete deck slabs shall be analyzed for positive and negative bending moments resulting from loads applied on the slabs. The analysis shall consider the bending moments induced in the longitudinal direction that agree with the assumptions used in the analysis of the transverse bending moments. The cantilever portions of concrete deck slabs shall be analyzed for transverse negative bending moments resulting from loads on the cantilever portions of the slabs or horizontal loads on barriers and railings. The cantilever portions of concrete deck slabs may be analyzed using Clause 5.7.1.6.1 while the deck slabs are analyzed using Clause 5.7.1.7.1. The design of sections, however, should be conducted according to Section 8 when steel bars are used and Section 16 when FRP reinforcing bars are used.

When the concrete deck slabs are designed according to the flexural design method for CL-625 truck, the design bending moments are determined based on a maximum wheel load of 87.5 kN. The design service load for the deck slabs is taken as 1.4 × 0.9 × 87.5 = 110.25 kN, where 1.4 is the impact coefficient and 0.9 is the live-load combination factor, while the design factored load is taken as 1.4 × 1.7 × 87.5 = 208.25 kN, where 1.7 is the live-load combination factor (CAN/CSA S6, 2014).

According to Section 16 in the CHBDC (CAN/CSA S6, 2014), the design of flexural members reinforced with GFRP bars should consider the following:

(a) For concrete components reinforced with FRP bars or grids, the overall performance factor, *J*, shall be at least 4.0 for rectangular sections and 6.0 for T-sections. (Clause 16.8.2.1).

(b) The factored resistance, M_r, shall be at least 50% greater than the cracking moment, M_{cr}. This requirement may be waived if the factored resistance, M_r, is at least 50% greater than the factored moment, M_f. If the ultimate limit state (ULS) design of the section is governed by FRP rupture (under reinforced section), M_r shall be greater than 1.5 M_f. This condition may be waived if $M_r > 1.5\ M_{ULS}$. (Clause 16.8.2.2).

(c) When the maximum tensile strain exceeds 0.0015, the crack width has to not exceed 0.5 mm for members subjected to aggressive environments and 0.7 mm for other members. (Clause 16.8.2.3).

(d) The maximum stress in FRP bars under loads at service limit state (SLS) shall not be more than $F_{SLS} f_{FRPu}$, where F_{SLS} is 0.25 for GFRP bars. (Clause 16.8.3).

(e) The longitudinal reinforcement provided by Clause 8.18.7 of the CAN/CSA S6-06 (2010), both top and bottom when the main reinforcement is perpendicular to traffic shall be $120/(S)^{0.5}$, up to a maximum of 67% of the transverse reinforcement. In addition, as mandated by Clause 16.8.8.2, the spacing of the reinforcement in each direction shall not exceed 300 mm and the diameter of the reinforcement shall not be less than 15 mm.

2.5.1.2. **The Empirical Design Method**

As stated by the CHBDC (CAN/CSA S6, 2014) Clause 8.18.4.1, the empirical method is applicable for that portion of the deck slab which is of nearly uniform thickness and bounded by the exterior supporting beams. However, they have to meet the conditions specified in Clause 8.18.4.1 in the CAN/CSA S6 (2014). These conditions are:

a) The deck slab is composite with the supporting beams, which are parallel to each other, and the lines of supports for the beams are also parallel to each other.
b) The ratio of the spacing of the supporting beams to the thickness of the slab is less or equal to 18.0. The spacing of the supporting beams used in calculating this ratio is taken parallel to the direction of the transverse reinforcement.
c) The spacing of the supporting beams does not exceed 4.0 m and the slab extends sufficiently beyond the external beams to provide full development length for the bottom transverse reinforcement.
d) When the supporting beams or their lines of supports are not parallel to themselves, engineering judgment shall be used to determine whether the empirical design method for the design of the deck slab is to be adopted.

In addition, for the empirical design method to apply, a full-depth cast-in-place deck slab should satisfy the conditions specified by Clause 8.18.4.2 (for steel reinforcement) and Clause 16.8.8.1 (for FRP reinforcement) in addition to those of Clause 8.18.4.1. Clause 16.8.8.1 for Design by empirical method specifies the following:

a) The deck slab contains two orthogonal assemblies of FRP bars with the clear distance between the top and bottom transverse bars being a minimum of 55 mm.

b) For the transverse FRP bars in the bottom assembly, the minimum area of cross-section in mm^2/mm is $500ds/E_{FRP}$, where d_s is the distance from the top of the slab to the centroid of the bottom transverse FRP bars (mm) and E_{FRP} is the mean modulus of elasticity of FRP bars (MPa).

c) Longitudinal bars in the bottom assembly and both the transverse and longitudinal bars in the top assembly are of GFRP with a minimum of 0.0035.

For the empirical design method to apply, a full-depth cast-in-place deck slab shall satisfy the following conditions in addition (Clause 8.18.4.2) to those of Clause 8.18.4.1:

a) As shown in Figure 2.18, the deck slab contains two orthogonal assemblies of reinforcement, near the top and bottom of the slab, respectively, with ρ in each direction in each assembly being at least 0.003, except as specified in Item (c). For calculating ρ, the effective depth of concrete, *d*, is assumed to be the distance between the top of the slab and the centroid of the lower reinforcement assembly.

b) When the slab is supported on parallel beams, the reinforcement bars closest to the top and bottom of the slab are laid perpendicular to the axes of the supporting beams or are laid on a skew parallel to the lines of beam supports.

c) The reinforcement ratio, ρ, may be reduced to 0.002 where deck slabs with the reduced reinforcement can be satisfactorily constructed and the reduction of ρ below 0.003 is approved.

d) Where the transverse reinforcing bars are placed on a skew, the reinforcement ratio for these bars is not less than $\rho / \cos^2\theta$, where θ is the skew angle.

e) Where the unsupported length of the edge stiffening beam, S_e, exceeds 5 m, the reinforcement ratio, ρ, in the exterior regions of the deck slab is increased to 0.006, as shown in Figure 2.19.

f) The spacing of the reinforcement in each direction and in each assembly does not exceed 300 mm.

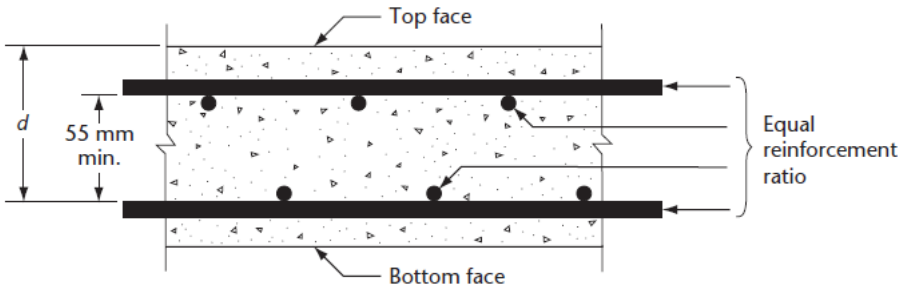

Figure 2.18 - Reinforcement in cast-in-place deck slab, Empirical design method, Clause 8.18.4.2, CAN/CSA S6 (2014)

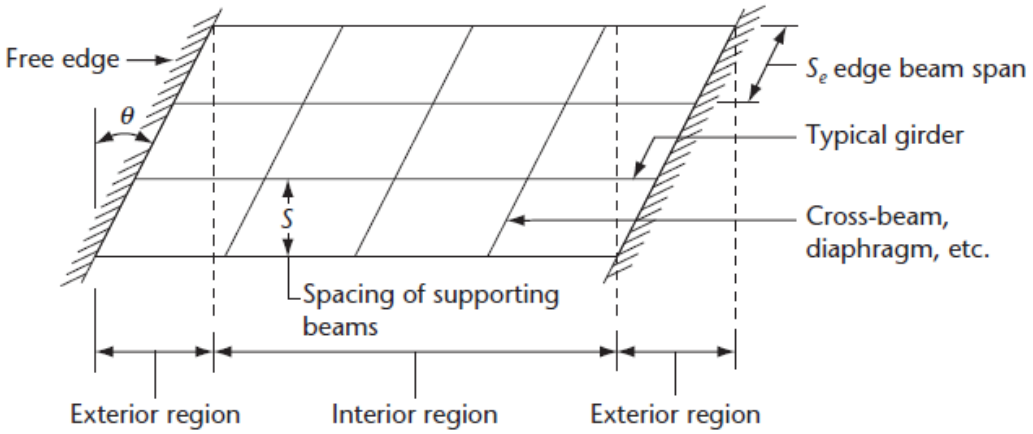

Figure 2.19 - Reinforcement for cast-in-place deck slabs designed using the empirical method, (Clause 8.18.4.2, CAN/CSA S6, 2014)

2.5.2. Design Approaches in the AASHTO-LRFD

AASHTO-LRFD (AASHTO, 2009 and 2012) specify different design methods for bridge decks reinforced with steel and FRP reinforcing bars. Article 9.7.1 states some design provisions for designing concrete deck slabs, these provisions can be summarized as follows:

- The depth of a concrete deck, excluding any provision for grinding, grooving, and sacrificial surface, should not be less than 7.0 in.
- Minimum cover shall be in accordance with the provisions of Article 5.12.3.
- Shear connectors shall be designed in accordance with the provisions of Section 5 for concrete beams and Sections 6 and 7 for metal beams.
- In case of skewed decks, If the skew angle of the deck does not exceed 25 degrees, the primary reinforcement may be placed in the direction of the skew; otherwise, it shall be placed perpendicular to the main supporting components.
- The edge of the deck shall either be strengthened or be supported by a beam or other line component. The beam or component shall be integrated in or made composite with the deck. The edge beams may be designed as beams whose width may be taken as the effective width of the deck specified in Article 4.6.2.1.4.

- The overhanging portion of the deck shall be designed for railing impact loads and in accordance with the provisions of Article 3.6.1.3.4.

2.5.2.1. **Empirical Design**

The empirical design process is exclusively for concrete deck slabs supported by longitudinal components. The method may be used only if the following conditions are satisfied (Article 9.7.2.4):

- Cross-frames or diaphragms are used throughout the cross-section at lines of support;
- For cross-section involving torsionally stiff units, such as individual separated box beams, either intermediate diaphragms between the boxes are provided at a spacing not to exceed 25.0 ft, or the need for supplemental reinforcement over the webs to accommodate transverse bending between the box units is investigated and reinforcement is provided if necessary;
- The supporting components are made of steel and/or concrete;
- The deck is fully cast-in-place and water cured;
- The deck is of uniform depth, except for haunches at girder flanges and other local thickening;
- The ratio of effective length to design depth does not exceed 18.0 and is not less than 6.0;
- Core depth of the slab is not less than 4.0 in., see Figure 2.20;
- The effective length, as specified in Article 9.7.2.3, does not exceed 13.5 ft;
- The minimum depth of the slab is not less than 7.0 in., excluding a sacrificial wearing surface where applicable;
- There is an overhang beyond the centerline of the outside girder of at least 5.0 times the depth of the slab; this condition is satisfied if the overhang is at least 3.0 times the depth of the slab and a structurally continuous concrete barrier is made composite with the overhang;
- The specified 28-day strength of the deck concrete is not less than 4.0 ksi; and

- The deck is made composite with the supporting structural components.

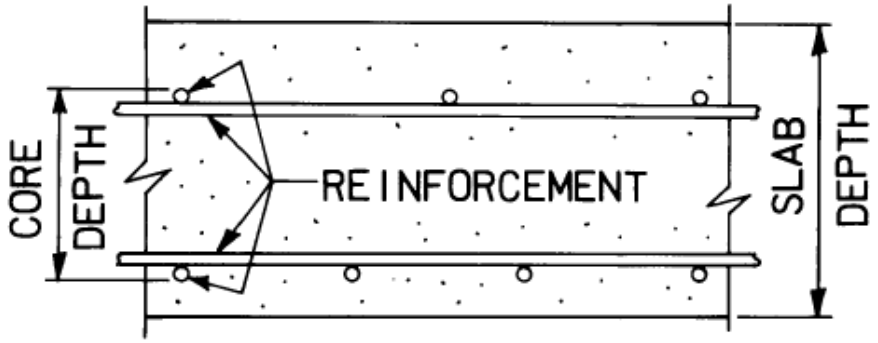

Figure 2.20 - Core of a concrete deck slab Empirical design method, Article 9.7.2.4, AASHTO (2012)

Four layers of isotropic reinforcement shall be provided in empirically designed slabs. Reinforcement shall be located as close to the outside surfaces as permitted by cover requirements. Reinforcement shall be provided in each face of the slab with the outermost layers placed in the direction of the effective length. The minimum amount of reinforcement shall be 0.27 in^2/ft of steel for each bottom layer and 0.18 in^2/ft of steel for each top layer. Spacing of steel shall not exceed 18.0 in. Reinforcing steel shall be Grade 60 or better. All reinforcement shall be straight bars, except that hooks may be provided where required.

Both lap splices and mechanical splices shall be allowed. Mechanical splices shall be tested and approved to conform to the limits for slip in Article 5.11.5.2.2, Mechanical Couplers, and for fatigue in Article 5.5.3.4, Welded or Mechanical Splices of Reinforcement. Sleeve wedge-type couplers shall not be permitted on coated reinforcing.

If the skew exceeds 25 degrees, the specified reinforcement in both directions shall be doubled in the end zones of the deck. Each end zone shall be taken as a longitudinal distance equal to the effective length of the slab specified in Article 9.7.2.3.

2.5.2.2. **Traditional Design**

The traditional design is based on flexure. The live load force effect in the slab may be determined using the approximate methods of Article 4.6.2.1 or Article 4.6.3.2. It is applied to concrete deck slabs that have four layers of reinforcement, two in each direction. Reinforcement shall be placed in the secondary direction in the bottom of slabs as a percentage of the primary reinforcement for positive moment as follows:

- For primary reinforcement parallel to traffic: $100/\sqrt{S} \leq 50$ %.
- For primary reinforcement perpendicular to traffic: $220/\sqrt{S} \leq 67$ %.

Where: S = the effective span length taken as equal to the effective length.

2.5.2.3. **Approximate Method**

An approximate method of analysis in which the deck is subdivided into strips perpendicular to the supporting components shall be considered acceptable for decks (Article 4.6.2.1.1). Where the strip method is used, the extreme positive moment in any deck panel between girders shall be taken to apply to all positive moment regions. Similarly, the extreme negative moment over any beam or girder shall be taken to apply to all negative moment regions.

In determining the strip widths, the effects of flexure in the secondary direction and of torsion on the distribution of internal force effects are accounted for to obtain flexural force effects approximating those that would be provided by a more refined method of analysis. Depending on the type of deck, modeling and design in the secondary direction may utilize one of the following approximations:

- Secondary strip designed in a manner like the primary strip, with all the limit states applicable;
- Resistance requirements in the secondary direction determined as a percentage of that in the primary one as specified in Article 9.7.3.2 (i.e., the traditional approach

for reinforced concrete slab in the previous editions of the AASHTO Standard Specifications); or

- Minimum structural and/or geometry requirements specified for the secondary direction independent of actual force effects, as is the case for most wood decks.

The approximate strip model for decks is based on rectangular layouts. Currently about two-thirds of all bridges nationwide are skewed. While skew generally tends to decrease extreme force effects, it produces negative moments at corners, torsional moments in the end zones, substantial redistribution of reaction forces, and a number of other structural phenomena that should be considered in the design. More details about approximate method for bridge decks are available in AASHTO 2012 in Article 4.6.2.1.3 through Article 4.6.2.1.9.

2.6. Closure Joints between Prefabricated Elements

Considerable research studies have been conducted to investigate the behavior of closure joints between precast bridge elements. Most of these studies have used conventional or epoxy-coated steel (Li et al., 2010; Graybeal, 2010; Au et al., 2011; Ma et al., 2012; Graybeal, 2014; Hwang and Park, 2014; Lee and Lee, 2015; Yuan and Graybeal, 2015; Haber and Graybeal, 2018) with different joint shapes and reinforcement configurations. A few studies used GFRP bars (Khalafalla and Sennah, 2013; Sayed-Ahmed and Sennah, 2015; Arafa et al., 2016; Sayed-Ahmed, 2016; Sherif and Sennah, 2017), although the closure joints had different reinforcement configurations.

Zhu et al. (2011a) tested four pairs of full-scale slabs connected by a U-bar detail with one of the selected closure-pour (CP) materials. Continuous longitudinal U-bar joint details for accelerated bridge construction were investigated. The specimens were tested under static and fatigue loadings. The test parameters were shear and flexure loading setup, curing times for the closure material, static and fatigue loading. Specimen details and test setup are shown in Figure 2.21. The actual moment capacity depends on the interaction between

the closure-pour material and steel as well as the steel arrangement. The main conclusions of this investigation are summarized as follows:

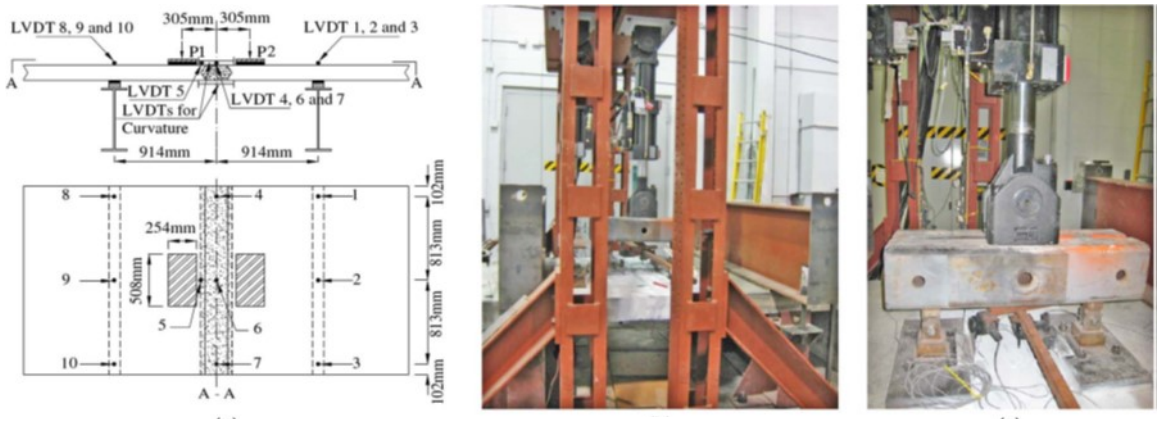

Fatigue shear test setup

Fatigue flexure test setup

Apparatus applying fatigue forces

Figure 2.21 - Specimen details and test setup (Zhu et al. 2011a)

1. The fatigue loading was found to have little influence on the U-bar joint behavior including average curvature (deflection) of the joint, crack width, and reinforcement strain under service live load.
2. Cracks at the interface between the grouted joint and the concrete slab were observed. Cracks initiate above the service load level for some specimens and below for others depending on the compressive strength of the joint material. No de-bonding between the slab and the joint is noticed. The crack widths of specimens with the U-bar detail are developed at a smaller rate with the increasing of the loading than those of the headed bar detail. At the failure loads, the U-bar detail develops similar or even smaller cracks than the headed bar detail when the same joint materials are used. Generally, crack widths are less than 0.15 mm at the service load level.
3. The joint moment capacity not only depends on the compressive strength of the closure-pour material at the compression side but also on the tension side where tensile steel is located. Also, it is noticed that the joints with lower closure-pour compressive strengths tend to have lower moment capacities.

4. All specimens with U-bars exceed the calculated capacity; whereas, only two of four specimens with headed bars do. All specimens experience a ductile failure. On the basis of these tests, the U-bar joint detail is a viable connection system for the longitudinal joint in bridge decks.

Zhu et al. (2011b) investigated continuous transverse U-bar joint details for accelerated bridge construction. Four full-scale specimens connected by the developed U-bar detail together with the selected closure-pour (CP) materials were tested. The test variables were curing times (i.e., overnight cure and seven-day cure), static and fatigue tension loading. The test setup is shown in Figure 2.22. Test results were evaluated based on tension capacity, cracking, and steel strain. The findings of this investigation are summarized as follows:

Figure 2.22 - Tension test setup (Zhu et al. 2011b)

i) The fatigue loading has no influence on tensile capacity. When the closure-pour material is poured and cured appropriately to get the compressive strength of 41.4 MPa, the calculated tensile capacity using nominal yield strength of 414 MPa for the steel reinforcement can be exceeded.

ii) The lacer bars provide confinement of concrete within the joint and serve as restraints for the U-bars when the joint closure-pour material fails. The lacer bars allow the ductile failure in all specimens.

iii) As the tension loading increases, transverse cracks (parallel to the joint interface) continue to appear in various locations within the joint zone. The first two cracks occur at the interfaces: crack 1 at the interface with two U-bar sides and crack 2 at the interface with three U-bar sides. Under the service load level, the maximum width of crack 1 is about 0.7 mm, while the maximum width for crack 2 is about 0.1 mm. When approaching the capacities of the specimens, longitudinal and diagonal cracks can be observed.

iv) At the same load level, fatigue loading increases the maximum crack width during the first 0.5 million cycles. However, the maximum crack width does not further increase after the first 0.5 million cycles. Instead, it tends to decrease because additional smaller cracks open in the joint zone under fatigue loading.

v) The compressive strength of closure-pour materials has an impact on the joint stiffness response. Specimens with the lowest closure-pour strength have the softest response, especially under above-service-level loading. Fatigue loading does not change the joint stiffness response.

vi) The span length of the bridge has the largest effect on the maximum negative moment in the transverse joint. For the bridge with the same span length, the difference of the maximum negative moment between the two-span bridge systems and three-span bridge systems is negligible. Based on the test results, the developed transverse U-bar joint detail is a promising connection system.

Hwang and Park (2014) evaluated the flexural behavior of lap-spliced joints that exploit the remarkable bonding performance of ultra-high-performance concrete (UHPC). Seven specimens have been fabricated using the same steel rebar and UHPC, the properties of steel reinforcement and concrete were identical for all test specimens. The test variables were the lap-spliced length and joint width. Concrete cover was 30 mm and the bar spacing was 100 mm for all test specimens. The failure pattern, load–deflection relationship, and load–strain relationship obtained by the static loading test were analyzed with respect to

the details of the joints, Figure 2.23 shows the four-point bending test setup. A modified model was suggested considering the bonding performance of UHPC at the joint interface and the yield behavior of the reinforcement in previous studies. The corresponding results for this model were compared with the test results. The following conclusions were derived from the static loading test results and the predictions of the modified analytical model:

Figure 2.23 - Four-point bending test (Hwang and Park, 2014)

i) Three types of failure mode were observed according to the joint details: failure mode 1, governed by cracks propagating in the center of the joint owing to inadequate lap-spliced length; failure mode 2, caused by lateral cracks in the joint; and failure mode 3, governed by the yield behavior of the rebar in the joint interface.
ii) Failure mode 3 occurred when sufficient lap-spliced length and joint length were secured. The values of lap-spliced length and joint length were determined by conditions such as the concrete cover and rebar spacing.
iii) To induce failure mode 3 and exploit the ductility of the rebar, a lap-spliced length longer than 150 mm and a joint length longer than 250 mm were required under the conditions of 30 mm for concrete cover and 100 mm for rebar spacing. However, a lap-spliced length longer than 200 mm should be arranged to ensure that ductility

reaches a level similar to when a continuous rebar is used. Such results were obtained from an experiment that used UHPC with reduced strength at the joint. If UHPC of sufficient strength had been employed, the bond between the rebar and UHPC should have been maintained even if a shorter lap-spliced length was used. Thus, this value represents a conservative result, and additional verification will be needed in the future.

iv) An analytical model to predict the flexural strength of thin UHPC members was proposed by modifying a model suggested in previous studies so as to consider the bonding performance of UHPC at the joint interface and the post-yielding behavior of the rebar. The use of 0.2 for the strength reduction factor introduced to express the bonding performance of UHPC at the joint interface as a ratio of the tensile strength provided conservative predictions in good agreement with the test results. Given that the predictions were derived from a small number of test results that correspond to those of test members with smooth interfaces, further validation tests with members that vary in the roughness of the interface will be required to derive more general conclusions. The analytical model should also be modified to consider the impacts of concrete cover and rebar spacing on interfacial bonding.

A study of improved continuous longitudinal joint details for decked precast prestressed concrete girder bridge systems has been investigated by Li et al. (2009a). Seven reinforced concrete beam specimens connected with either lapped headed reinforcement or lapped welded wire steel reinforcement were tested along with a specimen reinforced by continuous bars for comparison. The test variables were reinforcement details, lap length (64 mm, 102 mm, 152 mm), and longitudinal reinforcement spacing (102 mm, 152 mm). Each specimen was 610mm wide, 3048 mm long, and 152 mm deep with 51 mm cover at top and 25 mm cover at bottom. All the specimens had four layers of reinforcement both at the left side and the right side to simulate the deck reinforcement in the top flange of adjacent girders. All the reinforcement was grade 60 and epoxy coated. Test results were evaluated based on flexural capacity, curvature at failure, cracking, deflection, and steel strain. Figure 2.24 shows the four point load flexural test setup.

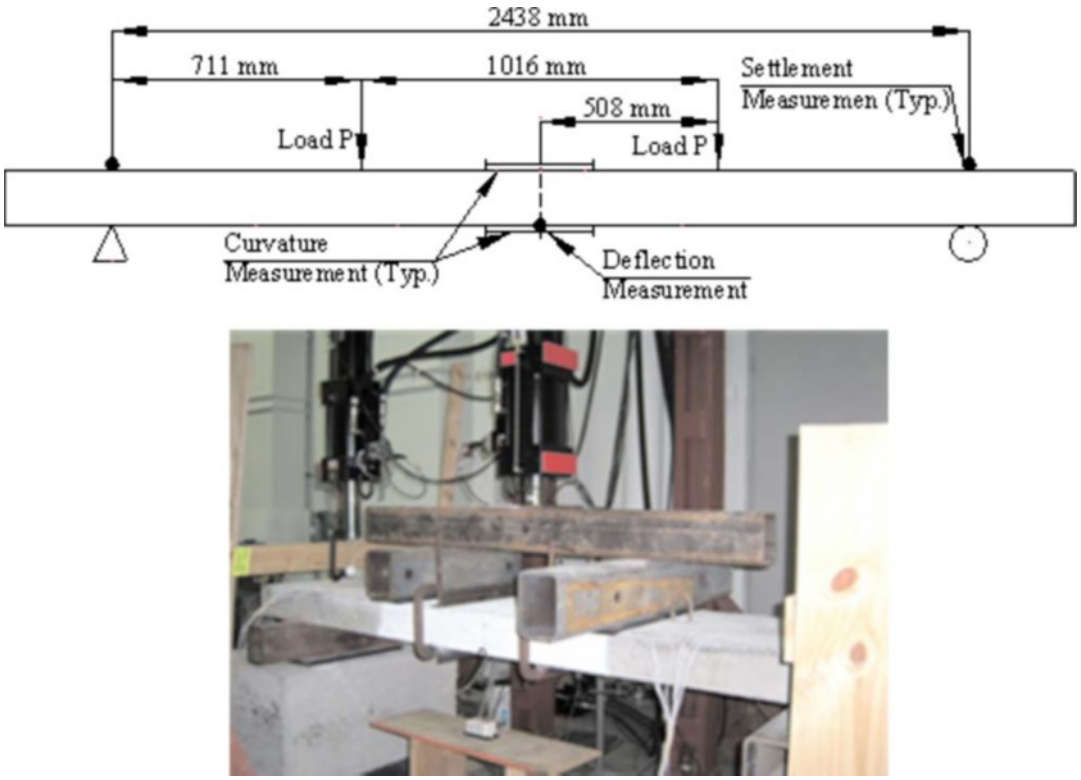

Figure 2.24 - The test setup (Li et al. 2009a)

The following conclusions were drawn: (1) The headed bar detail can provide a continuous force transfer in the longitudinal joint for decked bulb tee bridge system while minimizing the width of the joint to accelerate bridge construction. (2) The lap length for the headed bar detail is recommended to be 152 mm, this lap length provided full development of the bars to produce full load capacity and significant ductility. (3) The reinforcement spacing had an effect on the structural behavior, the smaller spacing provided more load resistance with less ductility because more steel was provided in the same cross section. (4) In the tested welded wire reinforcement connection details was used in the joint for decked bulb tee bridge, the joint width accommodating 25 mm spacing between cross wires failed to provide the required moment capacity. So, welded wire reinforcement connection detail with the same joint width as the headed bar detail cannot be recommended. (5) According to the moment capacity, curvature, cracking, deflection, and steel strain comparison, the headed bar detail with a 152 mm lap length was recommended for replacing the current welded steel connector detail as the improved longitudinal joint detail.

Li et al. (2009-b) investigated the improved continuous longitudinal joint details for decked precast prestressed concrete girder bridge systems. Four full-scale slabs with the same dimensions and reinforcement details were fabricated and tested. Each specimen consists of two panels of 1892 mm wide and 1626 mm long connected by 16 mm diameter headed steel reinforcement detail using a 152 mm lap length. The female to female shear key was provided at the vertical edge of both ends in the specimen length direction. An analytical parametric study was conducted to provide a database of maximum forces in the longitudinal joint. These maximum forces were then used to determine the loading demand necessary in the slab testing due to the service live load. Static and fatigue tests under four-point pure-flexural loading, as well as three-point flexural-shear loading, were conducted. Test results were evaluated based on flexural capacity, curvature behavior, cracking, deflection, and steel strain. Figure 2.25 shows the specimens dimensions and test setup. Based on the parametric study and the experimental program, the following conclusions were made:

a) The fatigue loading has little influence on the structure behavior including average curvature of the joint, deflection at midspan, relative displacement of the joint interface, as well as reinforcement strain under service live load.
b) The fatigue loading has no effect on the loading capacity of the structure. The slab, after 2,000,000 fatigue cycles, has the same loading capacity as the slab under static load test.
c) The fatigue loading inhibits the development of the plastic hinge under pure-bending load. The fatigue cycles reduce the ductility capacity significantly.
d) Based on these tests, the improved longitudinal joint detail is a viable connection system to transfer the forces between the adjacent decked bulb tee girders.

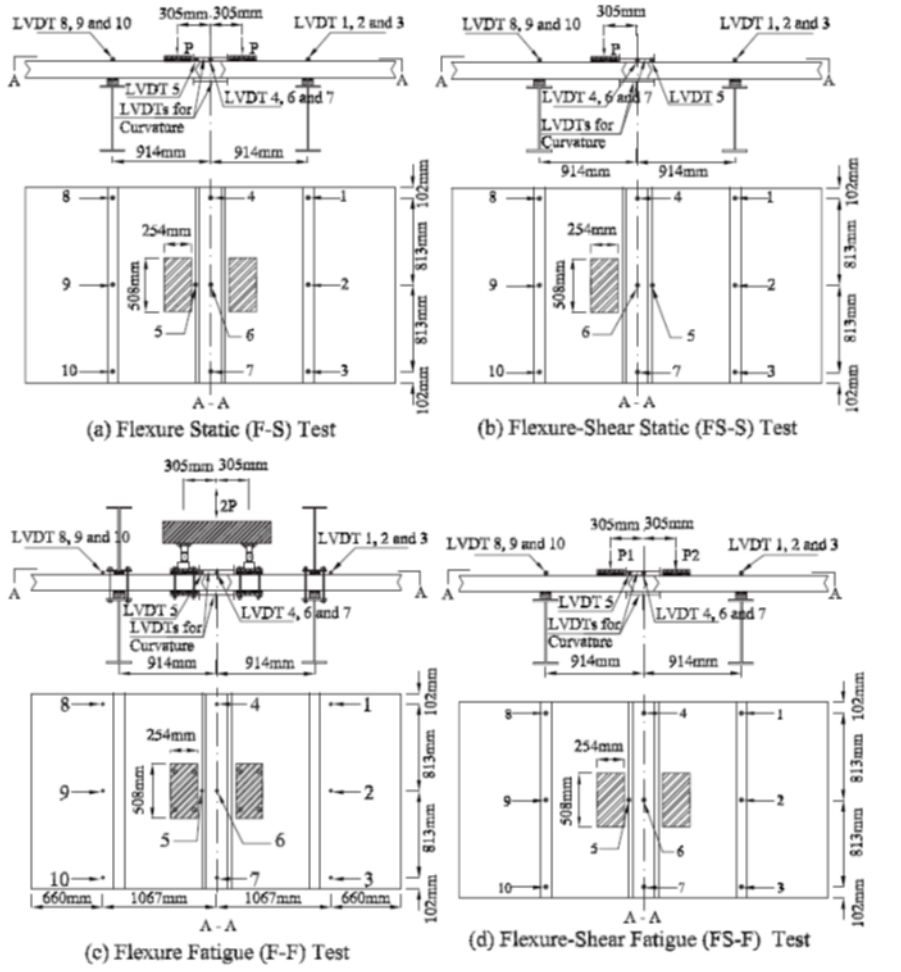

Figure 2.25 - The specimens' dimensions and test setup (Li et al., 2009-b)

Ma et al. (2012) studied longitudinal joint with Headed bar and U-bar details for accelerated bridge construction. A total of six specimens were fabricated and tested under static flexure test as shown in Figure 2.26, the specimens were 3048 mm long, 381 mm width, and 158.7 mm deep. The specimens made of stainless steel (SS) and deformed wire reinforcement (DWR) with the same joint detail configurations were tested and compared in Phase I, followed by the testing of U-bars (DWR) with varied concrete strengths, bar spacing, and overlap lengths in Phase II. Test results were evaluated based on moment capacity, cracking at service and failure load, and steel strains.

Figure 2.26 - The flexural test setup and specimen dimensions (Ma et al. 2012)

The test results indicated that: A 16 mm (No. 5) U-bar joint detail with a minimum bend diameter of three times the diameter of the bar ($3d_b$) can be used to facilitate accelerated bridge construction. The U-bar detail using DWR performed better than the headed bar detail in terms of moment capacity and service-level crack widths. Also, the U-bar joint zone is less congested than the headed bar detail. A reduction in joint concrete strength led to a reduction in the flexural capacity. When decreasing the joint overlap length from 152 mm to 102 mm, the crack widths were observed to be significantly larger and the flexural capacity was decreased by 17.7%. Increasing the spacing of the U-bar reinforcement from 114 mm to 152 mm did not change the behavior of longitudinal joints very much in terms of crack width and flexural capacity. To provide adequate ductility without significant loss of strength at ultimate, the joint overlap length should not be less than 152 mm when using 16 mm joint reinforcement.

An investigation of transverse joint details with tight bend diameter U-bars for accelerated bridge construction has been studied by Ma et al. (2011). Headed bar and U-bar [stainless steel and deformed wire reinforcement (DWR)] specimens with the same joint detail configuration were tested and compared in Phase I, followed by testing of U-bars (DWR) with varied concrete strength, bar spacing, and overlap length in Phase II. Test results were evaluated based on tension capacity, cracking at service loading and failure, and steel

strain. A strut-and-tie model (STM) was proposed to predict the tension capacity of a transverse joint. Figure 2.27 indicates the tension test setup.

Figure 2.27 - The tension test setup (Ma et al. 2011)

Based on the experimental program and strut-and-tie modeling, it can be stated that:

- The U-bar detail created a less-congested joint, which made it easier to construct than with headed bar detail. After consideration of capacity, service-level crack widths, constructability, and cost, the U-bar detail constructed of DWR was recommended.
- A reduction in concrete strength led to a reduction in the tensile capacity. When decreasing the joint overlap length from 152 mm to 102 mm, the crack widths were observed to be significantly larger, and the tensile capacity was decreased by 18.9%. Increasing the spacing of the U-bar reinforcement from 114 mm to 152mm did not change the behavior of transverse joints very much in terms of crack width and tensile capacity.
- To provide adequate ductility without significant loss of strength, the joint overlap length should not be less than 152 mm where 16 mm diameter joint reinforcement is used. The STM model provided safe and consistent strength predictions for transverse joints with U-bar details.

Lee and Lee (2015) studied the flexural behavior of precast concrete moment connections filled with ultra-high-performance fiber-reinforced concrete (UHPFRC). The experimental program consisted of two phases. First, the bonding performance of steel reinforcing bars embedded in the UHPFRC was evaluated using lap-spliced beam specimens with three different volumes of steel fibers. Second, the flexural behavior of the UHPFRC moment connections was investigated using 14 precast concrete beam specimens. The precast connections width ranged from 100 mm to 250 mm with three splice details (straight bars, 90-degree hooked bars, and U-loop bars). The specimens were subjected to flexural loading using a four-point loading scheme, Figure 2.28 indicates geometry and test setup of the test specimens. The findings of this investigation can be summarized as follows:

a) The bonding strength developed over tension lap splices of 160 mm or $10d_b$ were sufficient for the lap-spliced UHPFRC beams to transfer the yield strength of the reinforcing bars. The ductility of the specimens increased as the volume of the steel fibers increased, and ductile failure was observed when the volume of the steel fiber was increased by 1.6%.
b) The flexural responses of the precast concrete beam specimens were observed to be equivalent to those of the monolithic concrete specimen when the lap splice length was longer than 110 mm $7d_b$.
c) The anchorage provided by the hooks and the U-loops along with the transverse reinforcement did not appreciably contribute to the bonding strength, so that straight bars (lap splices) are the most effective splice details for UHPFRC moment connection.
d) Initial cracks at the interfaces of the UHPFRC moment connection were observed in all precast beam specimens. The occurrence of these cracks is inherent but the crack width can be controlled to ensure the serviceability of the structure. These cracks were generally initiated at an earlier stage relative to those of other flexural cracks but progressed with depths and widths similar to those of other cracks during the tests.

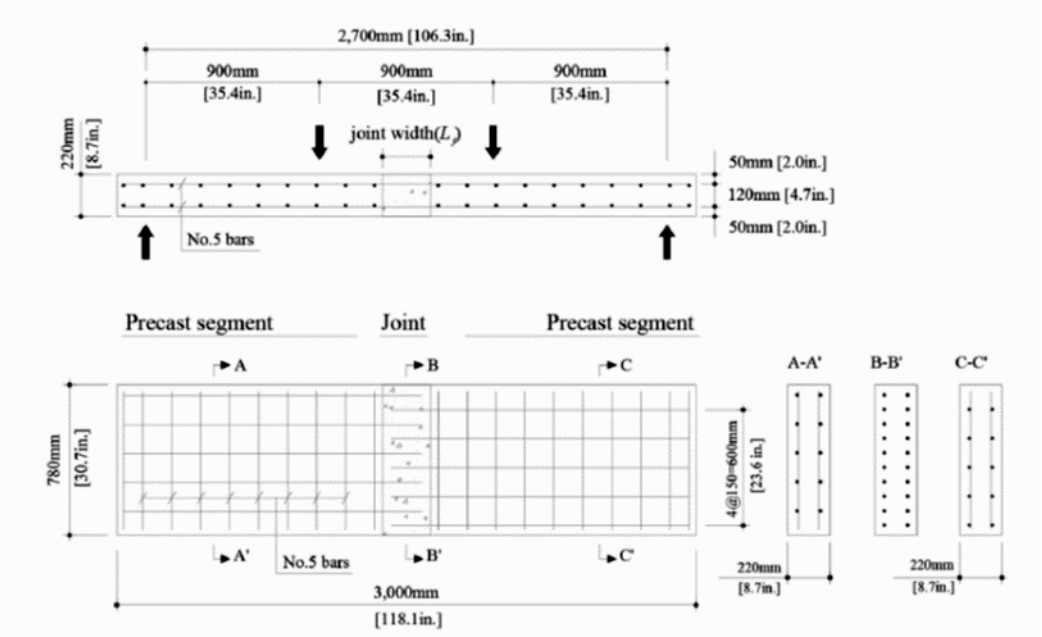

Figure 2.28 - Geometry and test setup of the test specimens (Lee and Lee, 2015)

Graybeal (2010) conducted a study to investigate the structural performance of field-cast UHPC connections for modular bridge deck components. The transverse and longitudinal connection specimens simulated the connections between precast deck panels and the connections between the top flanges of deck-bulb-tee girders respectively. Six specimens have been fabricated and tested including both cyclic and static loadings, four of them simulated transverse connections between full-depth precast deck panels and two simulated longitudinal connections between adjacent decked girders. The test parameters were reinforcement ratio, steel reinforcement type, and lap length. The test specimens were 2.4 m by 2.152 m with the connection running the length of the panel. Each of the specimens included a female-female diamond-shaped shear key with a 152 mm nominal minimum width at the top and bottom exposed surfaces. The connection reinforcement extended from the adjacent faces of the precast panels into the connection. Figure 2.29 and Figure 2.30 show the test setup for transverse and longitudinal connection specimens respectively.

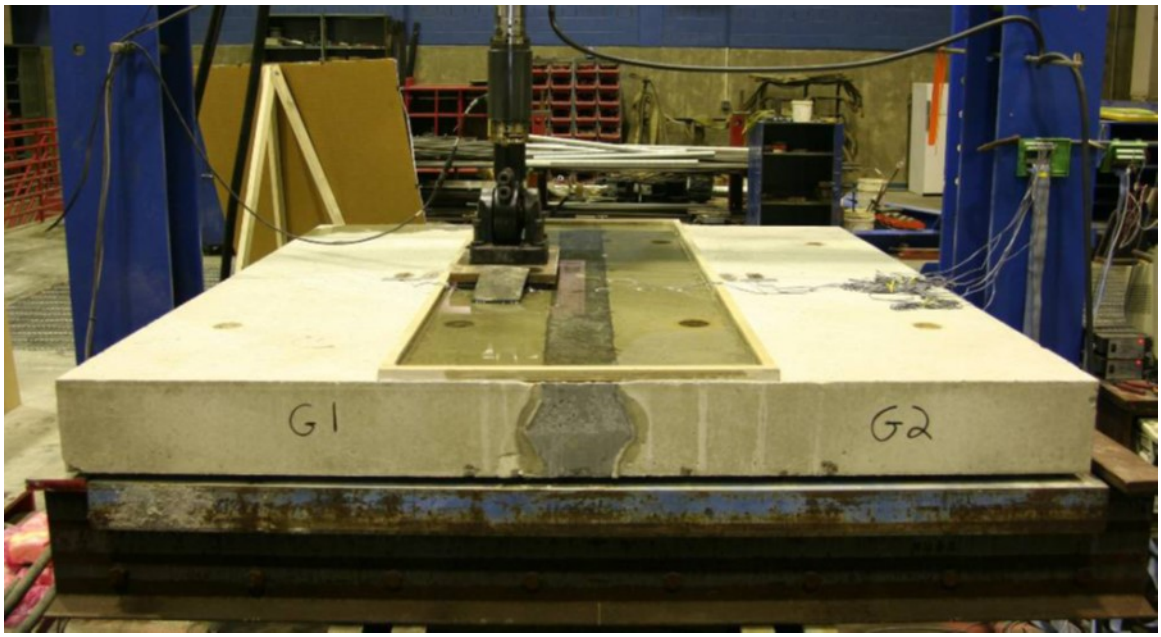

Figure 2.29 - Test setup for transverse connection specimens (Graybeal, 2010)

The main findings of this report can be summarized as follows:

i. No evidence of rebar debonding was observed in any of the longitudinal or transverse connection specimens.
ii. The development length of straight black 16M mild steel reinforcing bars was demonstrated to be equal to or less than 150 mm when lapped within a field-cast UHPC connection and subjected to flexural tensile loads.
iii. Structural cracks oriented perpendicular to a field-cast UHPC connection tend to follow straight across the connection and do not turn to run along the interface. In the tests simulating transverse connections, the structural loads applied throughout the test program caused flexural tensile cracking perpendicular to the connection along midspan on the tensile face of each of the specimens.
iv. An individual HPC panel crack of a given width will lead into a set of approximately ten cracks in the field-cast UHPC, each of which are on the order of ten times narrower than the adjacent HPC crack.

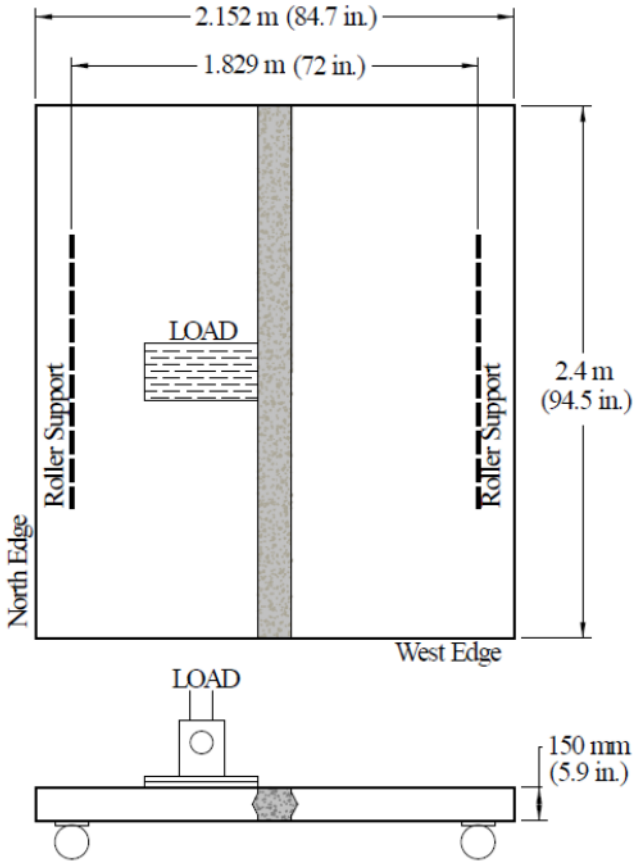

Figure 2.30 - Test setup for longitudinal connection specimens (Graybeal, 2010)

v. In transverse connection, the cracking load of the specimens was demonstrated to be greater than 71 KN and less than 95 KN. Cyclic application of structural loading for at least 2 million cycles to 71 KN did not result in any structural cracking in three of the four specimens, while the fourth specimen developed minor intermittent flexure cracks. The first subsequent loading cycle to 95 KN caused clear, discrete flexural cracking in each of the specimens.

vi. The repeated application of structural loading just above the cracking load does not significantly affect the structural performance of the field-cast UHPC connection. First application of a load peaking at 95 KN generally caused flexural cracking of the transverse connection test specimens. Cracking patterns and crack widths were not observed to be significantly affected by the continued application of cyclic loads through at least 5 million cycles to this load level.

vii. A simple analytical study focused on the behavior of the transverse connection specimens suggested that the testing configuration implemented herein with loads peaking at 71 KN generated elastic stresses which are similar to the stresses that might be observed in a conventional concrete deck spanning 3 m between adjacent girders and loaded to a peak wheel patch load of 125 kN (28 kips).

viii. In the two longitudinal connection specimens tested, interface debonding was observed in one of the specimens, while HPC panel cracking was observed approximately 50 mm away from the connection in the other specimen.

Pirayeh Gar et al. (2014) constructed and evaluated a full-scale bridge deck slab consisting of two full-depth 200 mm thick, 5490 mm long, and 2440 mm wide precast panels reinforced and pre-stressed with AFRP bars, the slab panels were connected by 150 mm wide female-to-female wet transverse joint and supported by three reinforced concrete beams rested on the floor. The reinforcement ratio in the x and y directions were 0.003 and 0.005 respectively. Test setup is shown in Figure 2.31, the specimen was tested in terms of load capacity, deformation, crack pattern, and failure mode. The test results indicated that:

- The average failure load of the interior spans and overhangs were, respectively found 3.9 and 1.4 times the maximum AASHTO LRFD (2010) factored wheel load, 200 KN.
- Flexural cracks were fully transferred from the loaded panel to the adjacent panel with no evidence of local failure at the joint.
- Apart from shear cracks that developed near the panel-to-panel seam, the failure mode of the bridge deck slab was essentially governed by flexure. The crack patterns at the slab interior span and overhang, respectively resembled elliptical and trapezoidal shapes, implying a flexural mechanism.
- When the wheel loads are adjacent to the joint, the performance of ultimate strength is influenced (but not governed) by shear at the panel-to-panels' wet-jointed seam connection.

Figure 2.31 - The test setup (Pirayeh Gar et al. 2014)

- The sequence of cracking and the consequent redistribution of moments results in increased deflections and provides significant deformability. Cracked elastic performance is achieved in a ductile fashion until the two-way failure mechanism is formed. The low elastic modulus of the AFRP bars provides a deformability capability similar to conventional steel reinforced slabs.

Au and Lam (2011) studied the connection details for the cast-in-place closure strips used to link prefabricated bridge elements. The reinforcement considered includes steel looped (U-shaped) bars and straight GFRP bars. Eleven closure strip models were constructed. The models are subjected to cyclic load tests, behavioral tests, and ultimate strength tests, the test setup is shown in Figure 2.32.

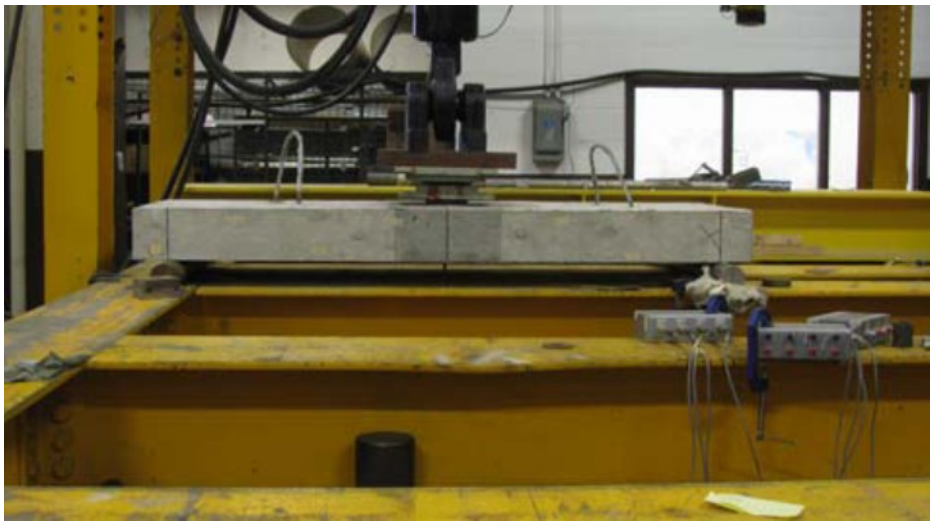

Figure 2. 32 - The test setup (Au and Lam, 2011)

The test specimens were 1800 mm by 600 mm by 150 mm, the closure pour was modelled by a 300 mm width in the middle of the specimen that connected two separately cast slabs representing the prefabricated deck panels, one specimen was built with a narrower closure pour 226 mm for use with an ultra-high-performance concrete. The test parameters were reinforcement configuration, reinforcement type, joint width, and type of loading. Based on the test results, the following conclusions can be drawn:

1) The use of both steel looped bars and GFRP rebars as reinforcing details in closure strip applications is satisfactory and provides an effective continuity of reinforcement in the connection pour.
2) The cyclic load tests did not have a major impact on the integrity of the closure strip connection. Therefore, the long-term live load effects on the closure pours should not be of concern.
3) The main failure mode for the ultimate strength tests of the samples was due to shear and the ultimate failure loads were all higher than that of the control samples. Therefore, all models satisfied the ultimate strength requirement.

4) The use of Ductal (UHPFRC) does not have a major effect on the overall stiffness and the ultimate strength of the closure strip. Its main advantage is it allows a significant reduction in the closure strip width requirement.

Honarvar et al. (2015) investigated the structural performance of full-depth precast Ultra-High-Performance Concrete (UHPC) waffle panels used in bridge replacement project to accelerate the bridge construction and increase bridge deck longevity. A combination of analytical modeling and field live-load testing of static and dynamic truck loads were made. Live load was applied by driving a loaded dump truck across the bridge, as shown in Figure 2.33. The total weight of the truck was 27,306 with a front axle weight of 8,233 kg, and two rear axles weight each of 9,525 kg. For static test, the truck was driven across the bridge at a speed 2.25 m/s. For dynamic test, the truck speed was increased to 13.4 m/s.

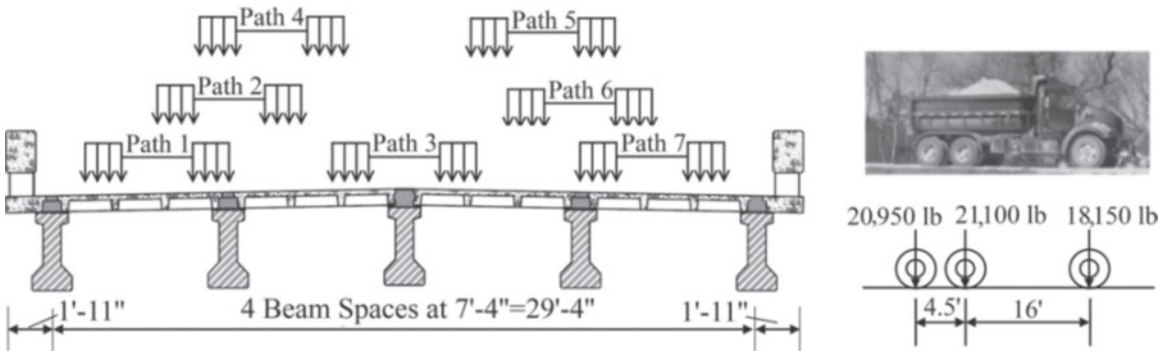

Figure 2.33 - Layout of the bridge loading (Honarvar et al. 2015)

The field test included monitoring of vertical deflections and strains at discrete, critical locations on the bridge deck. Using the FEM, the optimization of the waffle panels was undertaken by varying the number of ribs as well as spacing between ribs to minimize the UHPC volume and associated labor and material costs. The following findings from this study can be drawn:

- Only two strain gauges at the bottom of the deck panels adjacent to the abutment measured strains greater than the expected cracking strain of the UHPC, owing to pre-existing cracks observed prior to testing.

- The maximum live-load moment distribution factor (DF) for the interior girder was computed to be 0.51, this is acceptable compared to the AASHTO recommended value of 0.66. In addition, the maximum dynamic amplification factor (DAF) for the bridge girders was computed to be 1.4, which was close to the AASHTO recommended value of 1.33.
- Numbers of transverse and longitudinal interior ribs per panel were effectively reduced from six to two and four to two, respectively. This design was found to be appropriate, which reduced the UHPC volume by 8.8% compared with the original design.
- Longitudinal interior ribs could be completely removed without affecting the connectivity of the two adjacent panels. All longitudinal interior ribs were removed while retaining only two interior transverse ribs per panel. This alternative was also shown to be effective, which reduced the UHPC volume by 13.4% compared with the original design.

Sayed-Ahmed and Sennah (2015) conducted two precast full-depth deck panel (FDDP) with transverse trapezoidal zigzag-shape joint. Ultra-high performance fibre-reinforced concrete (UHPFRC) and high-modulus glass fibre reinforced polymer (GFRP) bars are utilized in the closure strip between the adjacent precast FDDPs for enhanced strength and durability. Each FDDP had 200-mm thickness, 2500-mm width and 3700-mm length in the direction of traffic and rest over braced twin-steel girder system. As shown in Figure 2.34(a), the transverse closure strip between connected precast FDDPs had a width of 100-mm with zigzag-shape from each side of the joint to increase moment capacity along the interface between the UHPFRC and the precast FDDP along the joint. GFRP bars in the precast FDDPs project into the closure strip with a development length of 175-mm. Two types of fatigue tests were performed using the foot print of the truck wheel loading specified in the Canadian Highway Bridge Design Code (CHBDC), namely: (i) high-cyclic constant amplitude fatigue loading followed by monotonically loading to-collapse; and (ii) low-cyclic accelerated variable amplitude fatigue loading. Figure 2.34(b) shows the test setup.

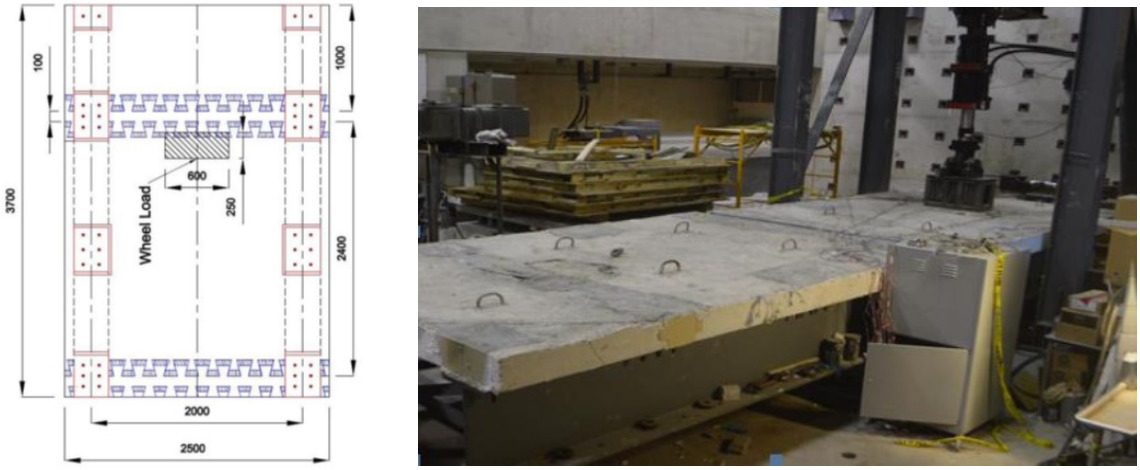

(a) Specimen dimensions (b) The test setup

Figure 2.34 - Specimen dimensions and the test setup (Sayed-Ahmed and Sennah, 2015)

Based on the experimental results, it can be concluded that the developed transverse panel-to-panel connection with projecting straight-ended high-modulus GFRP bars can provide a continuous force transfer in the transverse joints for the FDDPs. Experimental results also indicated that precast FDDP reinforced with high-modulus GFRP ribbed-surface bars showed high fatigue performance and there was no fatigue damage when subjected to 4,000,000 cycles under high-cyclic constant amplitude fatigue (CAF) loading of 122.5 KN specified in CHDBC. The tested precast FDDP under high-cyclic CAF loading sustained a failure load about 4.47 times the CHBDC factored design wheel load of 208.25 KN. While the tested precast FDDP under low-cyclic incremental step variable amplitude fatigue (VAF) loading sustained a failure load about 2.35 times the CHBDC factored design wheel load. The two laterally restrained precast FDDPs failed in punching shear mode. Finally, the first precast FDDP specimen's stiffness degraded by about 21.9% after 4 million cycles of (CAF) loading. On the other hand, the second precast FDDP specimen's stiffness degraded by 71.32% when subjected to low-cyclic (VAF) loading before complete collapse.

Ten specimens of high performance concrete connections between prefabricated concrete elements in bridges has been investigated by Harryson (2003) with the goal to design a

joint that makes the surrounding elements continuous, but still a very small joint that is easy and fast to produce. Laboratory tests as well as finite element (FE) analysis have been conducted. The test specimens were 2000 mm span, 440 mm width, and 260 mm height. The tests included static tests of flexural bending moments and shear forces as well as fatigue tests, Figure 2.35 shows the test setup and joint details. The test variables were joint width, concrete cover, transverse reinforcement, and loading type.

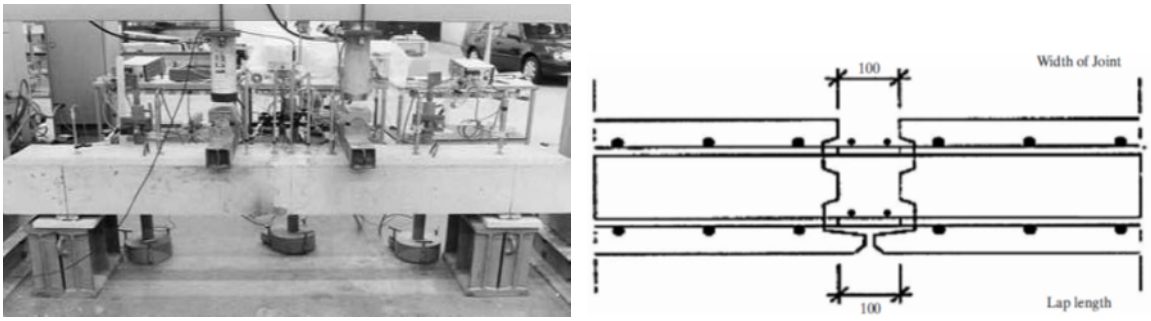

(a) Test setup (b) Joint details

Figure 2.35 - The test setup and joint details (Harryson, 2003)

It was concluded that a lap length of 100 mm was adequate if two transverse reinforcing bars were simply put on top of the spliced bars. So, continuous structural elements treated as a monolithic member in design can be created of precast concrete connected by this joint. Bond capacity of the joint without transverse rebar is about 75% of the capacity with the rebar present in the joint. In the fatigue tests, an anchorage failure in terms of a pullout was observed. Three-dimensional analysis provided additional understanding about the mechanical behavior of the joint, to be used in guidelines for design and construction.

Issa et al. (2007) conducted a full-scale, two-span continuous prototype bridge 25 m long and 5.5 m wide. The bridge was designed, constructed, and tested for service load, overload, and ultimate load to study the structural performance of the prefabricated full-depth precast concrete bridge deck system. The bridge superstructure is composed of 11 post-tensioned precast full-depth concrete panels placed on three steel beams and made fully composite with shear connector pockets and shear studs, see Figure 2.36. Finite element analysis and experimental test results indicated that a full composite action was

maintained between the post-tensioned precast concrete panels and the supporting system; also, no cracks were observed in the transverse joints at the negative moment regions. Based on analytical and experimental results, it was concluded that:

Figure 2.36 - Overall view of full-depth precast, post-tensioned concrete bridge deck system (Issa et al. 2007)

- The precast concrete bridge deck system showed an acceptable structural behavior without any cracking under service loads for both positive and negative bending;

- The effect of longitudinal post-tensioning was noticeable in maintaining the integrity of the bridge deck system under load levels representing approximately eight times the service load;

- The deflection for the maximum positive service load test was lower than the AASHTO (1996) limit for serviceability. In addition, the deflection for the maximum positive overload test was only approximately 73% of the AASHTO limit for serviceability;

- The full depth bridge deck system can be designed using the current AASHTO codes for the design of precast concrete slabs and shear connectors to achieve full composite action; and

- The FEA confirmed that a post-tensioning level of 3.45 MPa at the maximum negative moment region was reasonable to secure tightness of the transverse joints at

live load levels greater than the AASHTO truck service load plus impact even for modest surface preparation of the transverse joint faces.

Haber and Graybeal (2018) investigated the bond behavior between the UHPFRC joint and the precast slabs reinforced with Gr.420 M16 steel straight bars under cyclic loading (Figure 2.37). Five specimens were constructed to be representative of the prefabricated-bridge-deck systems. Each specimen was composed of two individual precast concrete panel elements jointed by UHPFRC joint. The splice length was 140mm ($8.8d_b$). Findings of this study indicated that the ultimate-loading response was consistent and ductile, and the failure was the result of concrete crushing. The embedment length for reinforcing bars M16 and smaller with fy ≤ 516 MPa and minimum clear cover between 25 mm and $3d_b$ should be $l_d = 10d_b$; this suggestion assumes that the compressive strength of the concrete is greater or equal to 97MPa.

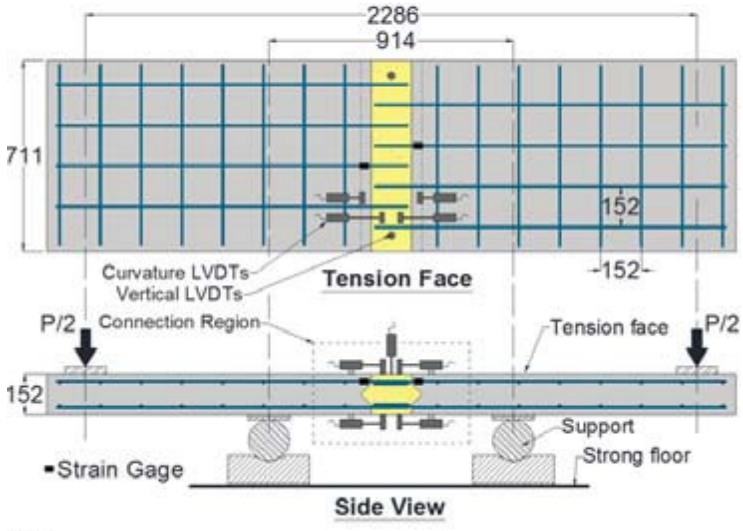

Figure 2.37 – Instrumentation and test setup (Haber and Graybeal, 2018)

2.7. Summary

The use of field-cast UHPFRC closure joints between full-depth reinforced concrete precast bridge-deck panels is a common technique of accelerated bridge construction (ABC). According to the literature review, many studies have focused on the behavior of

joints between prefabricated bridge elements reinforced with steel. Only a limited number of studies have been conducted on UHPFRC joints connecting GFRP reinforced concrete bridge-deck slabs. Moreover, the North American codes, such as the Canadian Highway Bridge Design Code CHBDC (CAN/CSA S6, 2014) and AASHTO LRFD (2009), do not provide guidelines or design recommendations for the UHPFRC joints in precast bridge-deck systems. Thus, there is lack of knowledge of such behavior and more studies are needed to well understand the structural performance of the UHPFRC joints between GFRP-RC precast bridge-deck panels.

This research project aims at investigating the structural behavior of the innovative UHPFRC closure joints between full-depth precast GFRP-RC bridge deck panels. Providing of solid design recommendations for UHPFRC closure joints is the primarily motivation of this study. Furthermore, the findings of this study will contribute to support the North American technical committees engaged in developing standards and design provisions for ABC techniques.

CHAPTER 3 EXPERIMENTAL PROGRAM

3.1. Introduction

Review of the literature has demonstrated the need for further investigations on the structural behavior of the field-cast UHPFRC closure joints between GFRP-RC bridge-deck slabs. This chapter reviews the detailed experimental program including material properties, specimens' details, instrumentation, and test setup.

The research program is conducted to investigate the structural behavior of ultra-high - performance fiber-reinforced concrete (UHPFRC) closure joints between normal strength concrete (NSC) precast bridge-deck slabs reinforced with GFRP bars. This common technique of accelerated bridge construction (ABC), however, requires narrow joints to minimize the onsite construction time. The closure joints are cast using UHPFRC infilling to achieve very high bond strength with the GFRP bars, which enables transferring the forces between the precast slabs through a short splice length.

3.2. Experimental Research Program

3.2.1. General

The experimental program focuses on the UHPFRC closure joints' structural behavior under different loading cases. A total of fourteen (14) full-scale slab specimens are included in the experimental program. Each specimen consists of two precast normal strength concrete slabs connected by UHPFRC closure joint. The details of test specimens, material properties, test matrix, fabrication, instrumentation, and test setup are discussed in this chapter.

3.2.2. Material Properties

High-modulus glass fiber-reinforced polymer (HM-GFRP) bars were used as longitudinal and transverse reinforcement for the test specimens. Two types of concrete were used: normal strength concrete (NSC) was used for precast slabs and ultra-high fiber-reinforced concrete (UHPFRC) was used for the closure joints. The characteristics of these materials are presented herein in the following sections.

3.2.2.1. **GFRP Reinforcement**

The HM GFRP bars used in this study were manufactured and developed by Pultrall Inc. (Thetford Mines, Quebec, Canada). The bars however, have a sand-coated surface to enhance bond and force transfer between bars and the surrounding concrete, Figure 3.1 shows the GFRP bars. No. 15 (15.9 mm) and No. 20 (19.1 mm) GFRP bars. The GFRP bars were manufactured by pultrusion process in a vinylester resin with E-glass fiber contents of 82.2% (Pultral 2016). The bars were classified as Grade III (modulus of elasticity 60 GPa) according to CAN/CSA S807 (2010). The guaranteed tensile strength (f_{fu}), ultimate strain (ε_{fu}), modulus of elasticity (E_f) of the GFRP bars were determined according to ASTM D7205 (ASTM, 2011). Table 3.1 provides the mechanical tensile properties of the GFRP reinforcing bars.

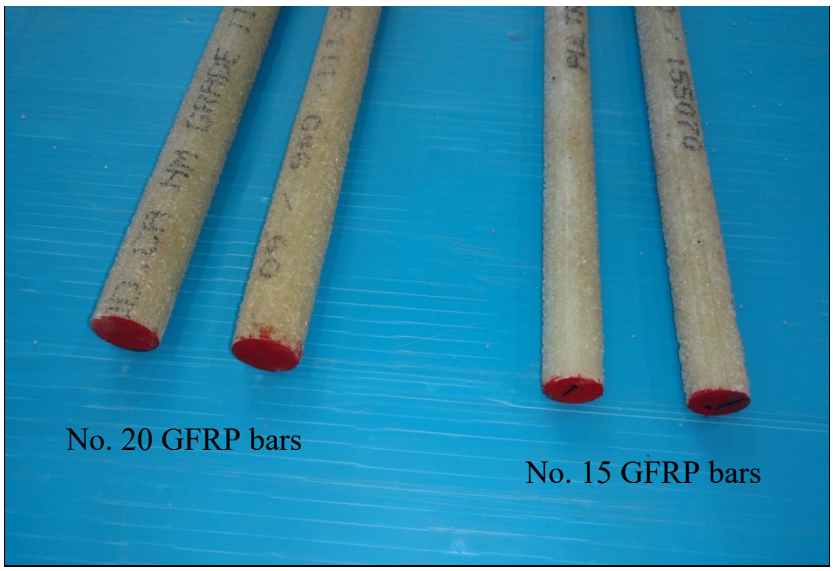

Figure 3.1 - GFRP bars

Table 3.1 - Mechanical properties of GFRP bars

Bar Size	Nominal bar Diameter d_b (mm)	Nominal Sectional Area A_f (mm^2)	Nominal tensile modulus E_f (GPa)	Guaranteed tensile strength f_{fu} (MPa)	Ultimate tensile strain ε_{fu} (%)	Surface configuration
No.15	15.90	199	64.2±0.6	1185	1.85	Sand Coated
No.20	19.10	284	64.5 ± 0.7	1105	1.72	Sand Coated

3.2.2.2. **Concrete**

Two types of concrete were used; ready-mixed normal-weight normal-strength concrete (NSC) and ultra-high-performance fiber-reinforced concrete (UHPFRC). The NSC was used for casting the reference specimens and the precast slabs of jointed specimens. The UHPFRC was used for casting the closure joints. The NSC had a 28-day target compressive strength of 40 MPa. The mix proportion for a cubic meter of concrete was 350 kg of cement, 813 kg of sand, 1032 kg of aggregate (maximum nominal size 20 mm), 155 liter water (water/cement ratio of 44%), and air content of 5-8%. The designed slump of the concrete was 90±30 mm. Nine concrete cylinders 100×200 mm were cast from each concrete batch and cured for 7 days under the same conditions as the test specimens. The actual compressive strength of NSC was determined as the average compressive strength of the concrete cylinders tested at the date of specimen testing according to ASTM C39 (ASTM, 2018).

The UHPFRC, known as Ductal® (JS1000) and developed by Lafarge-Holcim (Lafarge, 2009), was used for casting the closure joints to connect the precast slabs. The UHPFRC had a target 28-day compressive strength of 170 MPa and an average modulus of elasticity of 50 GPa. The mix proportion for a cubic meter of UHPFRC concrete (JS1000) was 2195 kg of Premix, 120 kg of water, 30 kg of Premia 150, and 156 kg of steel fiber. To

determine the actual concrete compressive strength of the UHPFRC, three 100 × 200 mm cylinders were cast and cured under the same conditions as the closure joints. The compressive strength of UHPFRC was determined by testing the UHPFRC cylinders on the day of specimen testing according to ASTM C1856 (ASTM, 2017).

3.2.3. Design, Parameters, and Specimens' Details

3.2.3.1. **Specimen Design**

The experimental program consisted of 14 full-scale slab specimens, including 2 reference specimens without closure joint and 12 jointed specimens simulating full-depth UHPFRC closure joints between GFRP-RC precast deck slabs. All the test specimens were designed according to the requirements of the Canadian Highway Bridge Design Code CHBDC (CAN/CSA S6, 2014). The test specimens were fabricated and tested under quasi-static line loading up to failure. The experimental program was divided into two main phases; Phase I included 7 specimens to simulate the closure joints at the zone of negative moment and subjected to combined flexural and shear stresses, while Phase II included 7 specimens to simulate the closure joints at constant positive moment zone and subjected to pure flexural stresses. The identification system of the test specimens is presented in Figure 3.2. The specimens were named according to reinforcement type, splice length, reinforcement diameter, and case of loading.

The effect of three main test parameters on the structural behavior of the UHPFRC closure joints was considered in this experimental program. Theses parameters are:

- The splice length, three splice lengths were considered (100, 150, and 200 mm), with a corresponding joint width of 120, 170, and 220 mm, respectively.
- GFRP longitudinal reinforcement ratio, two reinforcement ratios were tested (0.79 %, and 1.14 %), considering two diameters (No.15 and No. 20 GFRP bars) with the same spacing.

- Loading case, two test setups were conducted to test the two types of closure joints (closure joints subjected to pure flexural stresses and closure joints subjected to combined shear and flexural stresses).

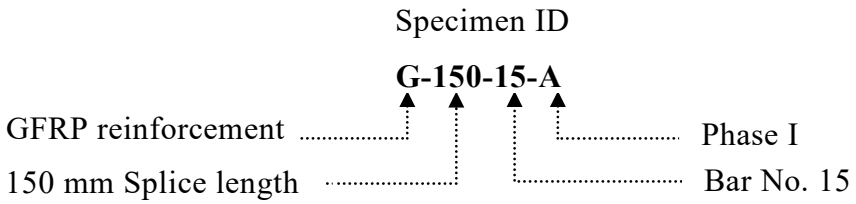

Figure 3.2 - Identification of test specimens

3.2.3.2. **Details of Test Specimens**

A total of 14 one-way slab specimens included in this experimental program measured 3000 mm length, 1000 mm width, and 225 mm depth. The test matrix consisted of two specimens were cast monolithically without a joint to serve as reference specimens and twelve jointed specimens. Each jointed specimen comprised of two precast GFRP-RC slabs, with GFRP splices projected from one side, and connected by UHPFRC closure joint. All specimens were reinforced with two mats of identical orthogonal reinforcing bars with top and bottom concrete covers of 40 mm, and the same reinforcement spacing in the longitudinal and transverse direction of 145 and 200 mm respectively. Table 3.2 shows the test matrix including the details of all specimens. The specimens were divided into two main phases as follows:

i) Phase I

This group included 7 full-scale one-way slab specimens which were fabricated and tested under quasi-static loading up to failure (six jointed specimens and a reference specimen). The reference specimen without closure joint (G-R-15-A) was reinforced with No. 15 GFRP bars in both longitudinal and transverse directions (top and bottom). Three of the jointed specimens (G-100-15-A, G-150-15-A, and G-200-15-A) were reinforce with No.15 GFRP bars in the longitudinal direction, with a splice length of 100, 150, and 200 mm, respectively, and a joint width of 120, 170, and 220 mm, respectively. The other three

jointed specimens (G-100-20-A, G-150-20-A, and G-200-20-A) were reinforced with No.20 GFRP bars, with 100, 150, and 200 mm splice length, respectively, and UHPFRC closure joints of 120, 170, and 220 mm in width, respectively. No. 15 GFRP bars were used as transverse reinforcement for all the jointed specimens. The closure joint was located over the support in the zone of maximum negative moment to investigate the joint behavior under combined flexural and shear stresses. Details of all test specimens included in Phase I are presented in Figure 3.3 through Figure 3.6.

ii) Phase II

Seven test specimens were included in this group (a reference specimen and six jointed specimens). The reference specimen (G-R-15-B) was reinforced with No.15 GFRP bars in both longitudinal and transverse directions (top and bottom). Each of jointed specimens consisted of a pair of identical NSC precast slabs connected by cast-in-place UHPFRC closure joint at the middle of each specimen. The three specimens (G-100-15-B, G150-15-B, and G-200-15-B) were reinforced with No.15 GFRP bars in longitudinal and transverse directions, top and bottom mats. The other three specimens (G-100-20-B, G-150-20-B, and G-200-20-B) were reinforced with No.20 GFRP bars as top and bottom main reinforcement, while No. 15 GFRP bars were used as a transverse reinforcement. In the jointed specimens, the longitudinal top and bottom reinforcing bars projected at one end forming three splice lengths namely, 100, 150, and 200 mm, and extended into the closure joints of width 120, 170, and 220 mm, respectively. Figure 3.7 through Figure 3.10 show the geometry and reinforcement details of Phase II test specimens.

Table 3.2 – Test matrix and specimens details

Phase	Specimen ID	f_c' (MPa)		Precast segments length(mm)	Splice length (mm)	Join width (mm)	GFRP longitudinal reinforcement
		NSC	UHPFRC				
I	G-R-15-A	40	170	N/A	N/A	N/A	NO.15
	G-100-15-A			940/1940	100	120	NO.15
	G-150-15-A			915/1915	150	170	NO.15
	G-200-15-A			890/1890	200	220	NO.15
	G-100-20-A			940/1940	100	120	NO.20
	G-150-20-A			915/1915	150	170	NO.20
	G-200-20-A			890/1890	200	220	NO.20
II	G-R-15-B	40	170	N/A	N/A	N/A	NO.15
	G-100-15-B			1440	100	120	NO.15
	G-150-15-B			1415	150	170	NO.15
	G-200-15-B			1390	200	220	NO.15
	G-100-20-B			1440	100	120	NO.20
	G-150-20-B			1415	150	170	NO.20
	G-200-20-B			1390	200	220	NO.20

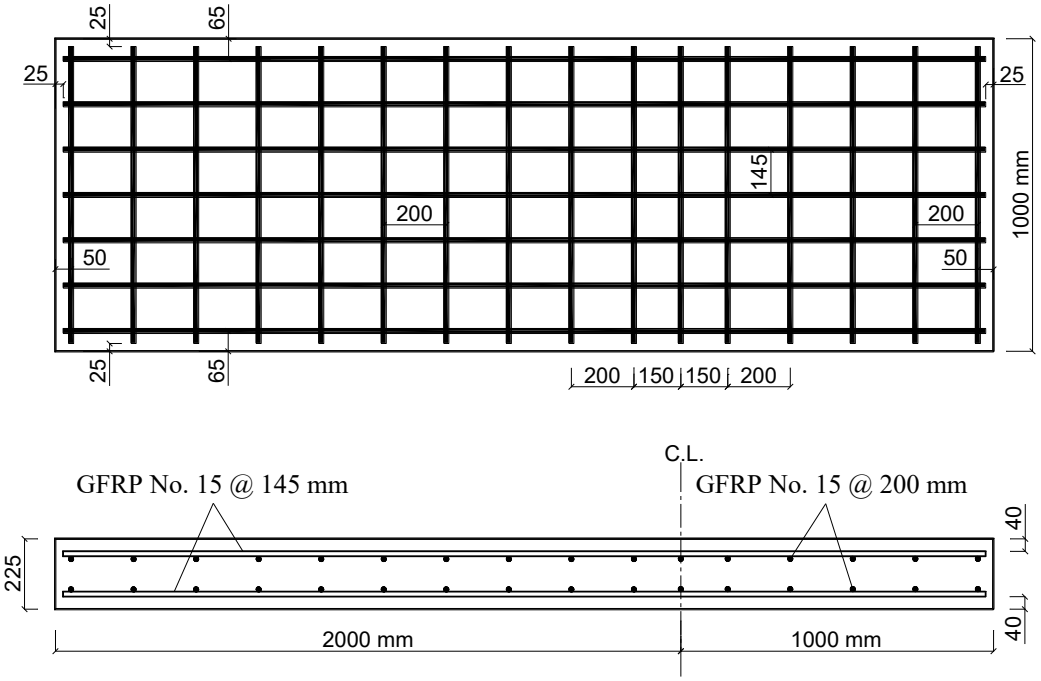

Figure 3.3 – Concrete dimensions and reinforcement details of reference specimen (G-R-15-A)

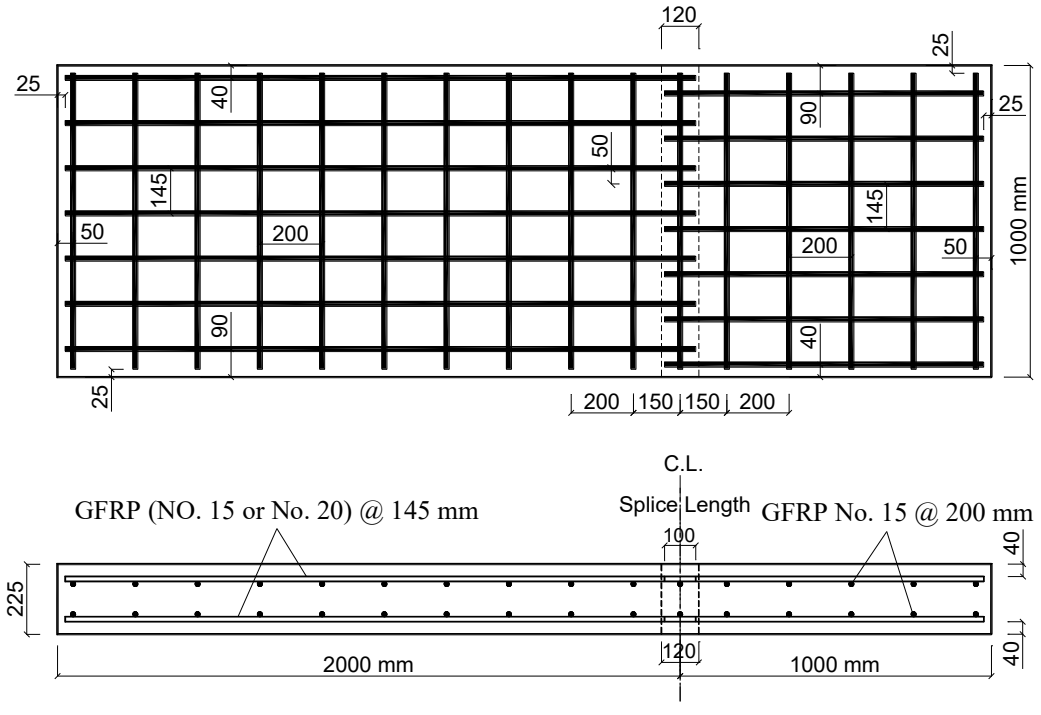

Figure 3.4 – Concrete dimensions and reinforcement details of specimens G-100-15-A and G-100-20-A

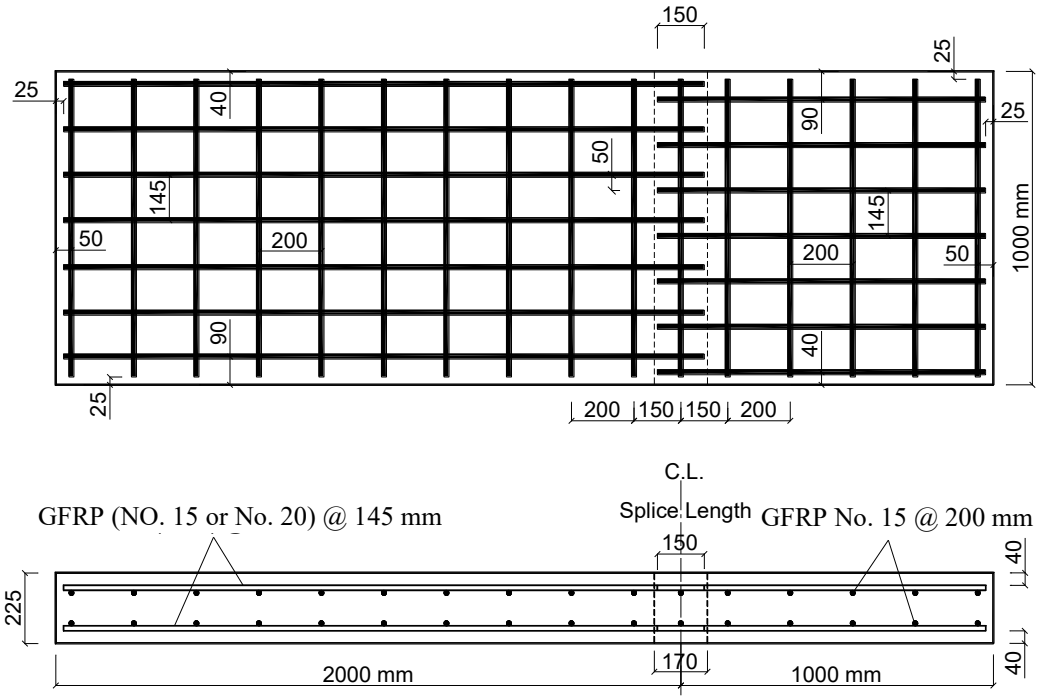

Figure 3.5 – Concrete dimensions and reinforcement details of specimens G-150-15-A and G-150-20-A

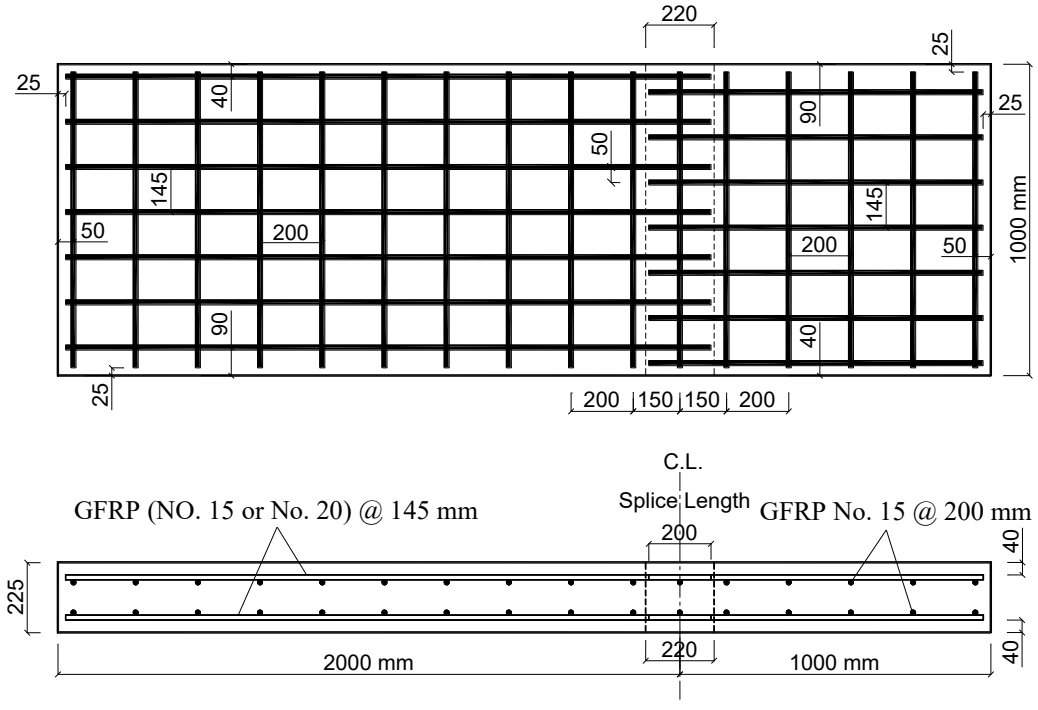

Figure 3.6 – Concrete dimensions and reinforcement details of specimens G-200-15-A and G-200-20-A

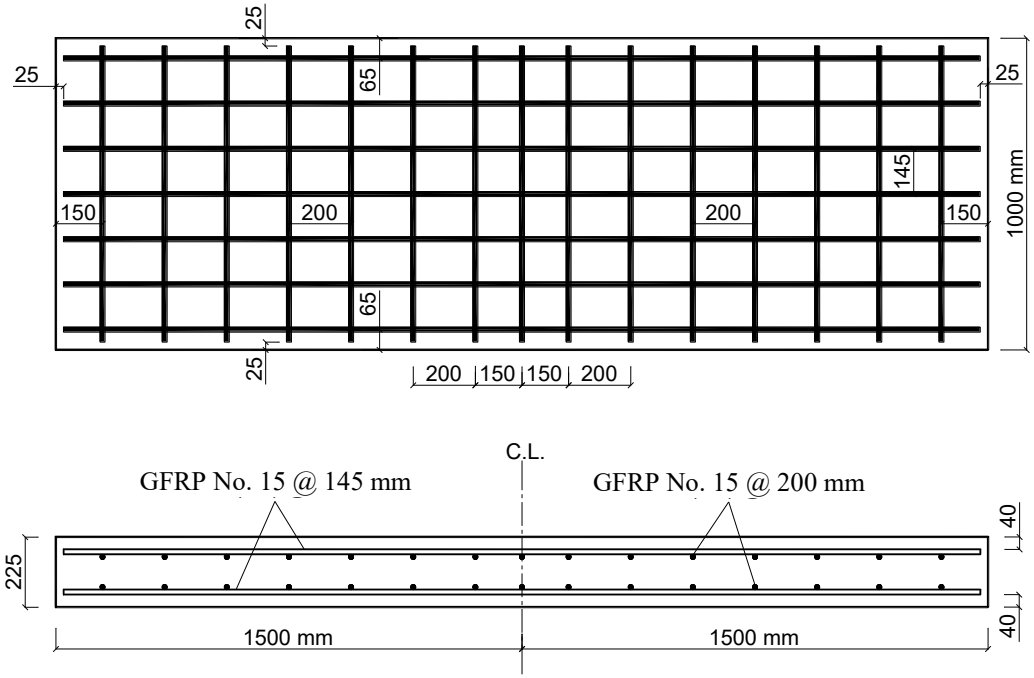

Figure 3. 7 – Concrete dimensions and reinforcement details of reference specimen (G-R-15-B)

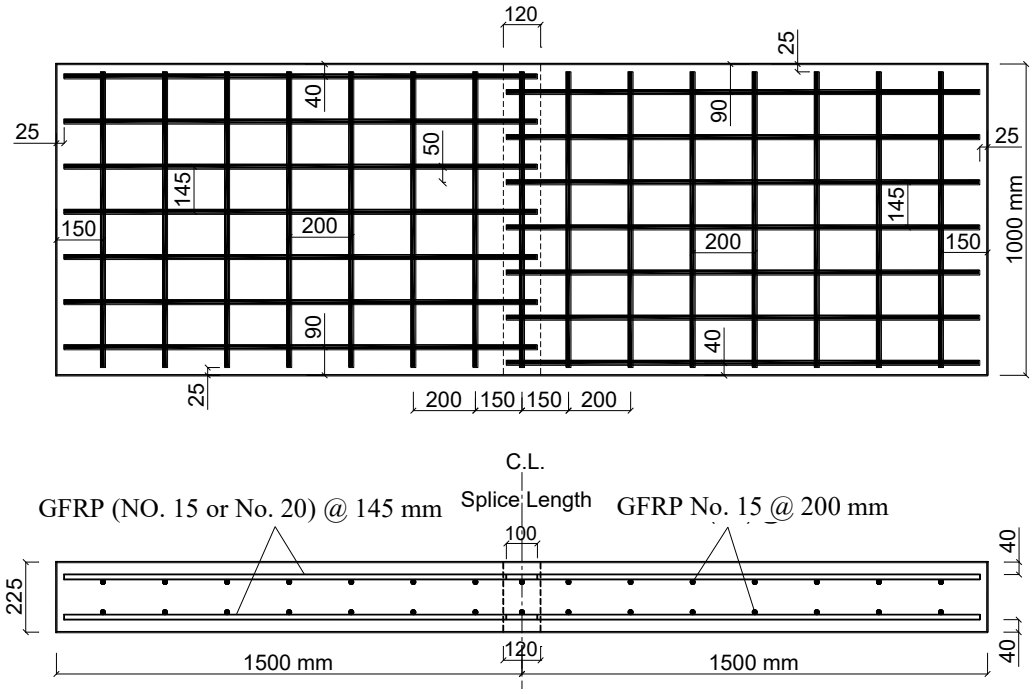

Figure 3.8 – Concrete dimensions and reinforcement details of specimens G-100-15-B and G-100-20-B

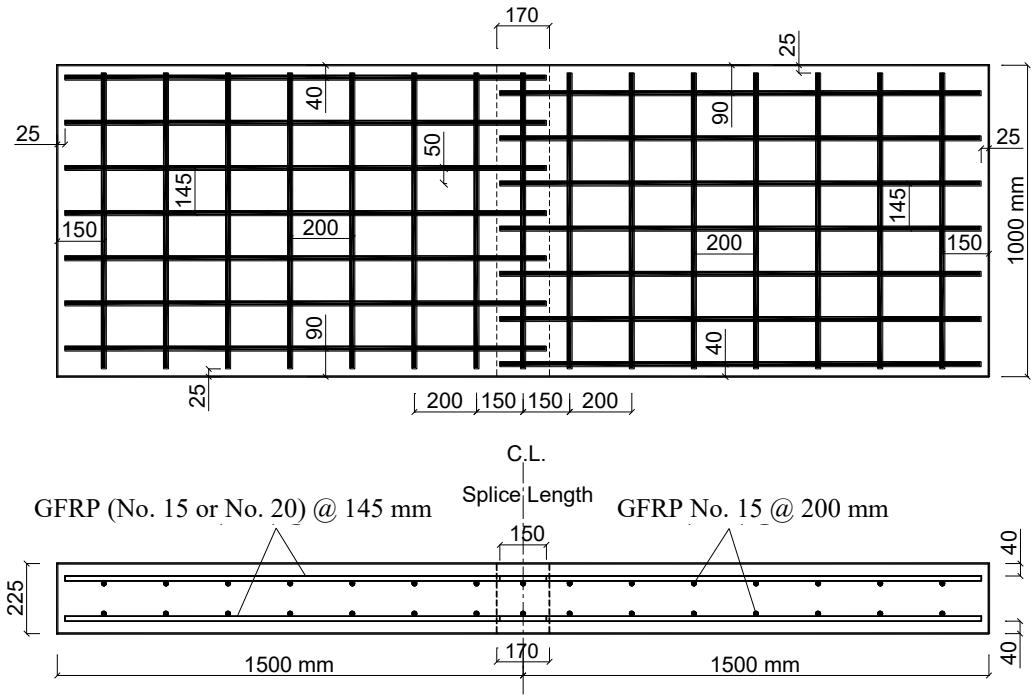

Figure 3.9 – Concrete dimensions and reinforcement details of specimens G-150-15-B and G-150-20-B

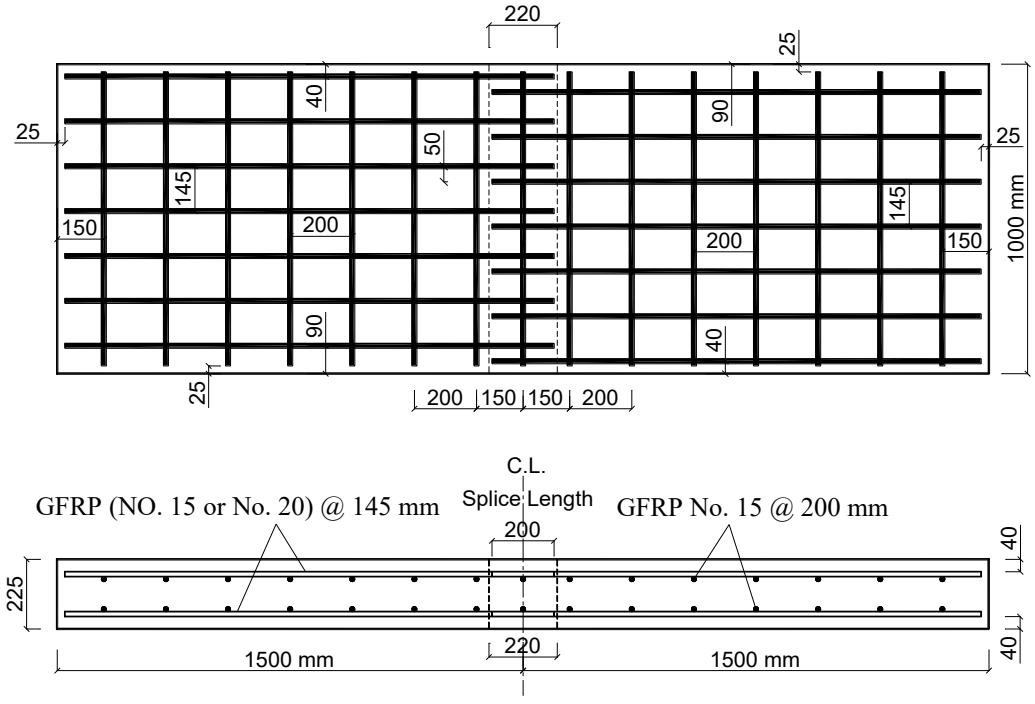

Figure 3.10 – Concrete dimensions and reinforcement details of specimens G-200-15-B and G-200-20-B

3.2.4. Fabrication of Test Specimens

3.2.4.1. **Formwork**

Two wooden large formworks were designed and fabricated, measuring 9750 mm clear length, 1000 mm clear width, and 225 mm clear height. Each formwork was individually levelled to ensure horizontality of the test specimens. For each of jointed specimens, two perforated wooden sheets, holed with the same diameter and spacing as the longitudinal reinforcement, were used to maintain the design spacing between the protruded splices. Sides of the formwork were supported by 50×50 mm steel angles at the top and bottom to avoid distortion in the slab width resulting during casting. Before placing the cages, the formwork was painted with oil to protect the formwork and to facilitate the de-molding of specimens from the formwork after concrete hardening. Overview of the formworks is shown in Figure 3.11.

3.2.4.2. **Reinforcing Cages**

The GFRP reinforcing bars were cut to the required lengths and assembled together according to design spacing and orientation of the bars. The GFRP longitudinal and transverse bars were connected using Plastic tie-wraps to form the top and bottom reinforcing meshes. After installation of the strain gauges on the top surface of the tension reinforcement, as shown in Figure 3.12, the reinforcing bars were placed inside the formwork. To ensure the required top and bottom concrete covers, big and small Plastic chairs were used, respectively. Figure 3.13 shows GFRP assembled cages, while Figure 3.14 shows the cages inside the formwork before concrete casting.

Figure 3.11 - Overview of the formworks

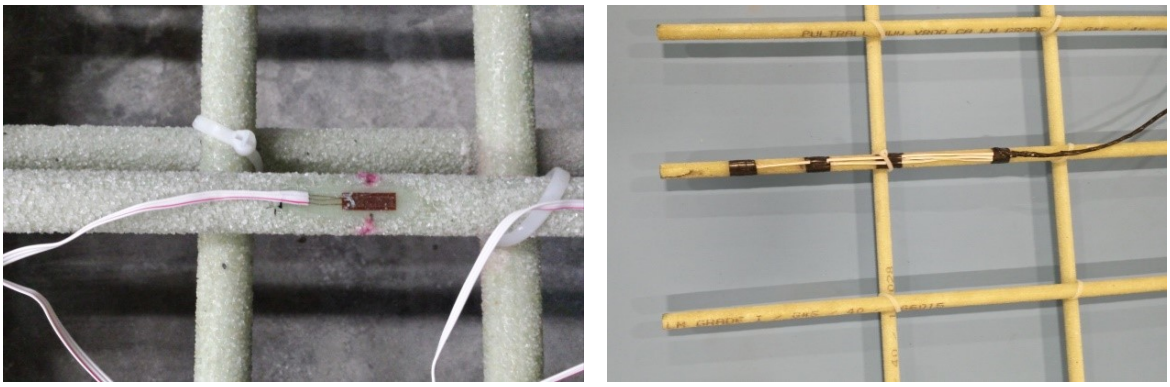

Figure 3.12 – Istallation of strain gauges

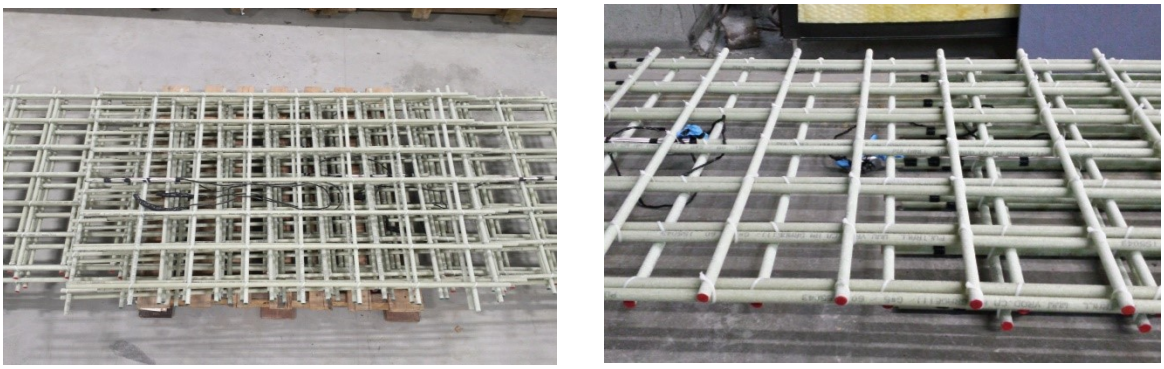

Figure 3.13 – Assembled GFRP cages

Figure 3. 14 - Typical views of GFRP cages inside the formwork before concrete casting

3.2.4.3. **Casting of NSC**

A normal-weight ready-mixed normal strength concrete (NSC) described earlier, with 28-days target compressive strength of 40 MPa, was used in casting the reference specimens and the precast segments of jointed specimens. Once poured, the NSC was compacted with an electrical vibrator and the surface was finished manually. Curing process started by covering the concrete surface with wet burlap and polythene sheet for 7 days. During casting and curing processes, the GFRP splices were tightly covered with polythene sheet to protect the bar surface. After curing, the precast slabs were removed from the formwork and stored until the date of casting the UHPFRC closure joints. Figure 3.15 to Figure 3.19 show fabrication of the precast slabs.

3.2.4.4. **Casting of UHPFRC Closure Joints**

The UHPFRC (Ductal® JS1000) was prepared using two portable mixers as shown in Figure 3.20, each of capacity 0.145 m^3. Each pair of the precast slabs was joined using a special formwork for casting the UHPFRC closure joints. The UHPFRC was poured directly into the joints and the testing cylinders (3 cylinders 100 × 200 mm from each batch) without vibration. To control the performance of the UHPFRC, a flow-table test was conducted right after mixing according to ASTM C230 (ASTM, 2014); the average flow diameter was 220 mm (Figure 3.21). Curing was carried out by covering the surface with polythene sheets to limit water evaporation. Figure 3.22 to Figure 3.25 show the fabrication of the UHPFRC closure joints. After curing, the full specimens were stored until the date of testing. The standard concrete cylinders of NSC and UHPFRC were subjected to the same environmental conditions as their correspondent slabs. The concrete compressive strengths of both NSC and UHPFRC for each batch were determined by testing three standard cylinders at the date of testing (ASTM C39, 2018 and ASTM C1856, 2017, respectively).

Figure 3.15 - Casting of NSC slabs

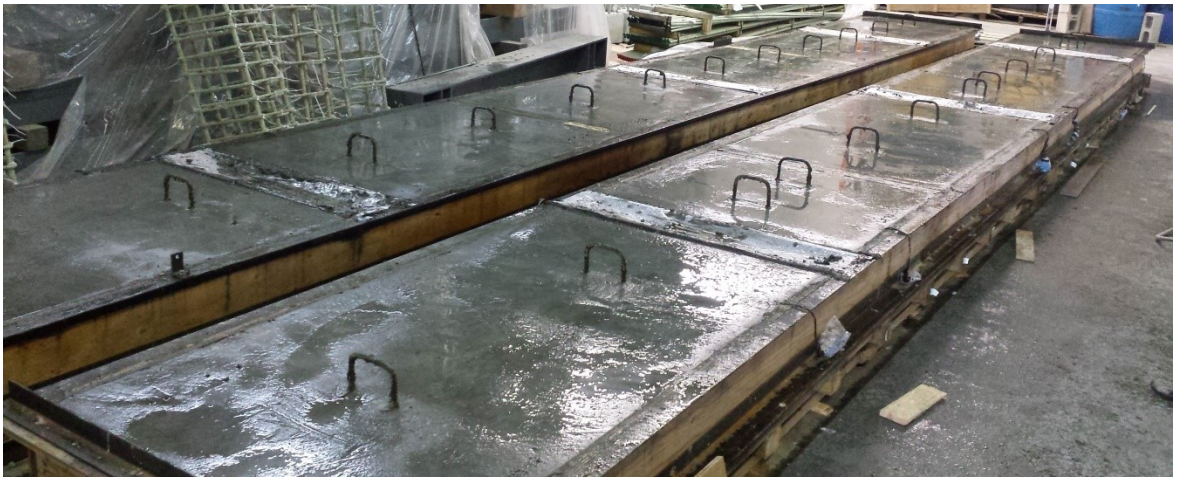

Figure 3.16 - Typical view of slabs after casting and surfacing

Figure 3.17 - Curing of NSC slabs

Figure 3.18 – De-molding of NSC slabs

Figure 3.19 - Storing of NSC precast slabs

Figure 3.20 – UHPFRC Portable mixers

Figure 3.21 – Flow-table test

Figure 3.22 – Formwork for casting the closure joints

Figure 3.23 – Filling the joints with UHPFRC

Figure 3.24 – Curing of UHPFRC closure joints

Figure 3.25 – Full specimens ready for testing

3.2.5. Instrumentation

To record the behavior of the tested specimens, different instruments were used to monitor deflection at critical locations, tensile strains in the longitudinal reinforcement, compressive strains in concrete, and the crack widths. Two potentiometers were used to record the deflection with a precision of 0.01 mm. Four Linear Variable Displacement Transducers (LVDTs), with a precision of 0.01 mm, were used to measure and record the crack widths. The tensile strain in GFRP reinforcement was measured by electrical resistance strain gauges produced by KYOWA Electronics Instruments CO., LTD, Tokyo, Japan with 120 ± 1 Ω resistance and 10 mm length. The concrete compressive strain was measured using strain gauges of 60 mm length installed on the compression side of concrete surface. Details of the instrumentation are shown in Figure 3.26 through Figure 3.33.

3.2.5.1. **Phase I Specimens**

To measure the tensile reinforcement strains, two strain gauges were installed on the GFRP bars at the maximum negative moment for the reference specimen G-R-15-A (Figure 3.26). For the jointed specimens, six strain gauges were attached to the tension GFRP splices (top splices) at the critical positions, as shown in Figure 3.27, to investigate the strain along the splice length. The concrete strains were measured with two strain gauges installed on the compression side of the slab 150 mm from the joint centerline and 200 mm

apart. Cantilever deflection was monitored with two potentiometers located under the load 900 mm from the joint centerline and 750 mm apart, as illustrated in Figure 3.28. Two LVDTs were installed on the closure joint sides to measure the interfacial-crack (joint opening) width at the closure joint–precast slab interfaces (J1 and J2). Two other LVDTs were used to record the crack width of the first two flexural cracks (Fig 3.29). A 50X handheld microscope was used to measure the initial crack widths. An automatic data-acquisition system connected to a computer was used to monitor load, deflections, crack widths, and strains in the concrete and reinforcing bars.

3.2.5.2. **Phase II Specimens**

Two strain gauges were installed on the middle of the GFRP longitudinal tension bars for the reference specimen (Figure 3.30). For the jointed specimens, six strain gauges were located at the critical positions of the longitudinal tension reinforcing bars as shown in Figure 3.31 to capture the strain along the splice length. Three strain gauges were affixed to the compression side of each specimen, at the mid-span and at 160 mm away from the center line to measure the concrete compressive strains. Deflection was monitored at the mid-span of the specimens using two potentiometers as illustrated in Figure 3.32. The cracks on the bottom surface of the test specimens were investigated using four LVDTs. Two LVDTs were used to monitor the two interfacial-crack widths at the closure joint-precast slab interfaces (J1 and J2), as depicted in Figure 3.33. The first two flexural cracks were recorded using two LVDTs. The initial crack widths were measured by a 50X hand-held microscope. An automatic data-acquisition system attached to a computer was used to record load, deflections, crack widths, and strains in concrete and reinforcement.

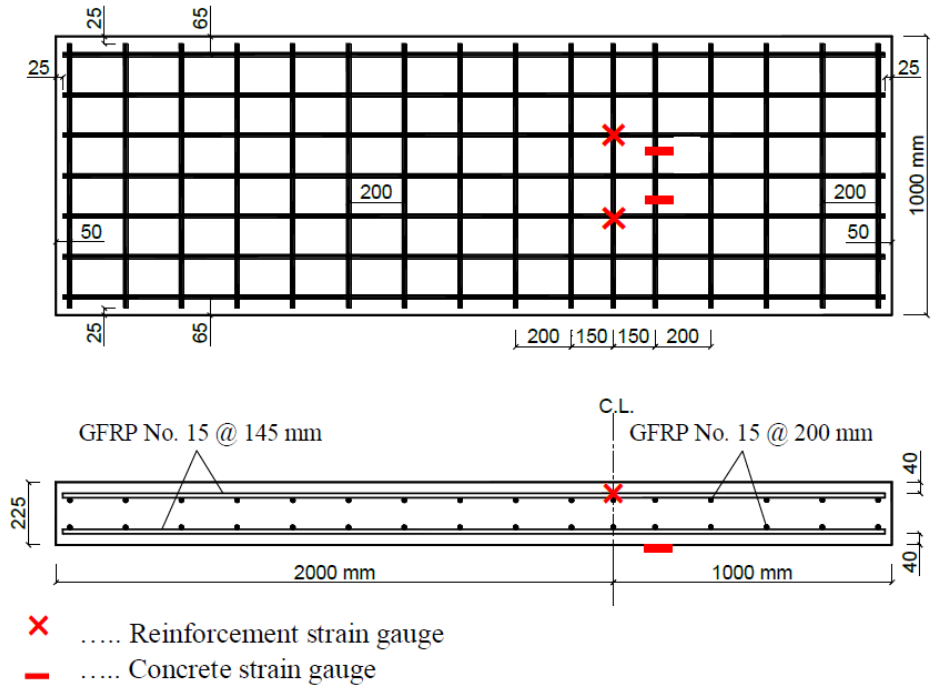

Figure 3.26 - Locations of reinforcement and concrete strain gauges for reference specimen G-R-15-A

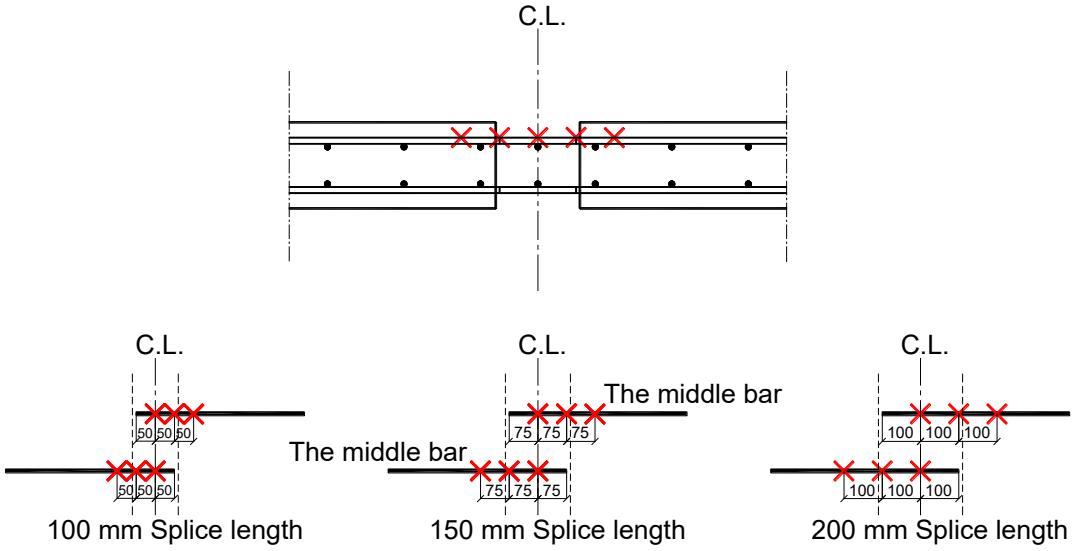

Figure 3.27 - Locations of reinforcement strain gauges for Phase I specimens

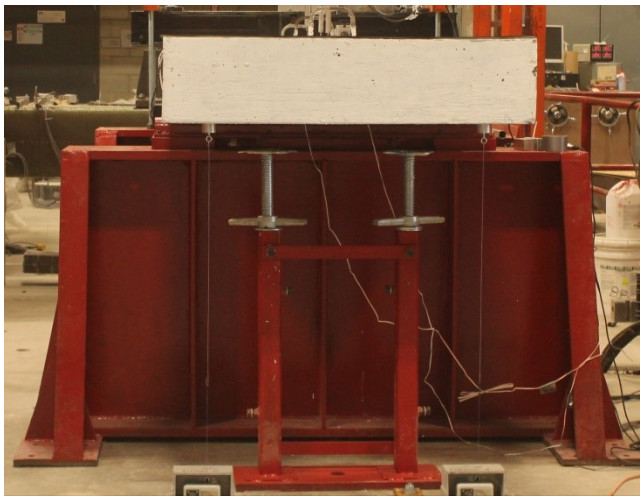

Figure 3.28 - Deflection measurements

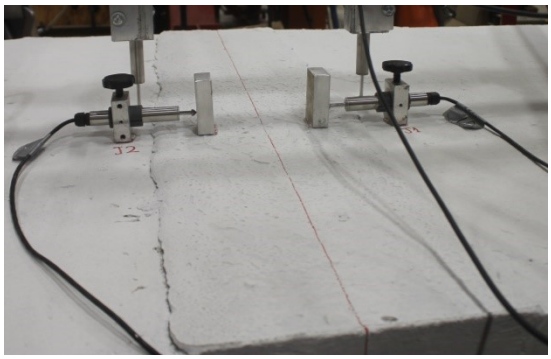

LVDTs for interfacial-cracks

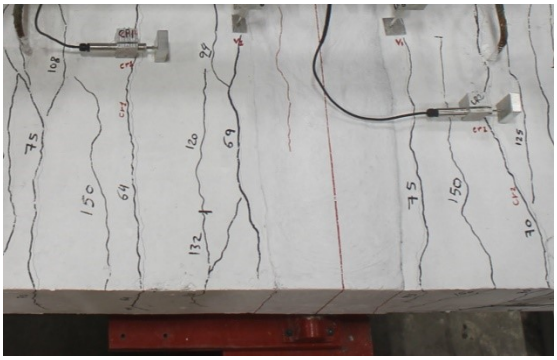

LVDTs for flexural-cracks

Figure 3.29 – LVDTs to record the crack widths

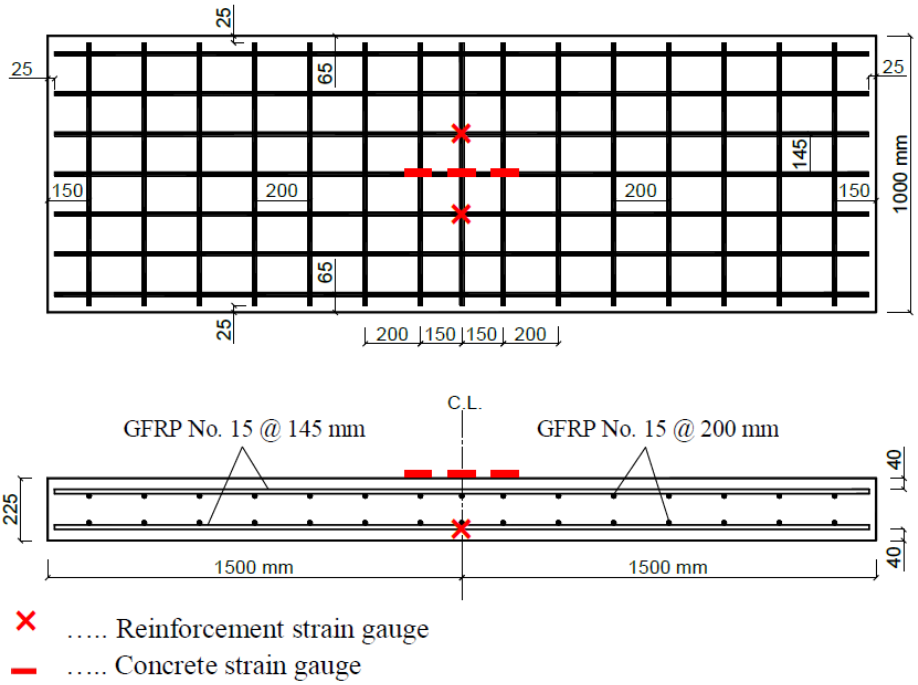

Figure 3.30 - Locations of reinforcement and concrete strain gauges for reference specimen G-R-15-B

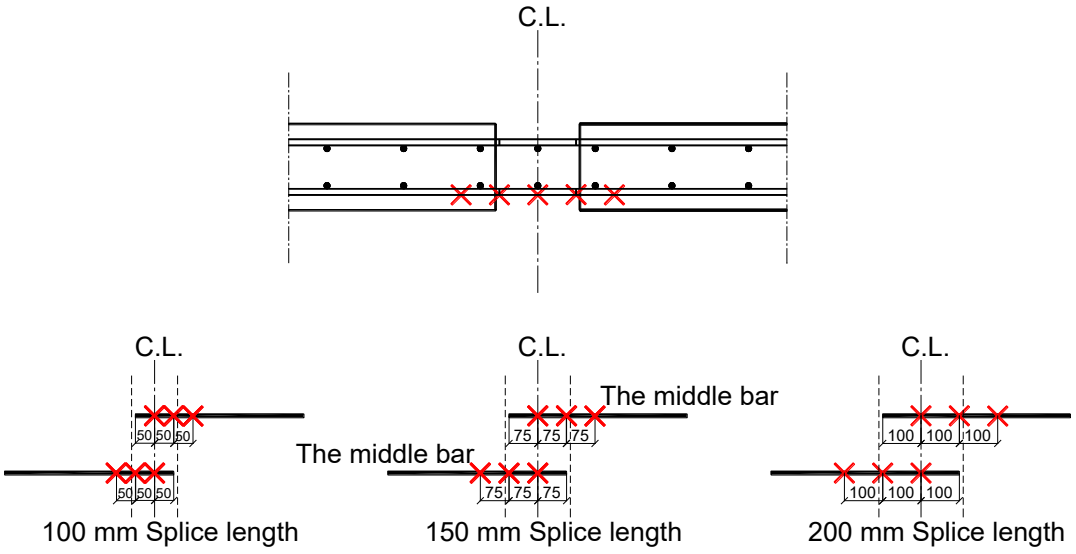

Figure 3.31 - Locations of reinforcement strain gauges for Phase II jointed specimens

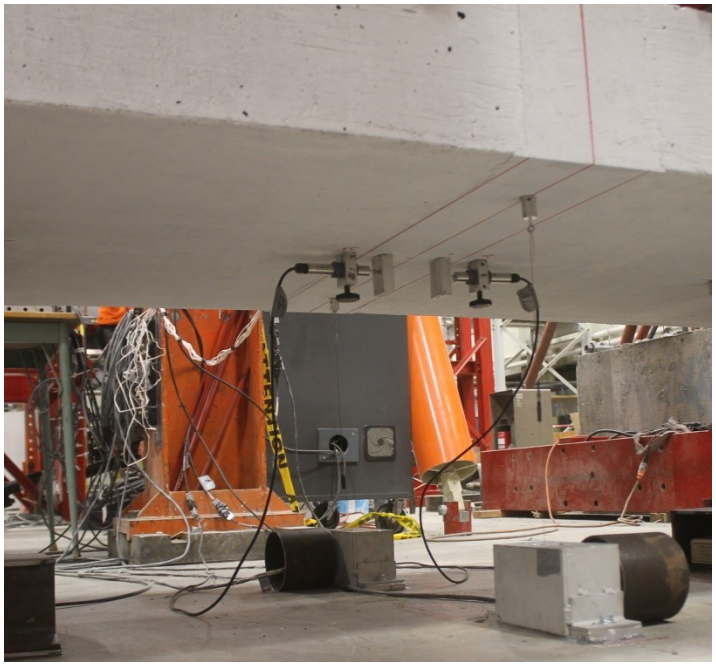

Figure 3.32 - Potentiometer for the deflection at mid-span

LVDTs for interfacial-cracks

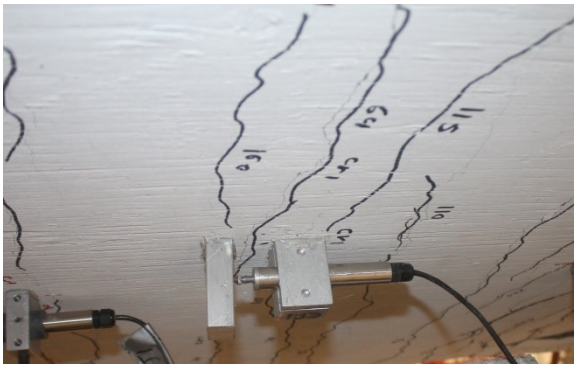

LVDTs for flexural-cracks

Figure 3.33 - LVDTs for crack-width measurements

3.2.6. The Test Setup and Procedure

The tests were performed at the Canadian Foundation for Innovation (CFI) structural laboratory at the University of Sherbrooke. The concrete cylinders were tested under compression to collapse at the same day as the test specimens. All tested specimens were loaded up to failure under stroke-control at a rate of 1.2 mm/min using 1000 kN hydraulic actuator and the test was completed when the specimen collapsed. The test setup was built considering the loading cases described earlier for each phase.

3.2.6.1. **Phase I Test Setup**

The specimens were tested as simply supported slabs with a clear span of 1750 mm and a 1000 mm of overhanging cantilever. Figure 3.34 and Figure 3.35 show overview and schematic details of the test setup, respectively. A hinged support located at one end of the specimen was designed to resist the upward reaction, while a roller support was located under the centerline of the UHPFRC closure joint at the zone of maximum negative moment (Figure 3.36). The hydraulic actuator load was applied as line load on the overhanging cantilever through a horizontal steel beam up to failure. The actuator was connected directly to the steel beam, applying the load to the tested specimens. In preparation of the test, two LVDTs were installed on the joint edges to monitor the joint opening (interfacial crack width) during testing. In addition, once the first two flexural cracks appeared, the load was paused and LVDTs were installed on the marked crack after measuring the initial crack widths with the handheld microscope. Thereafter, the subsequent cracks were marked and the loading continued until failure. Neoprene pads of 10 mm thickness were placed between the loading steel beam and concrete surface, and between the specimen bottom surface and the supports to ensure full contact and evenly distribute load.

3.2.6.2. **Phase II Test Setup**

All specimens were simply supported with a 2600 mm clear span, and tested in four-point bending scheme, as shown in Figure 3.37. A hinge support was located at one end of the specimen, while a roller support was located at the other end. The closure joint was positioned at the mid-span in a constant moment zone of 500 mm length. The specimens were loaded with two equal line loads spaced at 500 mm about the centerline. The load was transferred from the actuator to a steel spreader beam, then transferred equally to the tested slab through two horizontal steel beams. The LVDTs (J1 and J2) were installed at the joint-precast slab interfaces to measure the joint opening during the test, however, at the first two cracks appearance, the load was paused and LVDTs were installed on the marked cracks. Subsequent cracks were marked and the loading continued until failure. To ensure full contact and load uniform distribution, neoprene pads of 10 mm thickness were placed between the concrete surface and the supports, as well as between the steel beams and the concrete surface. Figure 3.38 shows schematic view of the test setup.

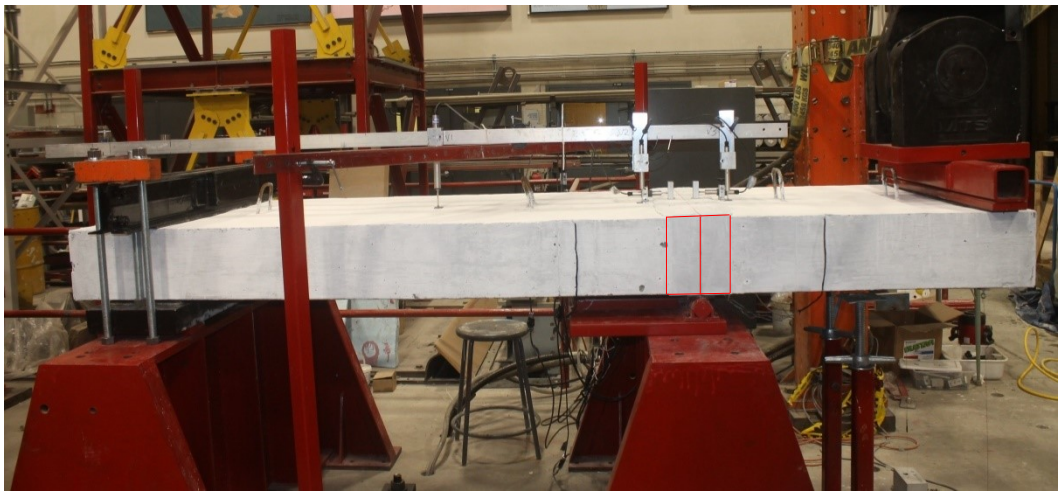

Figure 3.34 – Overview of the test setup for Phase I specimens

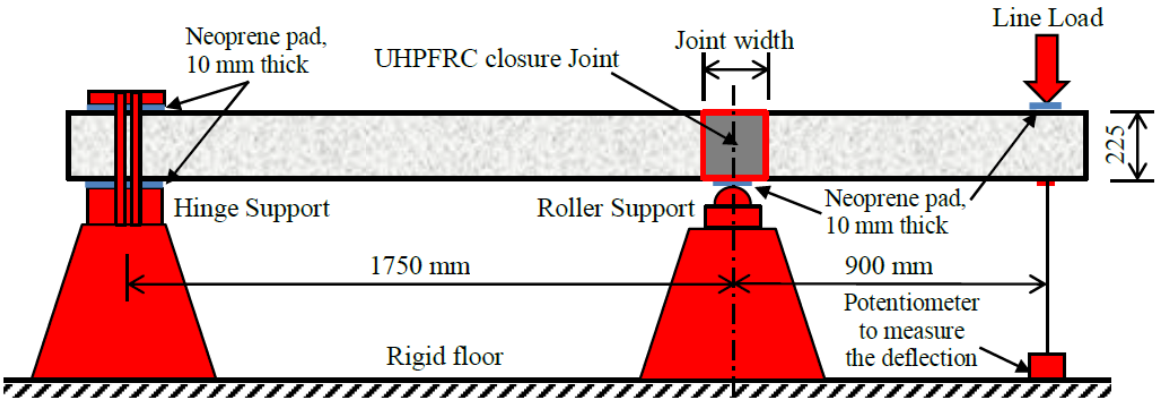

Figure 3.35 – Schematic view of the test setup for Phase I specimens

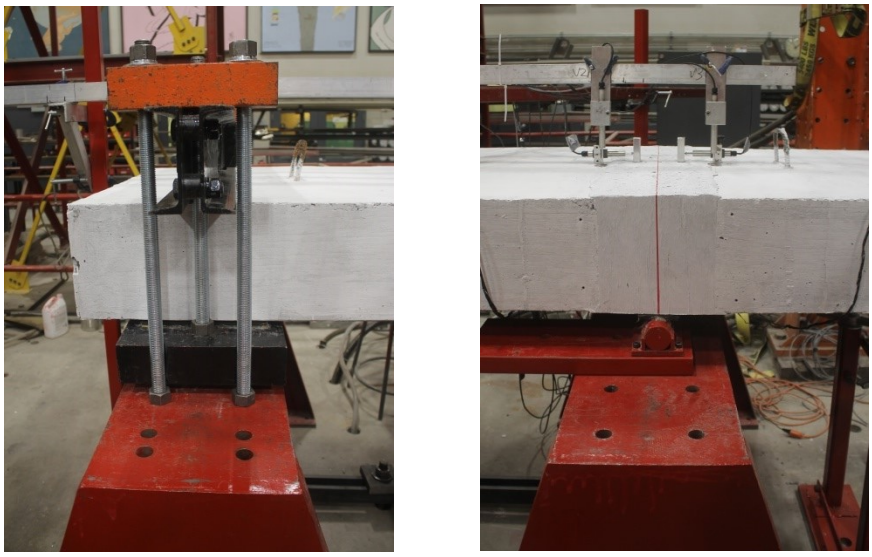

Figure 3.36 – The hinge and roller supports

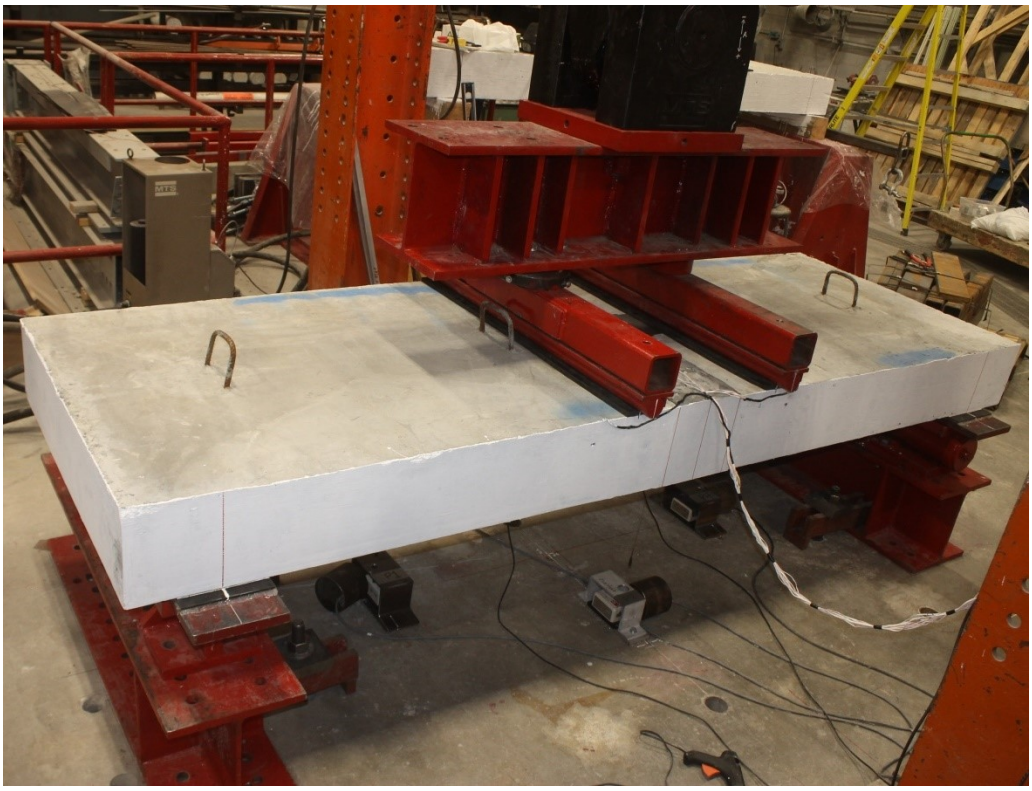

Figure 3.37 – Overview of the test setup for Phase II specimens

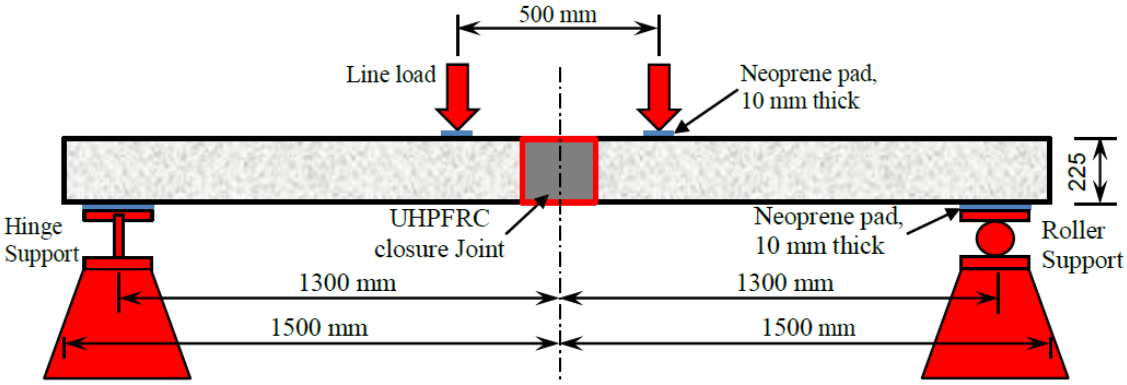

Figure 3.38 – Schematic view of the test setup for Phase II specimens

CHAPTER 4 STRUCTURAL BEHAVIOR OF GFRP-RC BRIDGE-DECK SLABS CONNECTED WITH UHPFRC JOINTS UNDER FLEXURE AND SHEAR

Foreword

Authors and affiliations:

- Mohamed Youssef, PhD Candidate, Department of Civil Engineering, University of Sherbrooke, Sherbrooke, QC, Canada.
- Ehab Ahmed, M. ASCE, Instructor, Concordia University, Montreal, Quebec, Canada; former Research Associate at the Department of Civil Engineering, University of Sherbrooke, Sherbrooke, QC, Canada.
- Brahim Benmokrane, Professor of Civil Engineering and Tier-1 Canada Research Chair in Advanced Composite Materials for Civil Structures and NSERC Research Chair in Innovative FRP Reinforcement for Concrete Structures, Department of Civil Engineering, University of Sherbrooke, Sherbrooke, Quebec, Canada.

Journal: Journal of Bridge Engineering, ASCE

Status: Submitted in October, 2018

4.1. Abstract

Recently, the use of ultra-high-performance fiber-reinforced-concrete (UHPFRC) closure joints between structural members has increased in accelerated-bridge-construction (ABC) applications. This paper presents an experimental study to investigate the structural behavior of UHPFRC closure joints between glass-fiber-reinforced-polymer reinforced-concrete (GFRP-RC) bridge-deck slabs. A total of seven full-scale specimens measuring 3,000 mm long × 1,000 mm wide × 225 mm thick were fabricated, comprised of a reference specimen without closure joints and six jointed specimens. The investigated parameters were: (1) the splice length (100, 150, and 200 mm with a corresponding joint width of 120, 170, and 220 mm, respectively), and (2) the reinforcement ratio (No. 15 and No. 20 GFRP bars with the same spacing). The specimens were tested up to failure in a cantilever-panel setup under monotonic line loading in which the UHPFRC closure joint was subjected to flexural and shear stresses. The test results are discussed and analyzed in terms of crack pattern, load–deflection response, crack width, and GFRP-reinforcement and concrete strains. The test results show that a minimum splice length of 100 mm in 120 mm UHPFRC closure joints yielded adequate strength and performance until failure. The UHPFRC closure joints remained intact without visible cracks and maintained the continuity between the precast slabs.

Author keywords: Accelerated bridge construction (ABC), ultra-high-performance fiber-reinforced concrete (UHPFRC), precast concrete slabs, bridge deck, GFRP, joints, deflection, shear strength, bridge design codes.

4.2. Introduction

North America's aging highway infrastructure is subjected to increasing traffic volume and must be continually renewed while accommodating traffic flow. The Federal Highway Administration (FHWA) (2019) states that the work that occurs from on-site construction activities can have significant social impacts in terms of mobility and safety. In many cases, the direct and indirect costs of traffic detours that result from the loss of a bridge during construction can exceed the actual cost of the structure itself. According to the FHWA (2019), full-lane closures in large urban centers, or on highways with heavy traffic volumes, can have a significant economic impact on commercial and industrial activities in the region. Partial lane closures and other bridge activities that occur alongside adjacent traffic can also lead to safety issues. Thus, the accelerated bridge construction (ABC), which is a technique that uses innovative planning, design, and materials to reduce the onsite construction time for new and existing bridges (Culmo, 2011) can minimize traffic disruption, improve work-zone safety, minimize impact to the environment, improve constructability, increase quality, and lower life-cycle costs. This technology is applicable and needed for both existing bridge replacement and new bridge construction (French et al. 2011).

Full-depth precast-concrete deck slabs are commonly used in ABC in which the slabs are placed on concrete or steel girders and the joints filled with ultra-high-performance fiber-reinforced concrete (UHPFRC). These closure joints, however, need to be durable to overcome any possible deterioration, and should have simple details and minimum width for ease of construction.

UHPFRC is a relatively new class of advanced cementitious materials, which often consists of Portland cement, fine sand, silica fume, ground quartz, steel fibers, water, and high-range water reducer (HRWR) (Russell and Graybeal, 2013). UHPFRC has approximately four to eight times the compressive strength and eight times the abrasion resistance of normal-strength concrete (NSC) as well has a 56-day compressive strength of over 150 MPa (Graybeal, 2007). Graybeal (2006a) measured the modulus of elasticity of

UHPFRC cylinders in compression under standard conditions and obtained an average value of about 42.7 GPa at 28 days. Thus, using UHPFRC in the closure joints between precast bridge-deck slabs is deemed an effective solution due to its exceptional durability, bonding performance, and strength.

The major cause of concrete deterioration is the corrosion of embedded black-steel reinforcing bars as a result of chloride ions in combination with moisture and oxygen (Virmani and Hooks, 2013). Deicing salts applied during winter months generally contain chloride. Chloride solutions penetrate existing cracks and diffuse through the concrete cover to the steel reinforcing bars, initiating corrosion (Azizinamini et al. 2013). In their study, Virmani and Hooks (2013) found that the average black-steel-reinforced concrete (RC) bridge deck in a snow-belt state showed spalling in about 7 to 10 years. Thus, the most effective approach to eliminate corrosion and extend the service life of concrete bridges in aggressive environments is to use noncorroding reinforcing bars such as glass-fiber-reinforced-polymer (GFRP) bars.

The Canadian Highway Bridge Design Code CHBDC (CAN/CSA S6, 2014) and AASHTO-LRFD Bridge Design Specifications for GFRP-Reinforced Concrete Bridge-Decks and Traffic Railings (AASHTO LRFD, 2009) allow the use of GFRP as the primary reinforcement in concrete bridges to eliminate the corrosion and related deteriorations. On the other hand, UHPFRC can develop tension cracks, although they are very small and tightly spaced, as opposed to wide intermittent cracks found in normal reinforced-concrete elements exposed to high tensile stresses. Furthermore, UHPFRC also has very low permeability, which should lead to a long service life (Culmo, 2011). Thus, combining the use of GFRP with UHPFRC will lead to innovative and durable concrete bridges.

UHPC became a commercially available construction material in North America in the late 1990s (Haber et al. 2018). The first North American bridge to use UHPC was a precast, prestressed pedestrian bridge that was constructed in Sherbrooke, Quebec, Canada in 1997 (Blais and Couture, 1999). Since 2006, the use of UHPC in bridges increased significantly where UHPC has been used in 100 bridges in USA and 87 bridges in Canada in 2016 (Haber et al. 2018). The typical uses of UHPC in these bridges are either for closure joints

between the precast concrete elements or for concrete rehabilitation. Recent innovative application of UHPFRC along with GFRP bars is achieved in Ontario's first cable stayed bridge - Nipigon River Bridge (Arafa et al. 2016) where UHPFRC was used in the closure joints between the precast GFRP-RC deck slabs.

Closure joints between prefabricated deck panels take various shapes, but the most common are rectangular and diamond shaped. The rectangular joint is easier to make, but the diamond-shaped joint maintains high interaction with the adjacent panels. Arafa et al. (2016) reported that the diamond-shaped joint exhibits high interaction with the adjacent panel but can involve a complicated construction process. In contrast, the rectangular joint is easy to build, but may have less interaction with the adjacent joint. There is, however, a need for design and construction recommendations for closure-joint geometry when GFRP is used as the primary reinforcement in concrete bridge-deck slabs. In addition, the minimum splice length and strength predictions are also needed for engineering practices since current bridge codes do not provide specific recommendations for UHPFRC-jointed members.

4.3. Literature Review

Several studies have investigated the behavior of full-depth UHPFRC closure joints between precast bridge-deck slabs. Most have used conventional or epoxy-coated steel (Li et al. 2010; Graybeal, 2010; Au et al. 2011; Ma et al. 2012; Graybeal, 2014; Hwang and Park, 2014; Lee and Lee, 2015; Yuan and Graybeal, 2015; Haber and Graybeal, 2018) with different joint shapes and reinforcement configurations. Graybeal (2014) presented a guide for the use of uncoated and epoxy-coated M25 steel and smaller bars, providing recommendations for cover and clear spacing, reinforcing-bar splice length, UHPC compressive strength, and fiber content. On the other hand, a few studies considered FRP bars (Khalafalla and Sennah, 2013; Sayed-Ahmed and Sennah, 2015; Arafa et al. 2016; Sayed-Ahmed, 2016; Sherif and Sennah, 2017), although the closure joints had different reinforcement configurations. Arafa et al. (2016) investigated GFRP-RC precast deck panels joined with rectangular UHPFRC closure joints, with a constant 200 mm splice

length under static loading. The test specimens were designed to simulate the bridge-deck panels of the Nipigon River Bridge. This study concluded that a 200 mm splice length for GFRP bars within a 220 mm wide UHPFRC closure joint was adequate to maintain continuity between the precast panels, allowing them to behave as if cast monolithically. The approval of the final design of the bridge-deck of Nipigon River Bridge was based on the test results for these panels. Sayed-Ahmed (2016) tested 3 details of transverse joints between full-depth and full-width precast NSC and HPC deck panels reinforced with straight-end GFRP bars under monotonic and cyclic loading. Khalafalla and Sennah (2013) studied the use of L-shaped and headed GFRP bars embedded in diamond-shaped UHPFRC closure joints between prefabricated bridge-deck slabs under static loading. They found that the jointed slabs with 125 mm wide UHPFRC closure joints with projecting headed-end or L-shaped GFRP bars had a load carrying capacity about 27% greater than that of a similar cast-in-place slab reinforced with steel bars. Au and Lam (2011) conducted an investigation for the Ministry of Transportation of Ontario (MTO) simulating different prefabricated bridge-deck slabs jointed with closure joints subjected to flexural fatigue stresses. They observed that GFRP bars with a 200 mm splice length in a 226 mm wide UHPFRC closure joint were satisfactory and provided effective continuity. Moreover, the ultimate failure loads of the tested specimens were higher than that of the control specimen. There remains, however, a need to optimize splice length and joint width.

Thus, this study investigated the structural performance of GFRP-RC bridge-deck slabs jointed with rectangular UHPFRC closure joints. A total of seven full-scale specimens measuring 3,000 mm long × 1,000 mm wide × 225 mm thick were fabricated (a reference specimen without a closure joint and six jointed specimens). The investigated parameters were: (1) the splice length (100, 150, and 200 mm with a corresponding joint width of 120, 170, and 220 mm, respectively), and (2) the reinforcement ratio (No. 15 and No. 20 GFRP bars with the same spacing). The specimens were tested up to failure in a cantilever-panel setup under monotonic line loading in which the UHPFRC closure joint was subjected to flexural and shear stresses. The test results are expected to shed the light on the splice length of GFRP bars in UHPFRC joints under combined flexural and shear stresses. The

findings of this study will support the work of the North American technical committees engaged in developing standards and design provisions for GFRP-RC bridge-deck slabs connected with UHPFRC closure joints.

4.4. Experimental Program

To investigate the performance of UHPFRC joints between GFRP-RC slabs, a total of seven full-scale one-way slabs were constructed and tested to failure. This section provides the materials properties, test specimens, fabrication and instrumentation, and test procedures.

4.4.1. Material Properties

No. 15 (15.9 mm diameter) and No. 20 (19.1 mm diameter) GFRP bars were used in this study. The bars were classified as Grade III (60 GPa modulus bars) according to CAN/CSA S807 (2010). The bars were manufactured using a pultrusion process involving a vinyl-ester resin with a fiber content of 82.2%. The bars had a sand-coated surface to enhance the bond with the concrete (Pultrall, 2016). The tensile properties of the GFRP bars were determined according to ASTM D7205 (ASTM 2011). Table 4.1 shows the mechanical properties of the GFRP bars.

Table 4.1 - Mechanical Properties of GFRP Bars

Bar size	d_b (mm)	A_f(mm^2)	E_f (GPa)	f_{fu} (MPa)	ε_{fu} (%)	Surface configuration
No.15	15.90	199	64.2 ± 0.6	1185	1.85	Sand-coated
No.20	19.10	284	64.5 ± 0.7	1105	1.72	Sand-coated

Notes:
d_b: nominal diameter; A_f: nominal cross-sectional area according to CAN/CSA S807 (2010); E_f: tensile modulus of elasticity; f_{fu}: guaranteed tensile strength = average value – 3 × Standard deviation (ACI, 2015); ε_{fu}: ultimate strain.

Two types of concrete were used: ready-mixed normal-weight / normal-strength concrete (NSC) (Ministry of Transportation of Quebec, MTQ Type 5, 40 MPa) and UHPFRC. The NSC had a target 28-day compressive strength of 40 MPa, a maximum aggregate size of 20 mm, and an air content of 5% to 8% for casting the reference specimen and the precast segments of jointed specimens. Nine concrete cylinders measuring 100×200 mm were cast from each NSC batch and cured under the same conditions as the test specimens. The UHPFRC, marketed as Ductal (JS1000) and developed by Lafarge-Holcim (Lafarge, 2009) with a steel fiber content of 2% (156 kg/m3), was used to fill the closure joints to connect the precast slabs. The UHPFRC, which had a target 28-day compressive strength of 170 MPa and an average modulus of elasticity of 50 GPa, was poured directly into the joint without any vibration. To determine the actual concrete compressive strength of the UHPFRC, six 100 × 200 mm cylinders were cast and cured under the same conditions as the closure joints. The properties of NSC and UHPFRC were determined by testing the concrete cylinders (ASTM C39, 2018 & ASTM C1856, 2017, respectively) on the date of testing.

4.4.2. Details of Test Specimens

Seven full-scale, one-way slab specimens were constructed and tested under quasi-static loading to failure. The test specimens were designed to simulate precast bridge-deck slabs connected by cast-in-place closure joints as in ABC applications. The dimensions of the test specimens were 3000 mm in total length (percast slabs and joint), 1000 mm in width, and 225 mm in thickness. The dimensions were selected based on the Sainte-Catherine Overpass Bridges (Ahmed et al. 2014) with an overhang cantilever of 1.0 m. The precast slabs varied in length to accommodate the variable joint widths while maintaining a total length of 3000 mm and a cantilever length of 1000 mm (from the edge to the joint centerline). Figure 4.1 shows the geometry of the test specimens. To meet CSA (2014) requirements, all specimens were reinforced with two mats of identical orthogonal reinforcing bars with top and bottom concrete covers of 40 mm. The reinforcing bars in the longitudinal direction were spaced at 145 mm. The reinforcement of the test specimens was selected based on the Sainte-Catherine Overpass Bridges (Ahmed et al. 2014) in

which the transverse reinforcement (main) was No. 20@140 mm and the longitudinal reinforcement was No. 20@210 mm. The main reinforcement of the test specimens tested herein was No. 20@145 mm and No. 15@145 mm to investigate the effect of the reinforcement ratio. The test parameters were: (1) the splice length (100, 150, and 200 mm) and (2) the longitudinal-reinforcement ratio (0.79% and 1.14%). The test matrix included (1) one NSC reference specimen without joints reinforced with No. 15 GFRP bars in both the longitudinal and transverse directions (G-R-15-A); (2) three jointed specimens reinforced with No. 15 GFRP bars (G-100-15-A, G-150-15-A, and G-200-15-A), with UHPFRC closure joints 120, 170, and 220 mm in width, respectively; and (3) three jointed specimens reinforced with No. 20 GFRP bars (G-100-20-A, G-150-20-A, and G-200-20-A), with UHPFRC closure joints 120, 170, and 220 mm in width UHPFRC, respectively. Figure 4.1 also shows the reinforcement details of the reference and jointed specimens, while Figure 4.2 shows the joint details. Table 4.2 presents the test matrix and details of the specimens.

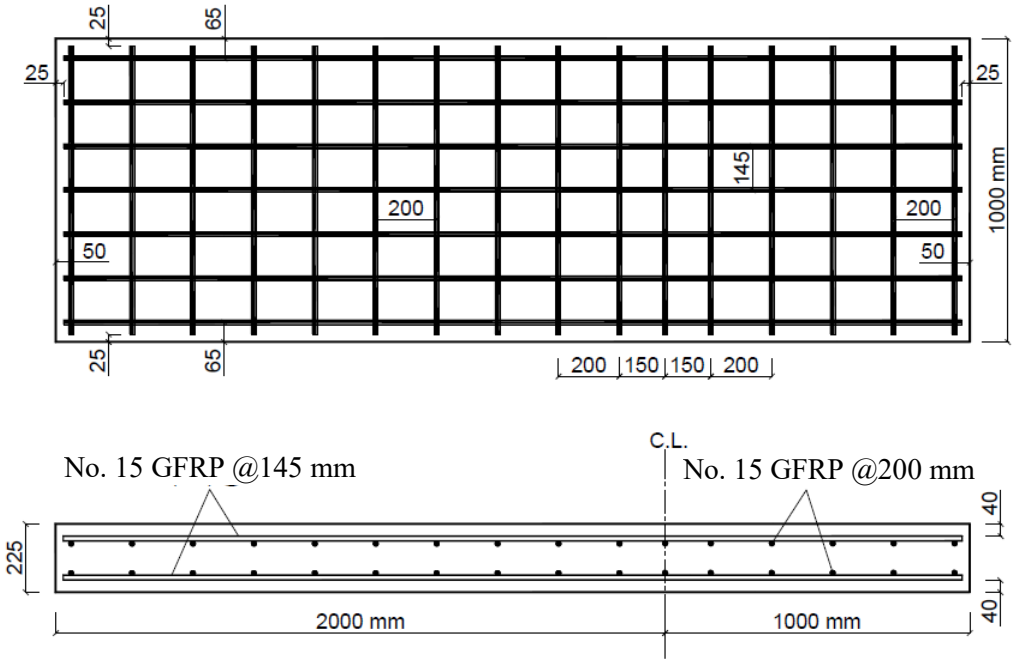

(a) Reference specimen

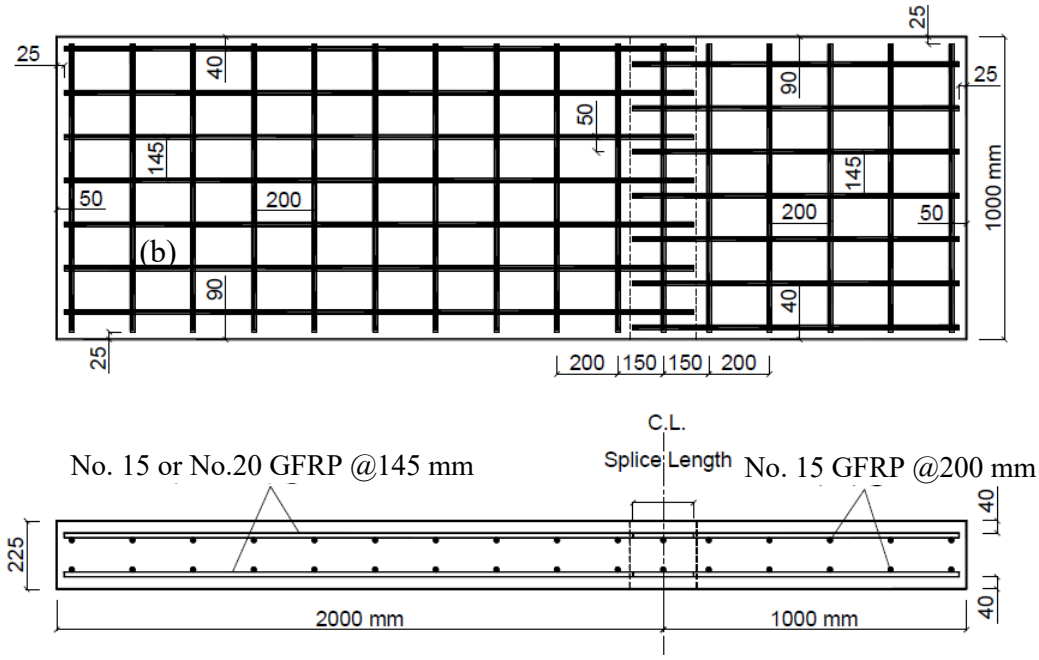

(b) Jointed specimens

Figure 4.1 - Typical concrete dimensions and reinforcement details

Table 4.2 - Concrete and Reinforcement Details of the Test Specimens

Specimen ID[a]	f_c' (MPa)		Joint Width (mm)	Splice Length (mm)	Reinforcement		ρ_{act}[b] (%)	$\rho_{act} \times E_f$[c] (N/mm^2)
	Slab	Joint			Type	Size		
G-R-15-A	40	N/A	N/A	N/A	GFRP	No. 15	0.79	507
G-100-15-A	40	170	120	100	GFRP	No. 15	0.79	507
G-150-15-A	40	170	170	150	GFRP	No. 15	0.79	507
G-200-15-A	40	170	220	200	GFRP	No. 15	0.79	507
G-100-20-A	40	170	120	100	GFRP	No. 20	1.14	735
G-150-20-A	40	170	170	150	GFRP	No. 20	1.14	735
G-200-20-A	40	170	220	200	GFRP	No. 20	1.14	735

Notes:
[a] (G) refers to GFRP-splice length-bar diameter (No. 15 and No. 20)-A, where A is used to differentiate the sample IDs throughout the extensive program.
[b] ρ_{act}: actual tensile reinforcement ratio.
[c] $\rho_{act} \times E_f$ = axial stiffness.

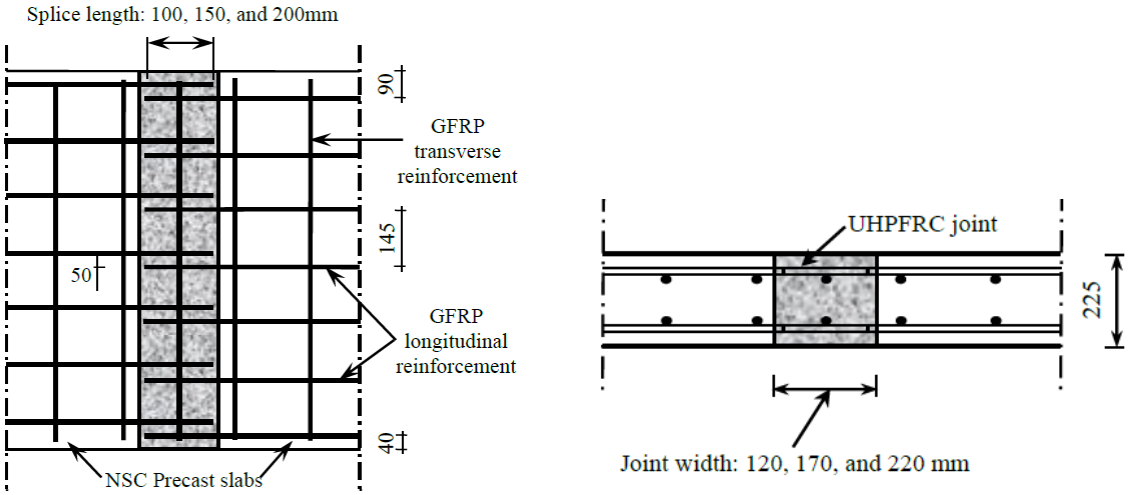

(a) Plan view (b) Side view

Figure 4.2 - Details of the joints and splices

4.4.3. Fabrication of Test Specimens

Two large formworks measuring 9750 mm long × 1000 mm wide × 225 mm high were constructed and used for the study. After instrumenting the GFRP bars, the reinforcing cages were assembled and placed inside the formworks. Figure 4.3 shows the fabrication of the test specimens.

(a) Cages (b) Casting

(c) Surfacing (d) Slabs after curing

Figure 4.3 - Fabrication of the reference specimen and precast slabs

The reference specimen G-R-15-A was cast with NSC without a joint, while all other specimens were fabricated as a pair of precast NSC slabs jointed with UHPFRC. The NSC had a target 28-day compressive strength of 40 MPa. After casting, the NSC was compacted with an electrical vibrator and the surface was finished manually. The slabs were then cured for 7 days with water and wet burlap covered with plastic sheets. After curing, the slabs were removed from the formwork and each pair of the precast slabs was joined in a special formwork for casting the UHPFRC closure joints. Figure 4.4 shows the

fabrication of the UHPFRC closure joints. Before pouring the UHPFRC, a flow-table test was conducted right after mixing according to ASTM C230 (ASTM 2014), the average flow was 220 mm (Figure 4.4(b)). The UHPFRC was poured directly into the joints and the testing cylinders without vibration (Figure 4.4(c)). Curing was carried out by covering the surface with plastic sheets to limit water evaporation.

(a) Alignment of slabs

(b) Flow-table test

(c) Joint casting

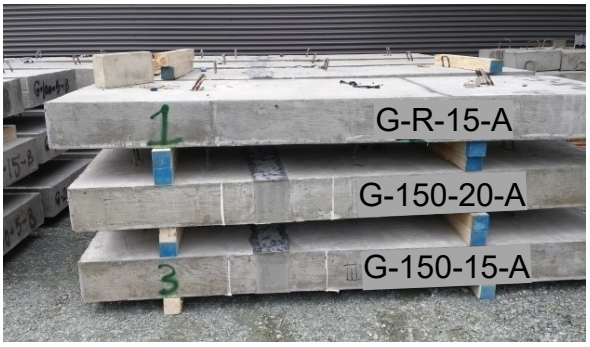

(d) Full specimens

Figure 4.4 - Construction of UHPFRC joint for the jointed specimens

4.4.4. Test Setup and Procedure

The specimens were tested at the Canadian Foundation for Innovation (CFI) structural laboratory at the University of Sherbrooke as simply supported slabs with a clear span of 1750 mm and a 1000 mm of overhanging cantilever. A hinged support located at one end of the specimen was designed to resist the upward reaction. A roller support was located under the centerline of the UHPFRC closure joint at the zone of maximum negative

moment. Neoprene pads 10 mm in thickness were placed between the bottom surface of the slabs and the supports to ensure full contact and distribute the load evenly. Figure 4.5 shows the details of the test setup. The load was applied as line load on the overhanging cantilever using a 1000 kN hydraulic actuator. The actuator applied the load to a steel beam, which, in turn, transferred the load to the slab. A neoprene sheet was used between the steel beam and concrete surface to ensure load distribution. The specimens were loaded at a stroke-controlled rate of 1.2 mm/min up to failure. Before starting the test, two LVDTs were installed on the joint edges to monitor the joint opening during testing. In addition, when the first two flexural cracks appeared, the load was paused and LVDTs installed on the marked crack after measuring the initial crack widths with the handheld microscope. Thereafter, the subsequent cracks were marked and the loading continued until failure.

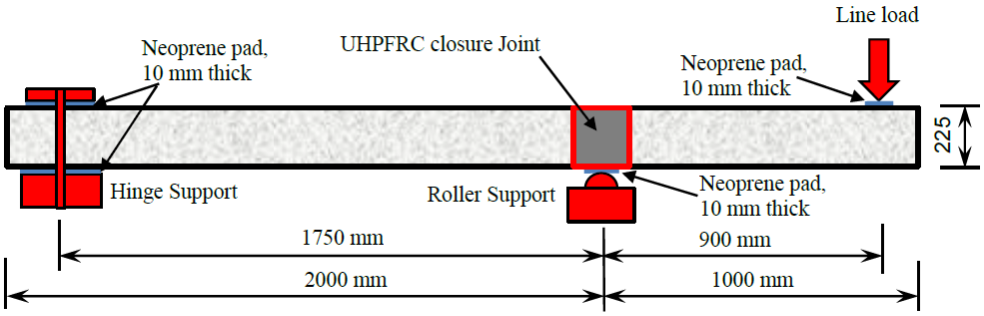

(a) Schematic

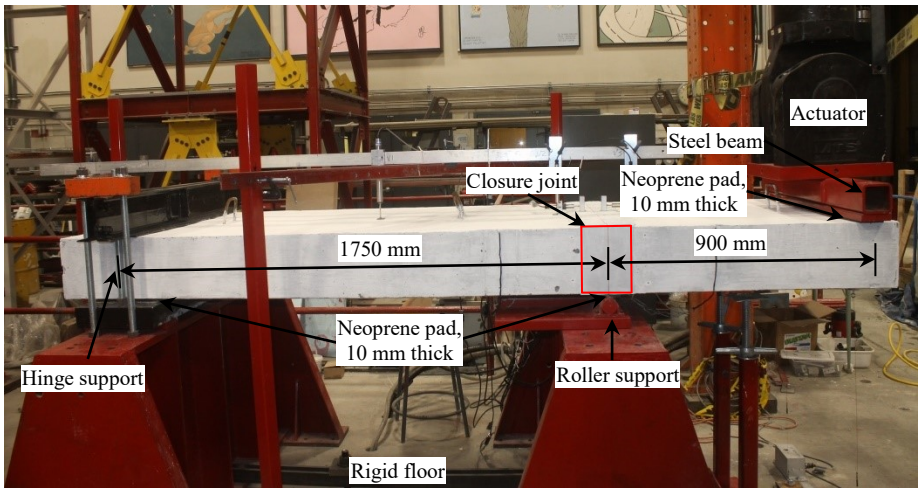

(b) Overview

Figure 4.5 - The test setup

4.4.5. Instrumentation

Figure 4.6 shows the typical instrumentation of the test specimens. The tensile strains in the GFRP reinforcing bars and the compressive strains in the concrete were measured with electrical resistance strain gauges. For the reference specimen, two strain gauges were installed on the GFRP bars at the maximum negative moment. For the jointed specimens, six strain gauges were attached to the longitudinal tension reinforcing bars at the critical positions, as shown in Figure 4.6(a), to investigate the strain along the splice length. The concrete strains were measured with two strain gauges installed on the compression side of the slab 150 mm from the joint centerline. Cantilever deflection was monitored with two potentiometers (Δ_A and Δ_B) located under the load 900 mm from the joint centerline, as illustrated in Figure 4.6(b). Two linear variable displacement transducers (LVDTs) with a precision of 0.01 mm were installed on the closure-joint sides to measure the interfacial-crack (joint opening) width at the closure joint–precast slab interfaces (J1 and J2). Two other LVDTs (0.01 mm in precision) were used to record the crack width of the first two flexural cracks (Figure 4.6(c)). A 50X handheld microscope was used to measure the initial crack widths. An automatic data-acquisition system was used to record loading, deflections, crack widths, and strains in the concrete and reinforcing bars.

4.5. Experimental Results and Discussion

Table 4.3 presents the summary of the test results. The results are discussed in terms of the crack pattern, crack load, crack width, ultimate capacity, deflection, strains, and mode of failure.

4.5.1. Crack Pattern and Mode of Failure

Figure 4.7 presents the typical crack pattern at failure of representative specimens. All tested specimens exhibited sudden shear failure (diagonal tension failure) within the cantilever region. The diagonal tension failure mode was expected due to the low modulus of elasticity of the GFRP reinforcing bars, which provided a shear capacity lower than the flexural capacity of the section.

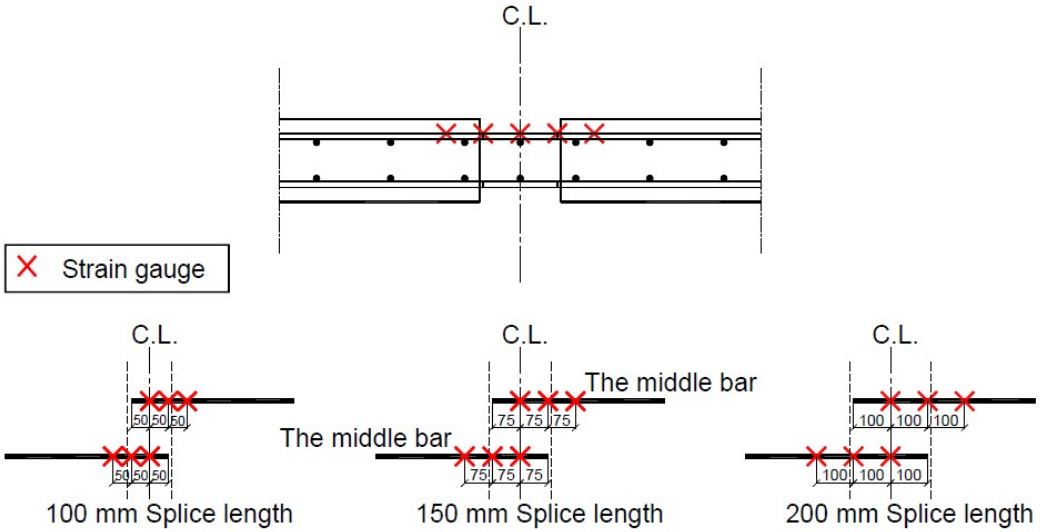

(a) Strain gauges for jointed specimens

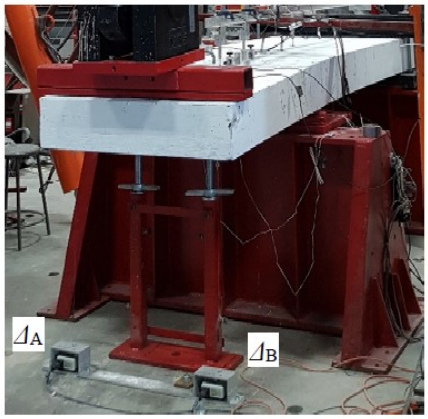

(b) Potentiometer for deflection

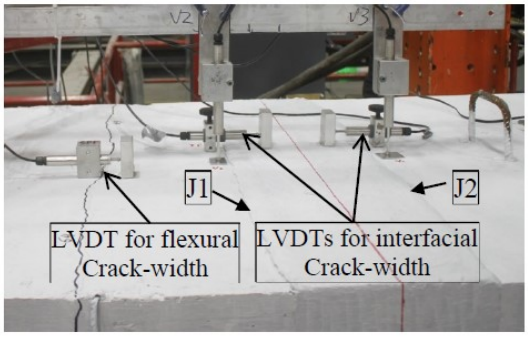

(c) LVDTs for the crack width

Figure 4.6 - Typical instrumentation

In the reference specimen without a joint (G-R-15-A), the first flexural crack appeared at a load of 28 kN (approximately 20% of the failure load) over the roller support at the line of maximum negative moment. Subsequent flexural cracks continued to appear within the cantilever and the interior span parallel to the first crack as the load increased. The cracks continued to propagate vertically through the slab thickness. At about 90% of the ultimate load, inclined cracks were observed along the cantilever sides, extending diagonally towards the roller support and upward towards the line load causing shear failure (diagonal

tension failure). The failure occurred at an ultimate load of 136 kN. Figure 4.7(a) depicts the crack pattern and mode of failure of reference specimen G-R-15-A.

Table 4.3 - Summary of the Experimental Results

Specimen	f'_c (MPa)		V_{cr}	V_{ser}	V_{exp}	Δ_{cr}	Δ_{ser}	Δ_{max}	Max Strain ($\mu\varepsilon$)		Failure
ID	Slab	Joint	(kN)	(kN)	(kN)	(mm)	(mm)	(mm)	FRP	Concrete	Mode
G-R-15-A	44.0	N/A	28	40.8	136	2.9	8.5	56.6	10,070	1,390	Shear
G-100-15-A	50.7	195	45	43.2	144	6.0	5.7	54.3	8,235[a]	2,179	Shear
G-150-15-A	50.7	195	44	47.1	157	5.7	7.3	60.0	8,650	1,678	Shear
G-200-15-A	50.7	195	40	45.6	152	5.1	7.1	51.8	7,920	1,830	Shear
G-100-20-A	51.7	195	44	47.7	159	5.7	6.6	45.6	7,600	1,885	Shear
G-150-20-A	51.7	195	43	50.4	168	5.1	7.1	45.3	6,880	1,917	Shear
G-200-20-A	51.7	195	63	50.1	167	6.4	5	40.0	6,050	1,515	Shear

Notes:
V_{cr}: first crack load; V_{ser}: service load; V_{exp}: experimental failure load; Δ_{cr}: deflection at the first crack; Δ_{ser}: deflection at the service load; Δ_{max}: maximum deflection at failure.
[a] Strain gauge malfunctioned before failure load.

In the jointed specimens reinforced with No. 15 GFRP bars (G-100-15-A, G-150-15-A, and G-200-15-A), the first flexural crack was observed within the interior span about 350, 260, and 250 mm from the joint centerline, respectively. The cracking load ranged from 26% to 31% of the ultimate load, with a value of 45, 44, and 40 kN, respectively, and an increase of 60%, 57%, and 43%, respectively, compared to the reference specimen (G-R-15-A). At the joint–slab interface, the interfacial crack started to open at an average load of 13 kN. Due to its very high tensile strength, the UHPFRC closure joint prevented the formation of cracks within the joint zone (maximum negative moment) and obviously increased the cracking load relative to G-R-15-A. Flexural cracks continued to appear on the top surface and propagated until the diagonal cracks appeared on the cantilever side and extended towards the roller support, causing diagonal tension failure. The failure loads were 144, 157, and 152 kN for G-100-15-A, G-150-15-A, and G-200-15-A, respectively, with increased ultimate capacities of 6%, 15%, and 12%, respectively, compared to G-R-

15-A. In addition, no visible cracks were observed within the UHPFRC closure joint due to its very high tensile strength compared to the NSC.

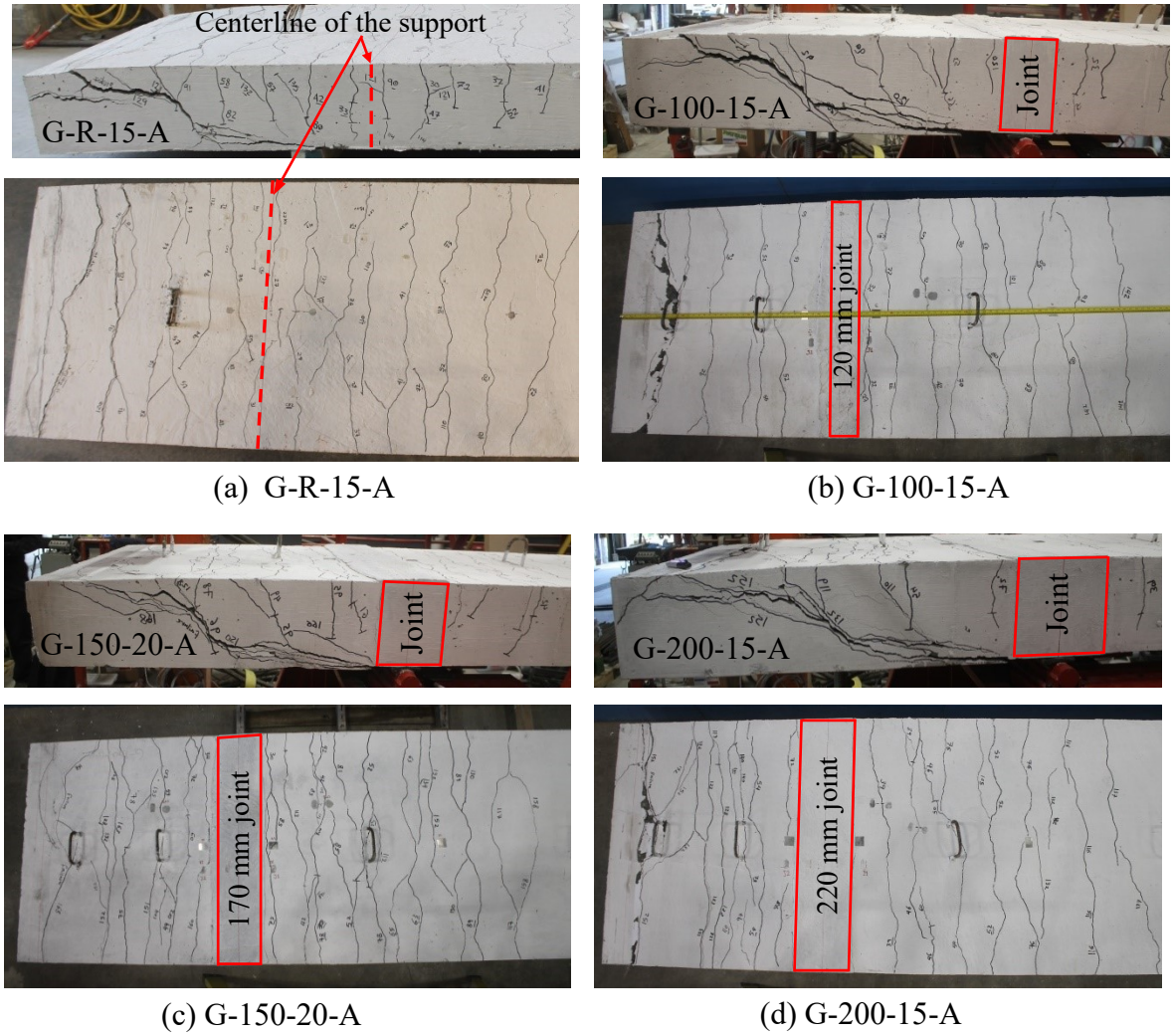

(a) G-R-15-A (b) G-100-15-A

(c) G-150-20-A (d) G-200-15-A

Figure 4.7 - Typical crack pattern and mode of failure

The jointed specimens reinforced with No. 20 GFRP bars (G-100-20-A, G-150-20-A, and G-200-20-A) behaved similarly to those with No. 15 GFRP bars, but more cracks were observed within the interior span. The first flexural crack loads were at 44, 43, and 63 kN at 320, 300, and 350 mm from the joint centerline, respectively. The cracking load ranged from 26% to 37% of the ultimate load at failure. The interfacial crack started to widen at an average load of 20 kN, representing an increase of 50% compared to the specimens with No. 15 GFRP bars. Flexural cracks appeared at higher loads and spread over the top

surface and extended through the slab thickness until the diagonal shear cracks appeared on the cantilever side, causing diagonal tension failure.

A comparison of the specimens with No. 15 and No. 20 GFRP bars revealed that G-100-20-A, G-150-20-A, and G-200-20-A failed at an ultimate load of 159, 168, and 167 kN, providing an increase of 10%, 7%, 10% compared to G-100-15-A, G-150-15-A, and G-200-15-A, respectively. Furthermore, increasing the reinforcement ratio by 44% (from No. 15 to No. 20) did not significantly affect the ultimate capacity because the specimens failed in shear, in which the failure was mainly governed by slab concrete strength. The joint width, however, had no clear effect on the crack pattern or mode of failure.

4.5.2. Load–Deflection Behavior

Figure 4.8 shows the applied load–deflection relationships for which the deflection was measured under the line load 900 mm from the roller support. Table 4.3 lists the deflection of the tested specimens at the first crack and failure. The reported values represent the average of the two potentiometers [Δ_A and Δ_B, shown in Figure 4.6(b)]. The reference and jointed specimens experienced typical bilinear relationships. As shown in Figure 4.8, the specimens showed the same linear relationships until cracking because the deflection was controlled by the gross cross-section. The response was not affected by the reinforcement ratio or splice length (joint width). Once the cracking load had been reached, the post-cracking stiffness decreased as the cross-section cracked. The deflection at cracking load of the reference specimen (28 kN) was 2.9 mm, while the average deflection of the jointed specimens at cracking (average cracking load = 46.6 kN) was 5.7 mm. The UHPFRC joint shifted the first crack away from the centerline of the roller support, which resulted in a higher cracking load and, consequently, higher corresponding deflection values. In addition, due to the very high modulus of elasticity of the UHPFRC, the jointed slabs with No. 15 GFRP bars experienced lower deflection values than the reference specimen.

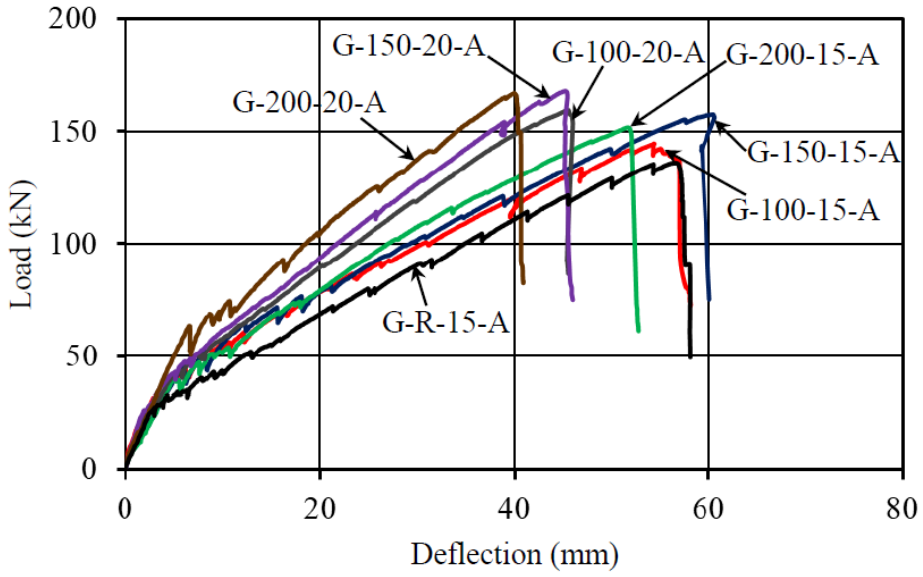

Figure 4.8 - Load–deflection relationships

On the other hand, unlike the pre-cracking stage, post-cracking deflection was affected by the reinforcement ratio and joint width. The maximum deflections at failure for G-R-15-A, G-100-15-A, G-150-15-A, and G-200-15-A were 56.6, 54.3, 60, and 51.8 mm, respectively. In addition, the load–deflection relationships were almost the same. This implies that the joints provided continuity, and the samples had the same deflection response and close deflection at failure. In addition, there was no significant difference between the responses of the specimens reinforced with No. 15 GFRP bars with 100, 150, and 200 mm splices.

Furthermore, the specimens reinforced with No. 20 GFRP bars (G-100-20-A, G-150-20-A, and G-200-20-A) had lower deflection values at failure compared to that of the specimens reinforced with No. 15 GFRP bars. for which the ultimate deflection was 45.6, 45.3, and 40 mm, respectively. For the three splices tested—100, 150, and 200 mm—increasing the reinforcement ratio by 44% [from No. 15 GFRP bars (199 mm^2) to No. 20 GFRP bars (284 mm^2)] decreased the ultimate deflection by 16%, 24.5%, and 24%, respectively. At the same load level, the specimens reinforced with No. 20 GFRP bars had 17% lower deflection due to increasing the splice length from 100 to 200 mm. The wider joints

accompanied with a higher reinforcement ratio contributed to enhancing the post-cracking stiffness, which resulted in lower deflection at the same load level.

Since the deflection is not a design criterion for bridge-deck slab in the CHBDC (CAN/CSA S6, 2014), the serviceability requirements of AASHTO LRFD (2009) where the deflection due to vehicular load on cantilever span was used as reference. AASHTO LRFD (2012) mandates that the deflection should not exceed the cantilever span, L, divided by 300 (L/300; L is in inches). The cantilever span, L, was set to the distance between the loading point and the centerline of the support and was equal to 900 mm. In addition, for comparison, the service load was set to 30% of the ultimate capacity of each specimen (0.30 V_{exp}). This value has been reported by many researchers as a service-load level (Mota at al., 2006, Bischoff, 2009, and El-Nemr et al. 2013, Lee and Lee, 2015, Elgabbas et al. 2016). Table 4.3 lists the service-load values and the corresponding deflections for the test specimens. The service-load levels ranged from 40.8 to 50.4 kN, and the corresponding deflection at service load ranged from 5.0 to 8.5 mm. It was confirmed that all the test specimens exhibited deflections at 0.30 V_{exp} larger than the AASHTO LRFD (2012) limit (L (in.)/300 = 3.0 mm). Thus, AASHTO LRFD (2009) deflection limit may be used as a service limit for such jointed slabs when deflection is of concern.

4.5.3. Crack Width

During the tests, cracks appeared and propagated on the top surface of the specimens; the first two flexural cracks and the two interfacial cracks were monitored. Table 4.4 provides the first flexural-crack widths and the average interfacial-crack width at both the service-load level and failure. Figure 4.9 depicts the relationship between the applied load and the flexural-crack width, and also introduces the best-fitting curves. The Figure shows that the test specimens had linear load–crack width relationships up to failure with an average coefficient of determination (R^2) equal to 0.99.

Table 4.4 - Comparison of Measured Crack Widths at Service and Failure Loads

Specimen ID	Flexural-Crack Width (mm)		Interfacial-Crack Width (mm)	
	V_{ser}	V_{exp}	V_{ser}	V_{exp}
G-R-15-A	0.43	1.72	---	---
G-100-15-A	---[a]	2.11	0.31	2.75
G-150-15-A	0.26	2.07	0.35	2.60
G-200-15-A	0.33	1.74	0.33	2.35
G-100-20-A	0.19	1.64	0.32	1.91
G-150-20-A	0.21	1.60	0.32	1.80
G-200-20-A	---[a]	1.39	0.23	1.30

Notes:
V_{ser}: shear at service load level; V_{exp}: shear at failure.
[a] The first crack load was higher than the service load.

At failure, the reference specimen G-R-15-A had a flexural-crack width of 1.70 mm, while specimens G-100-15-A, G-150-15-A, and G-200-15-A exhibited widths of 2.11, 2.07, and 1.74 mm, respectively. This represents an increase of 23%, 20%, 0%, respectively, relative to G-R-15-A. At the same load level, increasing the splice length from 100 mm to 150 and 200 mm decreased the flexural-crack width by 15 and 22%, respectively, see Figure 4.9. In addition, increasing the reinforcement ratio by 44% (No. 15 to No. 20) in G-100-20-A, G-150-20-A, and G-200-20-A decreased the flexural-crack width by about 20%. At the same load level, the higher reinforcement ratio contributed to reducing the stress in the GFRP bars at the same load level and consequently yielded smaller crack widths. Furthermore, the flexural-crack width decreased by 10% and 20% when the splice length was increased from 100 mm to 150 and 200 mm, respectively, at the same load.

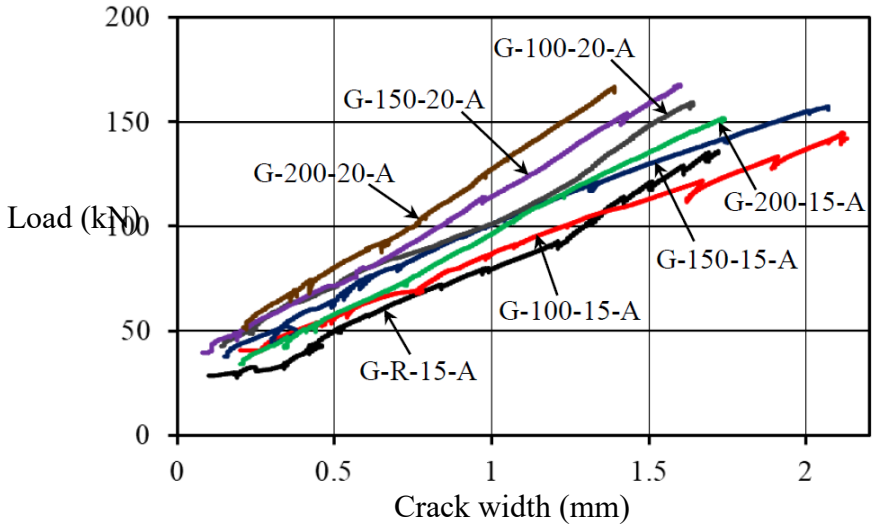

(a) Monitored cracks

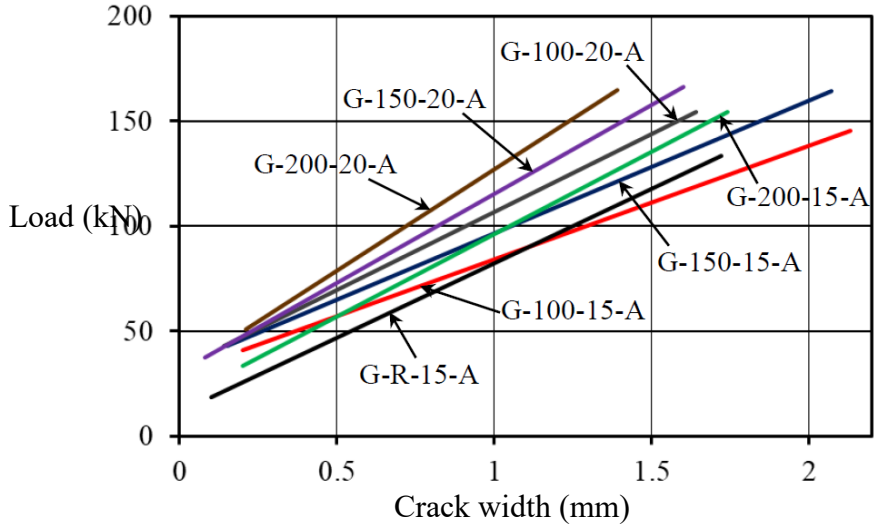

(b) Best fit

Figure 4.9 - Load–flexural-crack-width relationships

The relationships of the interfacial-crack widths on the cantilever side and the interior-span side are plotted against load in Figure 4.10, which provides the best fit. The relationships were almost linear with an average coefficient of determination, R^2, of 0.98. Specimens G-100-15-A, G-150-15-A, and G-200-15-A showed interfacial-crack widths at failure of 2.75, 2.60, and 2.35 mm, respectively. Increasing the splice length from 100 to 150 and 200 mm decreased the interfacial-crack width by approximately 10% and 18%,

respectively, while maintaining the same load level. In specimens G-100-20-A, G-150-20-A, and G-200-20-A, the interfacial-crack width at failure was 1.91, 1.80, and 1.30 mm, respectively. The crack width decreased by 35% at failure due to increasing the reinforcement ratio by 44%. At a given load level, increasing the splice length from 100 to 150 and 200 mm, resulted in decreased the interfacial-crack widths by 5% and 32%, respectively. It is worth mentioning that Lee and Lee (2015) reported that the load–interfacial-crack width relationship was not significantly influenced by the reinforcing-bar splice length. This, however, could be attributed to the use of low reinforcement ratios. Increasing the reinforcement ratio helped reduce the strain at the same load, which limited the interfacial-crack widths. Furthermore, the UHPFRC joints provided very high bond strength, which prevented any slip (relative moment and/or detachment of the reinforcing bar form the concrete), which can affect the joint opening, especially with short splice lengths such as 100 mm.

The flexural and interfacial-crack widths at an assumed service load of 0.30 V_{exp} were compared to 0.5 mm, limited for members subjected to aggressive environments (AASHTO LRFD, 2009 and CAN/CSA S6, 2014). Both specimens G-100-15-A and G-200-20-A had no flexural cracks at the service-load level, since the service load was less than the cracking load. The other specimens, including the reference, showed flexural-crack widths ranging from 0.19 to 0.43 mm, with an average value of 0.31 mm. The jointed specimens had an average interfacial-crack width ranging from 0.23 to 0.35 mm at service load of 0.30 V_{exp}, which is well below 0.50 mm.

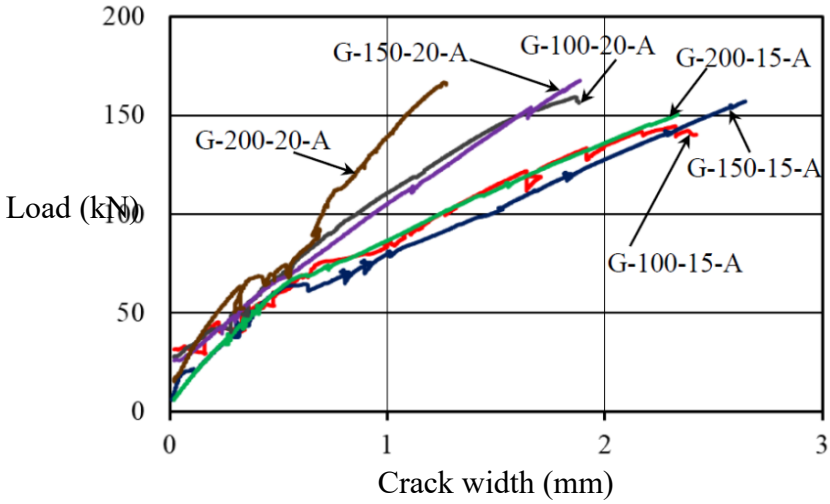

(a) Monitored interfacial cracks

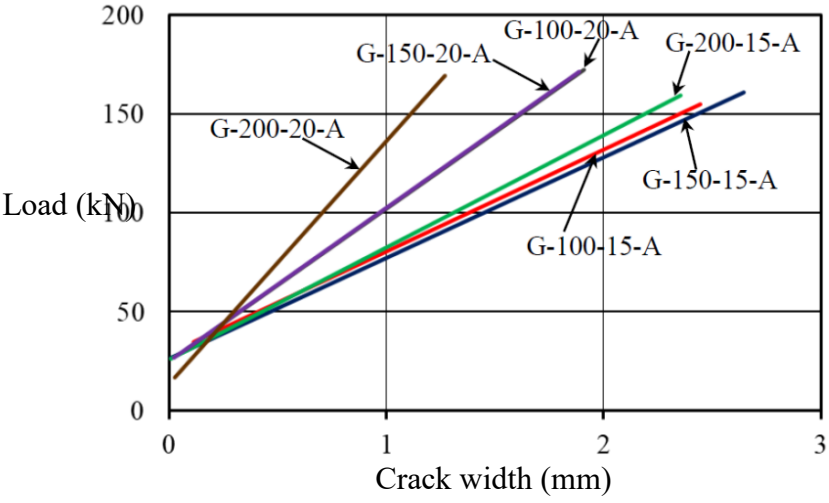

(b) Best fit

Figure 4.10 - Load–interfacial-crack-width relationships

4.5.4. Strains in Reinforcement and Concrete

Figure 4.11 shows the relationships between the maximum strains in the GFRP reinforcement and concrete versus the applied load. Table 4.3 lists the maximum strains at failure. The load–strain curves of the jointed specimens were typically bilinear relationships. After cracking, the strains in the GFRP and concrete varied linearly with increasing load up to failure. The load–strain relationships confirm that the GFRP bars

transferred the loads between the precast slabs, even with the short splice length of 100 mm, without experiencing pullout failures. This is consistent with the work reported by Arafa et al. (2016) for a splice length of 200 mm.

The maximum measured GFRP strain in the reference specimen at failure was 10,070 $\mu\varepsilon$ (54% of the ultimate strain). The six jointed specimens attained maximum measured strains in the GFRP between 6,050 and 8,650 $\mu\varepsilon$ (35% to 47% of the ultimate strain). The strain gauge in specimen G-100-15-A, however, malfunctioned before specimen failure. These measured strains were less than the ultimate strain for the GFRP indicated in Table 4.1 (Pultrall, 2016). The concrete strains ranged between 1,390 and 2,179 $\mu\varepsilon$; these values are less than the ultimate concrete compressive strain of 3,000 $\mu\varepsilon$ (AASHTO LRFD, 2009) or 3,500 $\mu\varepsilon$ (CAN/CSA S6, 2014). Figure 4.11 confirms that the tensile strain of the GFRP embedded in the UHPFRC closure joint increased as the splice length decreased. Increasing the splice length from 100 to 150 and 200 mm (comparing G-100-15-A to G-150-15-A and G-200-15-A, respectively) decreased the maximum strain in the GFRP bars by 8% and 13%, respectively, at the same load. The increase in GFRP-reinforcement ratio decreased the measured strains in both the GFRP bars and concrete. In G-100-20-A, G-150-20-A, and G-200-20-A, a 44% increase in the reinforcement ratio decreased the strain in the GFRP and concrete at failure by 22% and 10%, respectively. At the same load, however, the strain in the GFRP decreased by 10% and 20% due to increasing the splice length from 100 to 150 and 200 mm, respectively.

According to the CHBDC (CAN/CSA S6, 2014), the maximum tensile stress in GFRP under service load should not exceed 0.25 of the guaranteed tensile strength. At the service-load level (0.30 V_{exp}), the reference specimen G-R-15-A showed a maximum tensile stress in the GFRP bars of 150 MPa, which is less than 0.25 of the guaranteed tensile strength (0.25 × 1185 = 296 MPa). In addition, all the jointed specimens exhibited tensile stresses in the GFRP bars less than 0.25 of the guaranteed tensile strength. This was expected since the crack widths and interfacial-crack widths were less than 0.5 mm at a corresponding load of 0.30 V_{exp}.

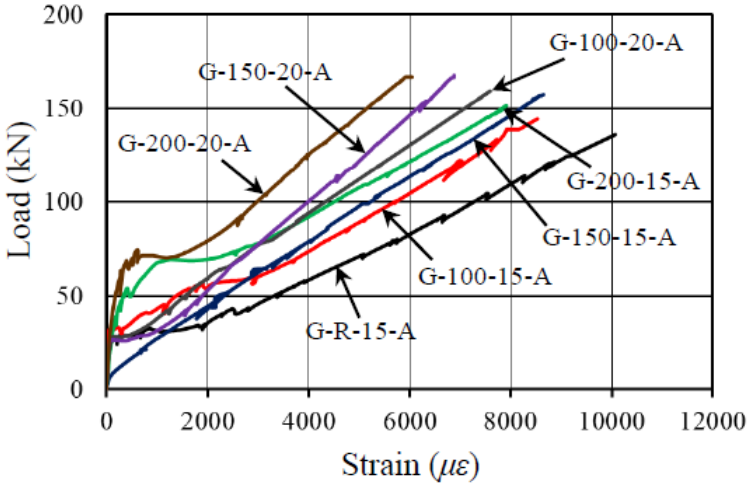

(a) Reinforcement strain

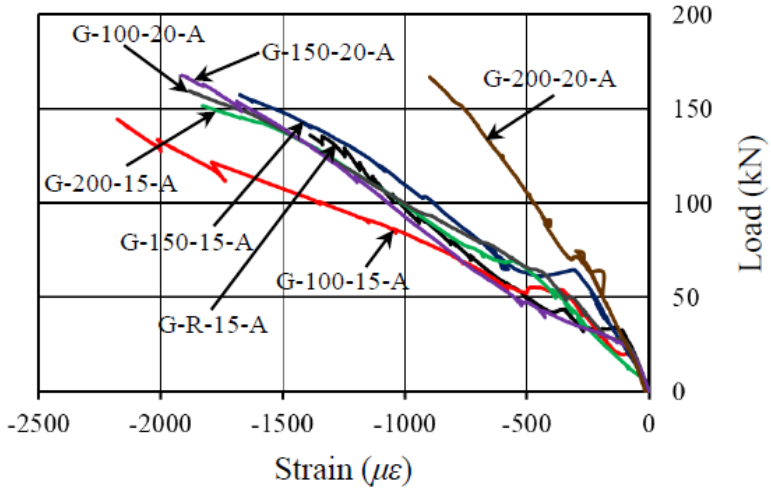

(b) Concrete strain

Figure 4.11 - Load–strain relationships

4.6. Comparison between Predicted and Experimental Shear Strength

The load-carrying capacities of the specimens were predicted using the available bridge-code shear provisions, namely AASHTO LRFD (2009) and the CHBDC (CAN/CSA S6, 2014). The predictions also included CAN/CSA S806 (2012) shear provisions for comparison. The predicted shear capacities were compared to the experimental shear capacities to assess the accuracy of the available shear provisions. As specimen failure

occurred in the slabs away from the closure joint, the prediction was performed using the properties of the NSC.

Table 4.5 gives the ratios of the measured to the predicted shear capacities (V_{exp}/V_{pred}) according to AASHTO LRFD (2009), CAN/CSA S6 (2014), and CAN/CSA S806 (2012). Figure 4.12 provides a comparison of the test-specimen V_{exp}/V_{pred} ratios. Generally, the provisions yielded conservative predictions when V_{exp}/V_{pred} was greater than unity.

Table 4.5 - Ultimate Shear-Strength Prediction

Specimen ID	V_{exp}[a] (kN)	AASHTO (2009)		CAN/CSA S6(2014)		CAN/CSA S806 (2012)	
		V_{pred}[b] (kN)	V_{exp}/V_{pred}	V_{pred}[b] (kN)	V_{exp}/V_{pred}	V_{pred}[b] (kN)	V_{exp}/V_{pred}
G-R-15-A	136	82	1.66	86	1.58	126	1.08
G-100-15-A	144	86	1.67	92	1.57	132	1.09
G-150-15-A	157	86	1.83	92	1.70	132	1.19
G-200-15-A	152	86	1.77	92	1.65	132	1.15
G-100-20-A	159	101	1.57	105	1.51	147	1.08
G-150-20-A	168	101	1.66	105	1.60	147	1.15
G-200-20-A	167	101	1.65	105	1.59	147	1.14
Mean			1.69		1.60		1.13
Standard deviation (SD)			8.27%		6.20%		4.25%
Coefficient of variation (COV)			4.90%		3.87%		3.77%

Notes: [a] $V_{exp:}$ experimental shear strength; [b] $V_{pred:}$ predicted shear strength at failure.

AASHTO LRFD (2009) yielded very conservative predictions with an average V_{exp}/V_{pred} of 1.69 and corresponding standard deviation of 8.27%. The CHBDC (CAN/CSA S6, 2014), however, gave reasonable yet conservative predictions compared to AASHTO LRFD (2009), with an average V_{exp}/V_{pred} of 1.60 and a standard deviation of 6.20%. Moreover, CAN/CSA S806 (2012) provided the most reasonable yet conservative V_{exp}/V_{pred} values with average and standard deviations of 1.13 and 4.25% respectively. Arafa et al. (2016) reported that CAN/CSA S806 (2012) accurately predicted the shear capacity of GFRP deck slabs spliced with UHPFRC joints for a joint width of 220 mm.

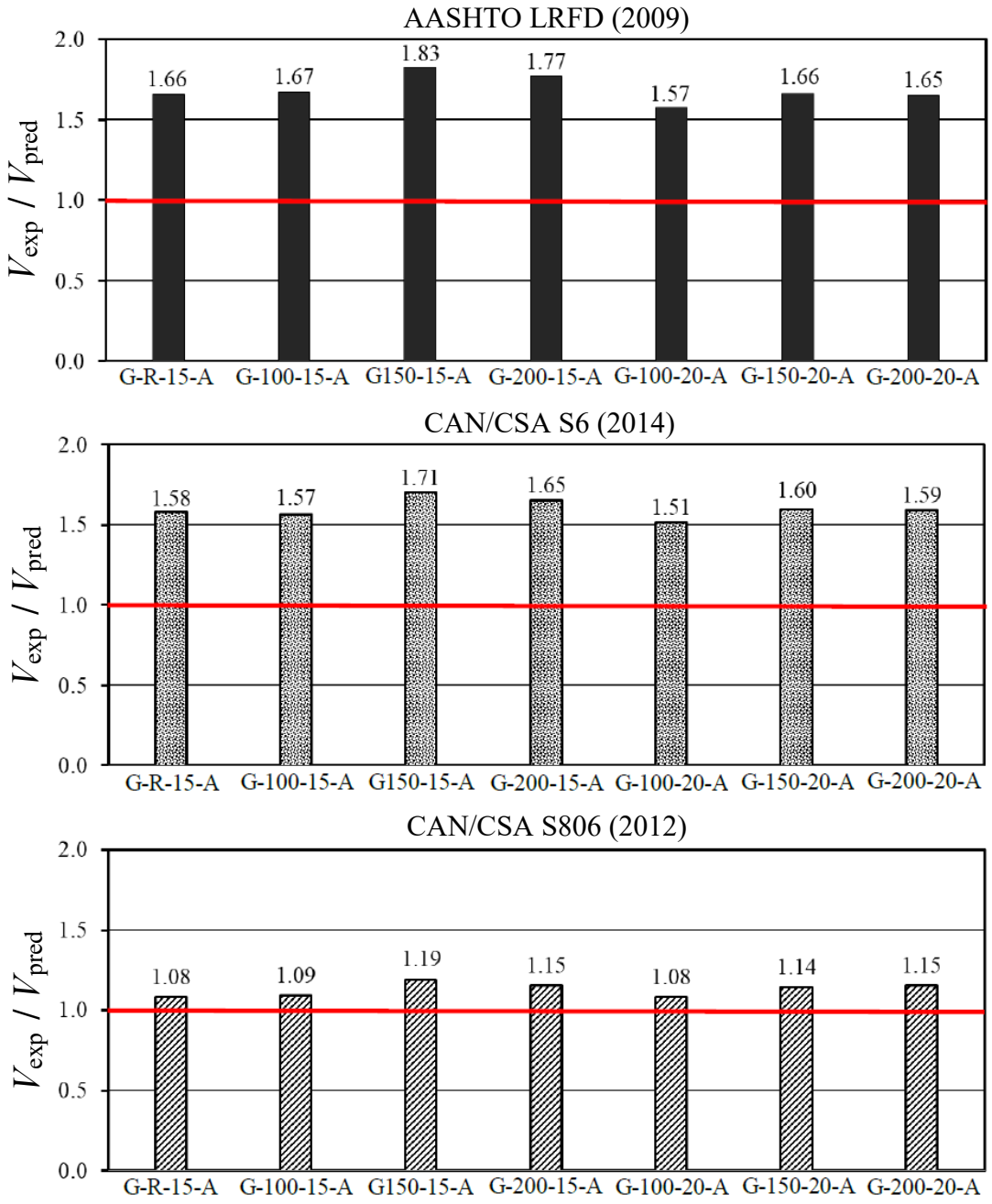

Figure 4.12 - Comparison between V_{exp}/V_{pred} values for the test specimens

As shown in Table 4.5 and Figure 4.12, the splice length in the UHPFRC closure joint had no significant effect on the V_{exp}/V_{pred} values because the GFRP bars showed no sign of slippage and the failure was governed by the NSC in the precast slabs and occurred away from the UHPFRC joints.

4.7. Conclusions

Seven full-scale one-way slabs measuring 3000 mm long × 1000 mm wide × 225 mm thick—including six jointed specimens and one reference without a closure joint—were fabricated and tested to failure. Two reinforcement ratios and three GFRP-bar splice lengths (100, 150, and 200 mm) were considered. The test specimens were loaded to failure as a cantilever, maintaining the UHPFRC closure joint subjected to flexural and shear stresses. Based on the test results and discussions presented herein, the following conclusions were drawn:

1. The observed mode of failure for all test specimens was diagonal tension failure within the cantilever zone (NSC slabs). The use of GFRP reinforcement with a splice length of 100 mm to 200 mm in the UHPFRC joint enabled the slabs to achieve their shear capacity when the same GFRP reinforcement as in the reference slab was used. Increasing the GFRP-reinforcement ratio slightly increased the shear capacity of the jointed slabs; the failure also occurred due to diagonal tension in the NSC slabs.
2. The very high tensile strength of the UHPFRC in the closure joint shifted the location of the first flexural crack from the zone of maximum negative moment (over the centerline of the support). Accordingly, the cracking capacity of the jointed specimens increased by an average of 54% compared to the reference specimen.
3. The ultimate capacity was dominated by the strength of the NSC precast segments, not by that of the UHPFRC closure joint. Thus, the GFRP-bar splice length did not significantly affect the ultimate capacity. Increasing the GFRP reinforcement from No. 15 to No. 20 (44%) increased the ultimate shear capacity of the test specimens by an average ratio of 9%.
4. The reference and jointed specimens experienced the typical bilinear deflection response up to failure. At the same load level, the deflection decreased with increasing bar splice length (closure-joint width), while the reinforcement ratio remained the same. The UHPFRC joint maintained the un-cracked inertia at this

location as the UHPFRC did not experience visible cracks. Consequently, the jointed slabs showed lower deflection than the reference specimen at the same load. Moreover, for a given load, increasing the GFRP-reinforcement ratio decreased deflection by about 22%.

5. The interfacial cracks initiated at earlier loading stages than the other flexural cracks, but no slippage of GFRP bars was observed and the joints remained intact until the slabs failed in shear away from the UHPFRC joints. Due to the UHPFRC having very high tensile strength, no cracks were observed within the closure joint and the joints allowed the specimens to maintain continuity.
6. The maximum measured tensile strains in the GFRP bars along the splice length ranged between 35% and 47% of bar ultimate strain. The maximum strain in the GFRP bars decreased with increasing splice length (closure-joint width). Increasing the reinforcement from No. 15 to No. 20 (44%) significantly decreased the strain in the GFRP bars by about 22%.
7. At 30% of the failure load (0.30 V_{exp}, assumed service load of the specimens), the stresses in the GFRP bars were less than 25% of the guaranteed tensile strength and the flexural and interfacial crack widths of the joints were less than 0.50 mm, even with 100 mm splices (120 mm joints).
8. AASHTO LRFD (2009) yielded conservative shear predictions with an average V_{exp}/V_{pred} of 1.69. CHBDC (CAN/CSA S6, 2014) had reasonable yet conservative predictions with an average V_{exp}/V_{pred} of 1.60. CAN/CSA S806 (2012), however, provided the most accurate yet conservative predictions with an average V_{exp}/V_{pred} of 1.13.
9. The use of a short splice length of 100 mm in 120 mm joints with No. 15 and No. 20 GFRP bars in UHPFRC performed adequately and achieved continuity of the spliced slabs. No slippage was observed; the failure of the jointed slabs was governed by slab strength. The jointed slabs experienced less deflection and strain than the reference specimen at the same load level. Nevertheless, the performance of this short splice under cyclic and fatigue loading should be investigated.

CHAPTER 5 BEHAVIOR OF FIELD-CAST FULL-DEPTH UHPFRC MOMENT CLOSURE JOINTS BETWEEN PRECAST BRIDGE-DECK SLABS REINFORCED WITH GFRP BARS

Foreword

Authors and affiliations:

- Mohamed Youssef, PhD Candidate, Department of Civil Engineering, University of Sherbrooke, Sherbrooke, QC, Canada.
- Ehab Ahmed, M. ASCE, Instructor, Concordia University, Montreal, Quebec, Canada; former Research Associate at the Department of Civil Engineering, University of Sherbrooke, Sherbrooke, QC, Canada.
- Brahim Benmokrane, Professor of Civil Engineering and Tier-1 Canada Research Chair in Advanced Composite Materials for Civil Structures and NSERC Research Chair in Innovative FRP Reinforcement for Concrete Structures, Department of Civil Engineering, University of Sherbrooke, Sherbrooke, Quebec, Canada.

Journal: Journal of Composites for Construction, ASCE

Status: Submitted in January, 2019

5.1. Abstract

The use of ultra-high performance fiber-reinforced concrete (UHPFRC) closure joints between precast deck slabs is a common technique of accelerated bridge construction (ABC). Bridge-deck slabs might be exposed to extreme weather. Glass fiber-reinforced polymer (GFRP) bars are used as successful alternative reinforcement in bridge-deck slabs to avoid steel corrosion problems and related deteriorations. This study presents an experimental investigation of the behavior of field-cast UHPFRC moment closure joints between precast bridge-deck slabs reinforced with HM-GFRP bars. The experimental program consisted of seven full-scale GFRP reinforced concrete specimens with a total length of 3,000 mm, 1,000 mm width, and 225 mm thick. One specimen without closure joint was fabricated monolithically as a reference specimen. Six jointed specimens were fabricated simulating the UHPFRC closure joint between precast bridge-deck slabs. The main test parameters were the GFRP splice length (100, 150, and 200 mm) and the reinforcement ratio (0.79 and 1.14%). The specimens were tested under monotonic load to collapse using a four-point bending scheme, the closure joints were positioned in the middle of the maximum constant moment region and subjected to pure flexural stresses. The experimental results were evaluated and compared to the current design codes and guidelines. The test results demonstrated that the GFRP splice length in the UHPFRC closure joint shall not be less than 150 mm or $9.5d_b$, whichever is greater, to maintain the continuity between the precast deck slabs.

Author keywords: Accelerated bridge construction (ABC); Ultra-high performance fiber-reinforced concrete (UHPFRC); precast slabs, bridge deck; glass fiber-reinforced polymer (GFRP) bars; joints; Connections.

5.2. Introduction

Bridge-deck slabs are the most vulnerable elements to deterioration due to direct exposure to harsh environment, deicing chemicals, and increasing traffic loads, which resulted in corrosion of steel reinforcement and decreased service life. The noncorrosive nature of fiber-reinforced-polymer (FRP) reinforcing bars helps to improve the durability, eliminate maintenance cost, and extend the service life of concrete bridges. The Canadian Highway Bridge Design Code CHBDC (CAN/CSA S6, 2014) and AASHTO-LRFD Bridge Design Specifications for GFRP-Reinforced Concrete Bridge-Decks and Traffic Railings (AASHTO LRFD, 2009) allow the use of GFRP as the primary reinforcement in concrete bridges.

Accelerated bridge construction (ABC) techniques have become increasingly commonplace alternatives to conventional construction techniques over the recent years. ABC systems use innovative planning, design, and materials to minimize the onsite construction time in building new bridges or replacing and rehabilitating existing bridges (Culmo, 2011). In North America, however, aging highway infrastructure is subjected to increasing traffic volume and must be continuously renewed while accommodating the traffic flow. Several advantages can be achieved in using ABC techniques such as: i) improve the quality and durability of the bridge elements as the elements are fabricated off-site under controlled conditions, ii) reduce the construction time and the traffic impacts, and iii) minimize the environmental impacts. One type of Accelerated Bridge Construction techniques uses full-depth precast concrete deck slabs placed on concrete or steel girders and connected by either longitudinal or transverse closure joints. The closure joints, however, need to be strong and durable to overcome any possible deterioration, and should have simple details and minimum width for constructability issues (Youssef et al. 2018a). Due to its exceptional durability and bonding performance, the ultra-high-performance fiber-reinforced concrete (UHPFRC) is used in filling the closure joints between the precast bridge-deck slabs.

Ultra-high-performance fiber-reinforced concrete (UHPFRC) indicates a class of advanced cementitious materials, which composed of Portland cement, fine sand, silica fume, ground quartz, steel fibers, water, and high-range water reducer (HRWR). UHPFRC has a targeted compressive strength over 150 MPa, which is approximately four to eight times the compressive strength of normal-strength concrete (NSC). The modulus of elasticity of UHPFRC cylinders in compression under standard conditions has an average value of about 42.7 GPa at 28 days (Graybeal, 2006b; Graybeal, 2007; Yuguang et al. 2008; Russell and Graybeal, 2013). Currently, the most popular application of UHPFRC in U.S. highway bridge construction is for closure joints between prefabricated bridge-deck elements. Thus, the advanced mechanical properties of UHPC allow for short development length with simple reinforcement details within the closure joint, which result in enhanced element constructability and simplified on-site assembly (French et al. 2011; Haber and Graybeal, 2018). So far, combining the use of GFRP bars with UHPFRC closure joints leads to accelerated, innovative, and durable bridge construction.

Figure 5.1 shows the load transfer mechanism through the closure joint. To transfer the moment, the load should be transferred between the precast segments through short splices embedded in the joint. The tension force is transferred between the bottom splices (tension splices) by bonding stress over the splice length. The splice length should be long enough which can decrease the tensile stresses to resist splitting or pull-out failure. Moreover, the high tensile strength of the UHPFRC improves the bond strength of the reinforcing bars.

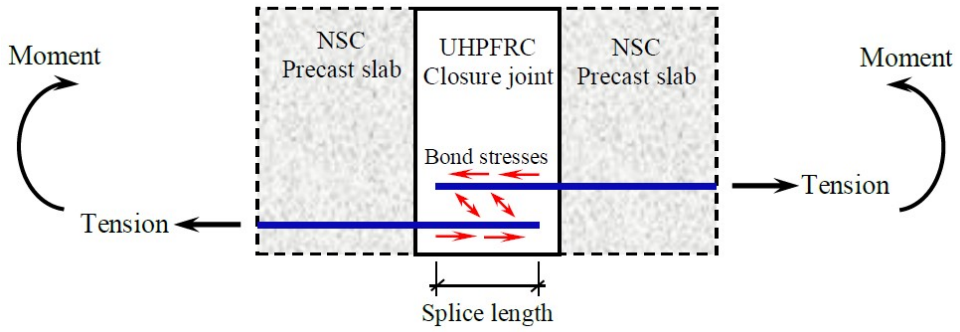

Figure 5.1 - Load transfer mechanism through the UHPFRC closure joint

5.3. Previous Research

Field-cast UHPFRC closure joints between prefabricated bridge components have been implemented in several field applications in North America, including the Rainy Lake Bridge, on Highway 11, Ontario in 2006; the Sunshine Creek Bridge, on Highway 11/17, Ontario in 2007; the Hawk Lake Bridge, on Highway 17, Ontario in 2008; the Buller Creek Bridge on Highway 105, Ontario in 2009; the Log River Bridge, on Highway 71, Ontario in 2009; the Route 31 Bridge in Lyons, New York in 2009; the Route 23 Bridge in Oneonta, New York in 2009; the Eagle River Bridge on Highway 17, Ontario In 2009/2010; The Wabigoon River Bridge on Highway 105, Ontario in 2010; the Chukuni River Bridge on Highway 105, Ontario in 2010; and the Nipigon River Bridge on Highway 11/17, Ontario in 2017 (Graybeal, 2010; Arafa et al. 2016).

Valuable research work have investigated the behavior of UHPFRC closure joints between precast bridge-deck slabs using conventional or epoxy-coated steel reinforcement, with different joint shapes and reinforcement configurations (Li et al. 2010; Graybeal, 2010; Ma et al. 2012; Graybeal, 2014; Hwang and Park, 2014; Lee and Lee, 2015; Yuan and Graybeal, 2015; Vella et al. 2017; Haber and Graybeal, 2018). Graybeal (2014) provided a guide for the use of uncoated and epoxy-coated M25 steel and smaller bars, including recommendations for bar splice length, UHPFRC compressive strength, and fiber content. On the other hand, limited research studies considered GFRP bars (Khalafalla and Sennah, 2013; Sayed-Ahmed and Sennah, 2015; Arafa et al. 2016; Sayed-Ahmed, 2016; Sherif and Sennah, 2017; Youssef et al. 2018(a, and b)). Khalafalla and Sennah (2013) investigated the use of L-shaped and headed GFRP bars embedded in diamond-shaped UHPFRC closure joints between prefabricated bridge-deck slabs under static loading. It was observed that the jointed slabs with 125 mm wide UHPFRC closure joints reinforced with headed-end or L-shaped GFRP bars had a load carrying capacity about 27% greater than that of a similar cast-in-place slab reinforced with steel bars. Moreover, the failure loads of the jointed specimens were higher than that of the reference specimen. Sayed-Ahmed (2016) tested 3 details of transverse joints between full-depth and full-width precast NSC

and HPC deck panels reinforced with straight-end GFRP bars under monotonic and cyclic loading.

A study by Au and Lam (2011) was conducted for the Ministry of Transportation of Ontario (MTO) to investigate different prefabricated bridge-deck slabs jointed with closure joints subjected to flexural fatigue stresses. It was recommended that GFRP bars with 200 mm splice length in a 226 mm wide UHPFRC closure joint were satisfactory and provided effective continuity. The MTO decided to use the GFRP bars with the UHPFRC closure joints in the first cable-stayed bridge in Ontario (Nipigon River Bridge). Moreover, the design of Nipigon River Bridge was accepted based on a study of full-scale prototypes (Arafa et al. 2016) due to the lack of applicable design recommendations. The study investigated eight GFRP-RC precast deck panels connected with rectangular UHPFRC closure joints, with a constant 200 mm splice length and 220 mm joint width under static loading. The test specimens were designed to simulate the bridge-deck panels of the Nipigon River Bridge. The findings of this study concluded that the GFRP splice length of 200 mm was sufficient to maintain continuity between the precast slabs, and the jointed specimens behaved like those cast monolithically. Since current bridge design codes (AASHTO LRFD, 2009 and CAN/CSA S6, 2014) do not provide specific recommendations for the UHPFRC closure joints, there is a need for solid design specifications for the joint geometry and the splice length using GFRP as a primary reinforcement in concrete bridge-deck slabs.

An extensive research program is being carried out at the University of Sherbrooke (Qc, Canada) to investigate the structural behavior of GFRP-RC bridge-deck slabs connected by rectangular UHPFRC closure joints with different splice lengths, splice details, and different loading types. The first group of specimens was conducted and tested at which the closure joints located at the zone of maximum negative moment and subjected to combined flexural and shear stresses. The results of this investigation (Youssef et al. 2018a) recommended the feasibility of using 100-mm or $6.5d_b$ GFRP splice length, whichever is greater, to perfectly transfer loads between the precast slabs without any slippage signs or bond-strength degradation.

This paper presents the test results in terms of flexural behavior and serviceability performance of one-way GFRP-RC bridge-deck slabs jointed with rectangular UHPFRC closure joints with different splice lengths and reinforcement ratios. The closure joints are subjected to pure flexural stresses. The findings of this study are expected to support the work of the North American technical committees engaged in developing standards and design provisions for ABC techniques, especially the GFRP-RC bridge-deck slabs connected with UHPFRC closure joints.

5.4. Experimental Program

5.4.1. Material Characteristics

The GFRP reinforcements used in this study, as shown in Figure 5.2, were No. 15 (15.9 mm diameter) and No. 20 (19.1 mm diameter) grade III bars. The high modulus HM-GFRP bars were manufactured by pultrusion process in a vinylester resin with E-glass fiber contents of 82.2% (Pultral 2015). The HM-GFRP bars had a sand-coated surface texture to enhance the bond and load transfer between the bars and the surrounding concrete. The guaranteed tensile strength (f_{fu}), ultimate strain (ε_{fu}), modulus of elasticity (E_f) of the GFRP bars were determined according to ASTM D7205 (ASTM 2011). Table 5.1 provides the mechanical tensile properties of the GFRP reinforcing bars.

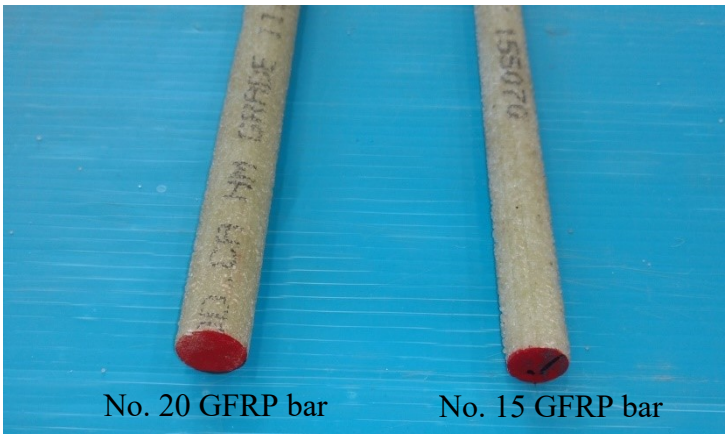

Figure 5.2 - HM-GFRP reinforcing bars

Table 5.1 - Mechanical Properties of GFRP Bars

Bar size	d_b (mm)	A_f (mm^2)	E_f (GPa)	f_{fu} (MPa)	ε_{fu} (%)	Surface configuration
No.15	15.90	199	64.2 ± 0.6	1185	1.85	Sand-coated
No.20	19.10	284	64.5 ± 0.7	1105	1.72	Sand-coated

Notes:
d_b: nominal diameter; A_f: nominal cross-sectional area according to CAN/CSA S807 (2010); E_f: tensile modulus of elasticity; f_{fu}: guaranteed tensile strength = average value – 3 × Standard deviation (ACI, 2015); ε_{fu}: ultimate strain.

The test specimens were fabricated using normal-weight ready-mixed normal-strength concrete (NSC) and ultra-high-performance fiber-reinforced concrete (UHPFRC). The NSC was used in casting the reference specimen and the precast segments of the jointed specimens. The NSC had a targeted compressive strength of 40 MPa at 28 days, and contained 20-mm maximum aggregate size and 5 to 8% air content. Nine concrete cylinders were cast from each concrete batch to determine the compressive strength of NSC. The UHPFRC, commercially knows as Ductal® (JS1000) and developed by Lafarge-Holcim (Lafarge 2009) was used as filling materials in the closure joints. The Ductal product of 170 MPa target compressive strength and 50 GPa average modulus of elasticity was cast directly into the closure joint without vibration. For UHPFRC, to determine the compressive strength, six 100×200 mm concrete cylinders were cast from each concrete batch. The NSC and UHPFRC cylinders were cured under the same conditions as the test specimens and tested on the day of testing. The actual compressive strength of NSC and UHPFRC was determined according to ASTM C39 (ASTM, 2018) and ASTM C1856 (ASTM, 2017), respectively.

5.4.2. Details and Fabrication of Test Specimens

A total of seven full-scale one-way slab specimens measuring 3000 mm length, 1000 mm width, and 225 mm thick were constructed and tested up to failure. The test specimens were designed to meet the requirements of the Canadian Highway Bridge Design Code CHBDC (CAN/CSA S6, 2014), each specimen was reinforced with two mats of identical

orthogonal GFRP reinforcing bars with top and bottom concrete covers of 40 mm. The study included a reference specimen was cast monolithically without a closure joint and six jointed specimens. The reference specimen (G-R-15-B) was reinforced with No.15 GFRP bars in both longitudinal and transverse directions (top and bottom). The six jointed specimens were designed to simulate an accelerated bridge system, each consisted of a pair of identical NSC precast slabs connected by cast-in-place UHPFRC closure joint at the middle of each specimen. Three of the jointed specimens (G-100-15-B, G150-15-B, and G-200-15-B) were reinforced with No.15 GFRP bars in longitudinal and transverse directions, top and bottom mats. The other three specimens (G-100-20-B, G-150-20-B, and G-200-20-B) were reinforced with No.20 GFRP bars as top and bottom main reinforcement, while No. 15 GFRP bars were used as a transverse reinforcement. In the jointed specimens, the longitudinal top and bottom reinforcing bars projected at one end with straight end bars forming three splice lengths namely, 100, 150, and 200 mm, and extended into the closure joints of width 120, 170, and 220 mm, respectively, the spliced bars offset was 50 mm. The specimens were named in accordance with the reinforcement type, splice length, and bar size. Figure 5.3 shows the geometry and reinforcement details of the test specimens, while Figure 5.4 provides overview of the joint details.

Table 5.2 presents the test matrix. The main reinforcements in the longitudinal direction were spaced at 145 mm, the transverse reinforcing bars were spaced at 200 mm. The top and bottom longitudinal bars protruded 110, 160, and 210 mm from one direction of the precast segments of length 1440, 1415, and 1390 mm, respectively, and extended into the UHPFRC closure joint to produce 100, 150, and 200 mm splice length, respectively. The main investigated test parameters herein were the splice length and the longitudinal reinforcement ratio (0.79 and 1.14%).

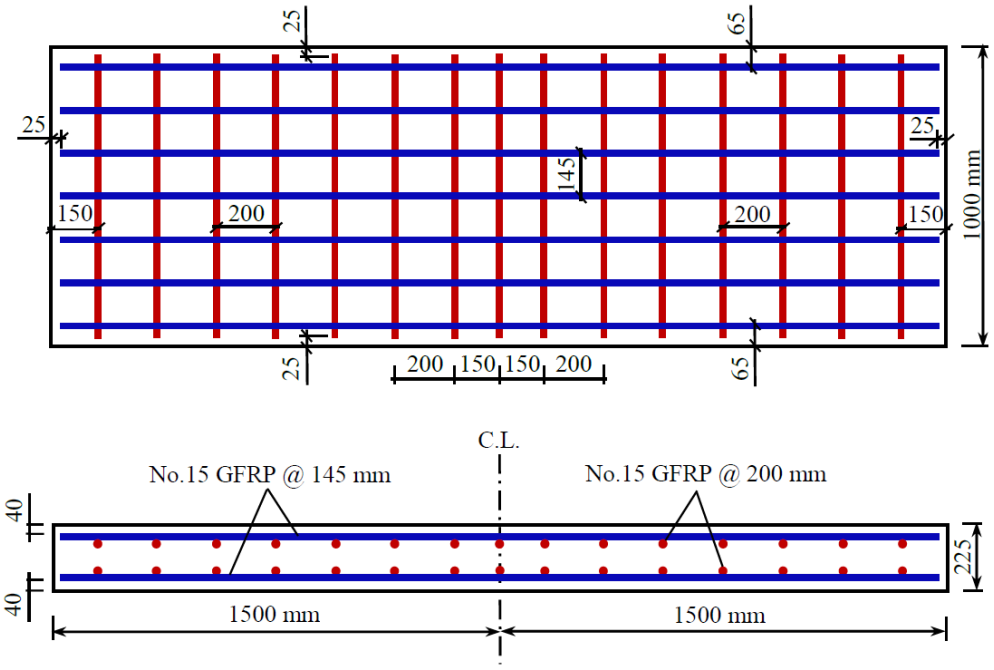

(a) Reference specimen

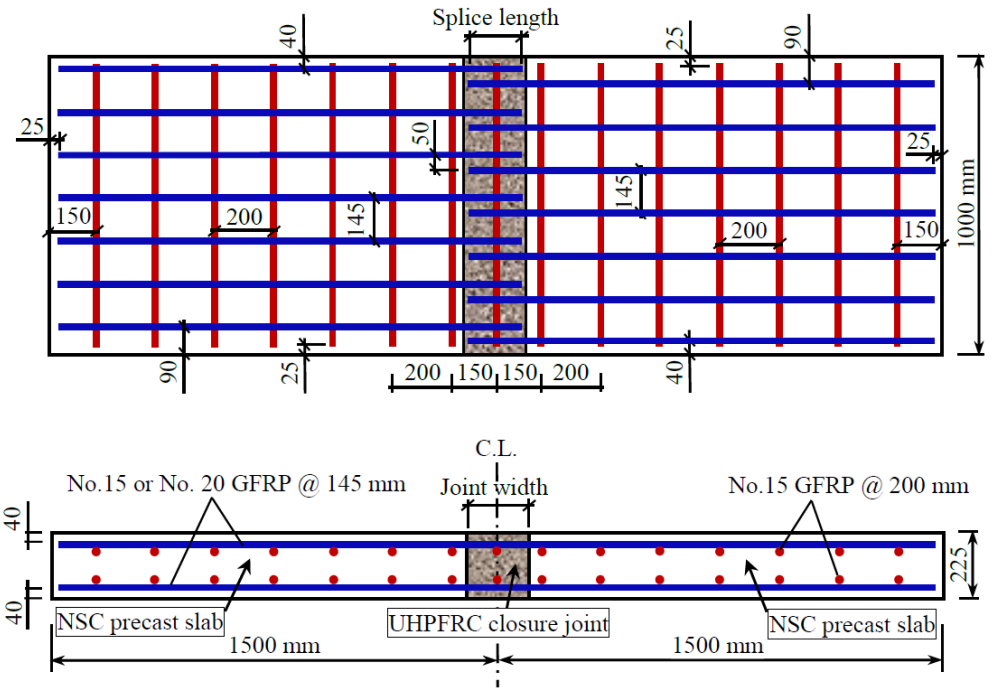

(b) Jointed specimens

Figure 5.3 - Geometry and reinforcement details of tested specimens

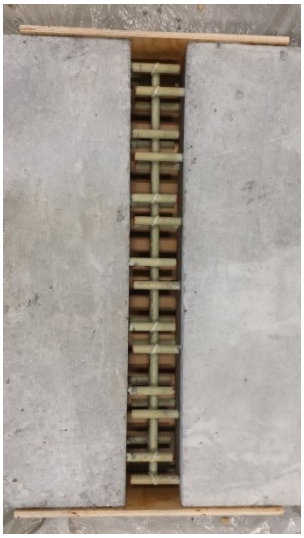

(a) 100 mm splice length

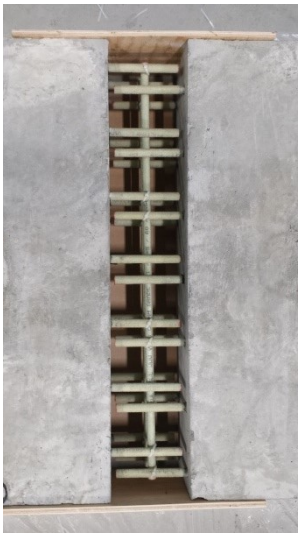

(b) 150 mm splice length

(c) 200 mm splice length

Figure 5.4 - The joint details

In preparation to the construction of the test specimens, as shown in Figure 5.5, The GFRP cages were assembled according to the longitudinal and transverse design spacing. Subsequently, the cages were instrumented and placed inside the formworks. The NSC was cast, compacted using an electrical vibrator, and leveled manually in fabricating the precast slabs. Moreover, curing was carried out at ambient temperature and humidity for 7 days, then the slabs were removed from the formwork. Each two identical precast segments were assembled beside each other in order to Construction of the UHPFRC closure joints. Once mixing was completed, the flow-table test was executed for each mix according to ASTM C230 (ASTM 2014) to ensure consistency of UHPFRC. The average flow diameter was 220 mm, as shown in Figure 5.5(d), which is in the acceptable range of 200 mm. Curing was carried out immediately after casting the UHPFRC by placing polythene sheet on the surface of the closure joints to eliminate water evaporation. Full specimens are presented in Figure 5.5(f).

Table 5.2 - Details of the Test Specimens

Specimen[a]	f_c' (MPa)		Precast segments Length (mm)	Splice length (mm)	Joint width (mm)	Main reinforcement	ρ_{act}[b] (%)	$\rho_{act} \times E_f$[c] (N/mm^2)
	Precast Slabs	Closure joints						
G-R-15-B	40	N/A	N/A	N/A	N/A	GFRP No. 15	0.79	507
G-100-15-B		170	1440	100	120	GFRP No. 15	0.79	507
G-150-15-B			1415	150	170	GFRP No. 15	0.79	507
G-200-15-B			1390	200	220	GFRP No. 15	0.79	507
G-100-20-B			1440	100	120	GFRP No. 20	1.14	735
G-150-20-B			1415	150	170	GFRP No. 20	1.14	735
G-200-20-B			1390	200	220	GFRP No. 20	1.14	735

Notes:
[a] (G) refers to GFRP - splice length - bar diameter (No. 15; No. 20) - B, where B is used to differentiate the samples ID through the extensive program.
[b] ρ_{act}: actual tensile reinforcement ratio.
[c] $\rho_{act} \times E_f$ = axial stiffness.

5.4.3. Instrumentation of Specimens

Different instruments were used to record the behavior of the tested specimens, as indicated in Figure 5.6 Electrical resistance strain gauges were used to measure the tensile strains in the GRRP reinforcing bars and the compressive strains in the concrete. Two strain gauges were installed on the middle of the GFRP longitudinal tension bars for the reference specimen. For the jointed specimens, however, six strain gauges were located at the critical positions of the longitudinal tension reinforcing bars as shown in Figure 5.6(a) to capture the strain along the splice length. Three strain gauges were affixed to the compression side of each specimen, at the mid-span and at 160 mm away from the center line, to measure the concrete compressive strains.

Four Linear Variable Displacement Transducers (LVDTs) with a precision of 0.01 mm were used to investigate the cracks on the bottom surface of the test specimens. The interfacial-crack width at the closure joint-precast slab interfaces was monitored using two

LVDTs (J1 and J2), as depicted in Figure 5.6(b). Moreover, the first two flexural cracks were recorded using two LVDTs (CR1 and CR2). The initial crack widths were measured by a 50X hand-held microscope.

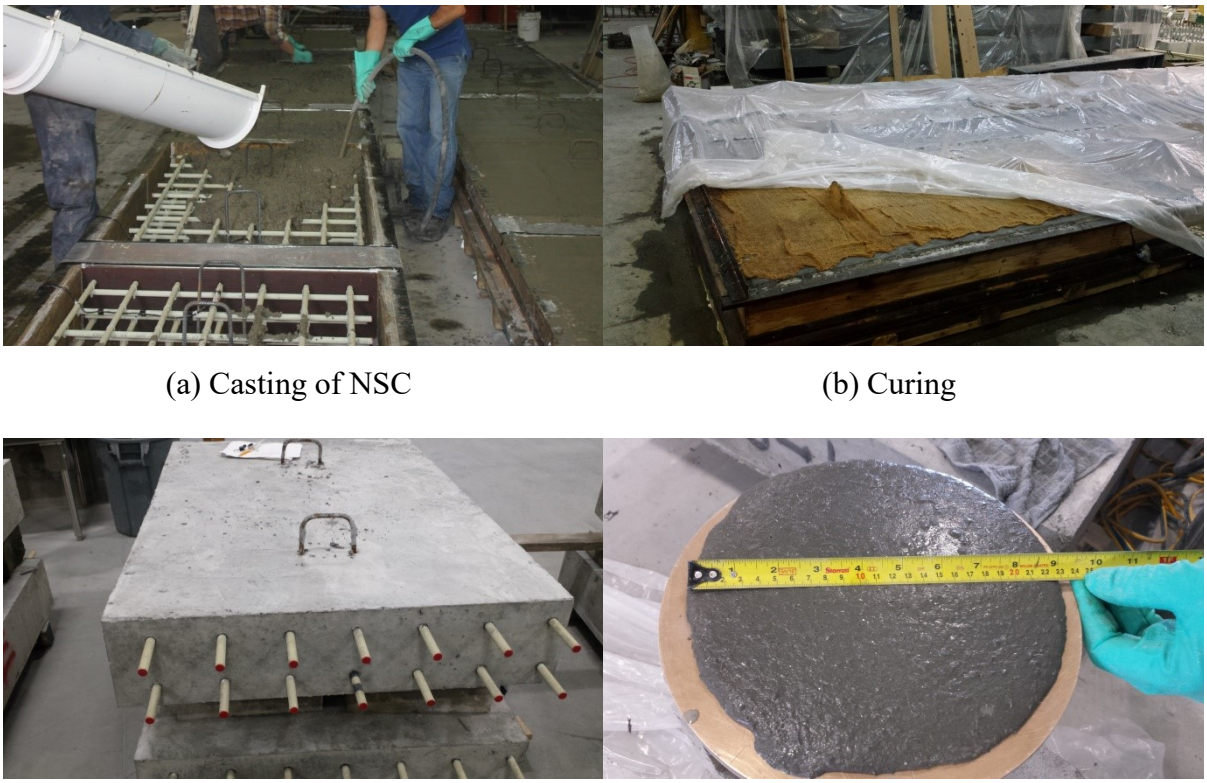

(a) Casting of NSC (b) Curing

(c) Slabs after curing (d) Flow-table test

(c) Joint casting (d) Full specimens

Figure 5.5 - Fabrication of the test specimens

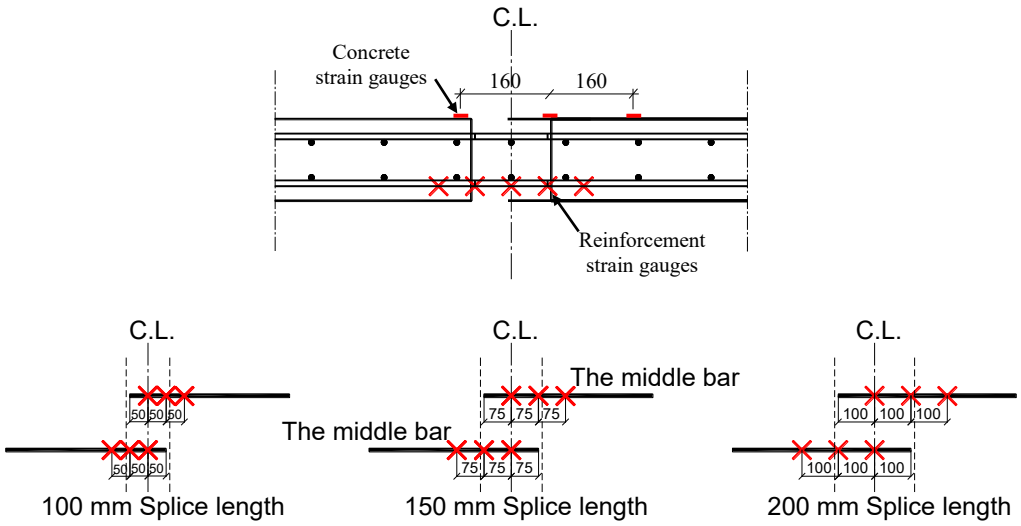

(a) Strain gauges for jointed specimens

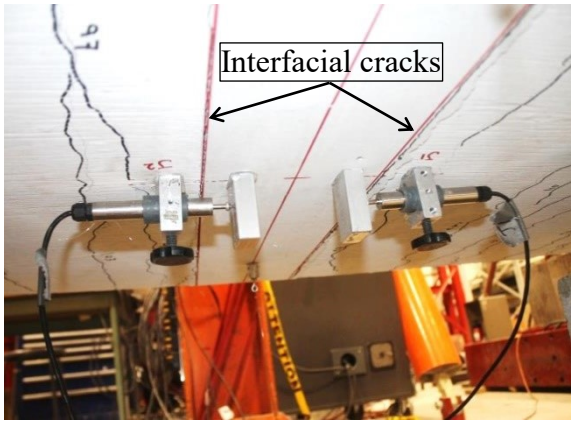

(b) LVDTs for the crack width

(c) Potentiometers for deflection

Figure 5.6 - Instrumentation of test specimens

Deflection of specimens at the mid-span was monitored using two potentiometers (Δ_A and Δ_B), as illustrated in Figure 5.6(c). An automatic data-acquisition system attached to a computer was used to record load, deflections, crack widths, and strains in concrete and reinforcement.

5.4.4. Test Setup and Procedure

The test specimens were loaded up to failure at the Canadian Foundation for Innovation (CFI) structural laboratory at the University of Sherbrooke. All specimens were simply supported with a 2600 mm clear span, and tested using a four-point bending scheme, as shown in Figure 5.7. A hinge support was located at one end of the specimen, while a roller support was located at the other end. The closure joint was located at the mid-span in a constant moment zone of 500 mm, and subjected to pure flexure without shear. To ensure full contact and load uniform distribution, neoprene pads of 10 mm thickness were placed between the concrete surface and the supports. The specimens were loaded with two equal line loads spaced at 500 mm about the centerline. The load was transferred from an actuator of capacity 1000 kN to a steel spreader beam, then transferred equally to the tested slab through two horizontal steel beams. 10-mm thick neoprene pads were placed between the steel beams and the concrete surface.

In preparation to the test, the LVDTs (J1 and J2) were installed at the joint-precast slab interfaces to monitor the joint opening during the test. During the test, however, at the first two cracks appearance, the load was paused and LVDTs (CR1 and CR2) were installed on the marked cracks right after measuring the initial crack widths with the hand-held microscope. The subsequent cracks were marked and the loading continued until failure. The test specimens were loaded in a stroke-controlled rate of 1.2 mm/min, and the test was completed when the specimen collapsed.

5.5. Test Results and Observations

The test results including effects of the test parameters are discussed herein in terms of crack load, failure load, crack pattern, mode of failure, mid-span deflection, Crack width, strains in GFRP splices and concrete, and deformability. Table 5.3 summarizes the test results.

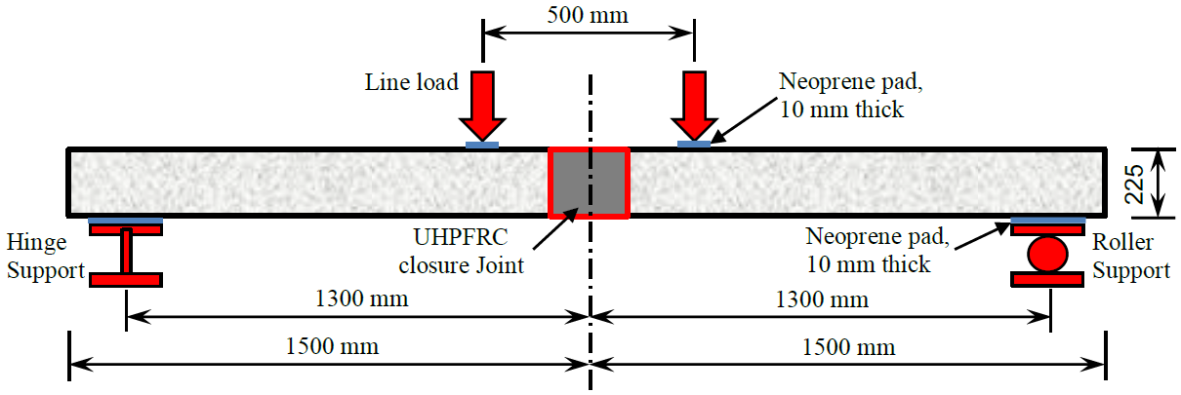

(a) Schematic

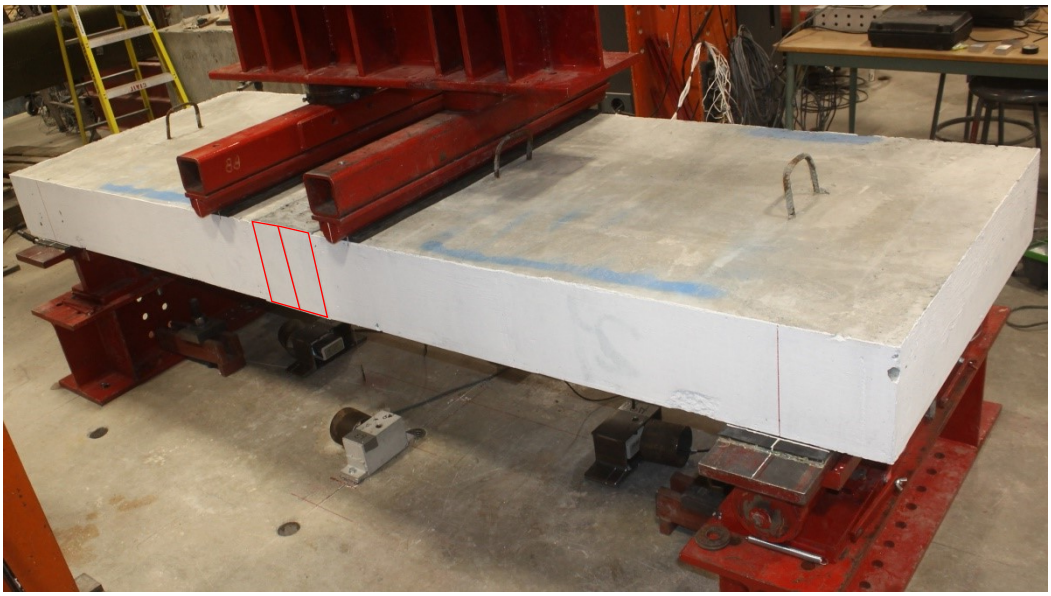

(b) Overview

Figure 5.7 - Testing setup

5.5.1. Crack Pattern and Failure Modes

In all of the tested specimens, the overall crack propagation followed the traditional crack pattern of simply supported slabs. Several flexural cracks extended along the bottom surface of the slabs, running adjacent and parallel to both loading steel beams. The cracking load (P_{cr}) ranged between 42.6 and 58.2 kN, with an average value of 50.4 kN. Figure 5.8 shows the typical observed modes of failure for all test specimens, while Figure

5.9 depicts the crack pattern for representative specimens at failure. Two different failure types were observed during testing; pull-out failure and diagonal tension shear failure. The specimens of 100-mm splice length (G-100-15-B and G-100-20-B) collapsed by a sudden pull-out failure between the splices and the UHPFRC. The pull-out failure resulted from high tensile stresses in the short splices embedded in the closure joint compared to their bond strength. The reference specimen and the other jointed specimens had a sudden diagonal tension failure. This mode of failure was expected due to the low modulus of elasticity of the GFRP bars, which provided a shear capacity lower than the section flexural capacity (Youssef et al, 2018a).

Table 5.3 - Summary of Test results

Specimen ID	f'_c (MPa)		P_{cr} (kN)	P_{ser} (kN)	P_{exp} (kN)	Δ_{cr} (mm)	Δ_{ser} (mm)	Δ_{max} (mm)	Failure Mode
	Slab	Joint							
G-R-15-B	44.0	N/A	48	87.3	262	1.4	8.5	44.8	Type I
G-100-15-B	51.7	195	43.3	84.7	254	1.6	8.1	46.4	Type II
G-150-15-B	51.7	195	45.3	88	264	2	9.5	47.2	Type I
G-200-15-B	51.7	195	42.6	95.3	286	1.3	8.5	48.8	Type I
G-100-20-B	50.7	195	58.2	83	249	2.2	5.9	31.1	Type II
G-150-20-B	50.7	195	57.1	109	327	2.5	9.1	40.7	Type I
G-200-20-B	50.7	195	52.8	108.7	326	2.1	8.1	39.5	Type I

Notes:
P_{cr}: first crack load; P_{ser}: service load; P_{exp}: experimental failure load; Δ_{cr}: deflection at the first crack; Δ_{ser}: deflection at the service load; Δ_{max}: maximum deflection at failure; Type I: shear failure; Type II: Pull-out failure.

In the reference specimen without a closure joint (G-R-15-B), the first flexural crack appeared at 300 mm from the centerline at a load of 48 kN (approximately 18% of the failure load). Subsequently, as the load increased, flexural cracks continued to appear within the flexural span and the shear span parallel to the first crack. Moreover, the cracks continued to propagate vertically upward through the slab thickness. At about 80% of the ultimate load, inclined cracks were observed along the shear span sides, extending diagonally towards the support and upward towards the loading point, leading to diagonal tension failure at an ultimate load of 262 kN.

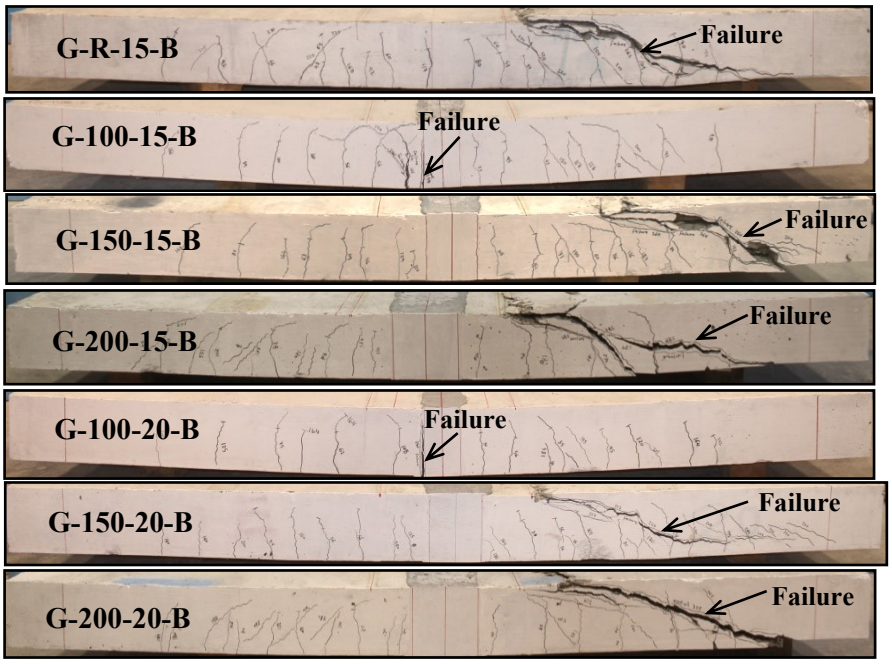

Figure 5.8 - Failure modes of the test specimens

In the jointed specimens (G-100-15-B, G-150-15-B, and G-200-15-B), the first flexural crack appeared at about 350, 340, and 260 mm from the joint centerline, respectively. The cracking loads were 43.3, 45.3, and 42.6 kN, respectively, ranged from 15 to 18 % of the ultimate load. The average cracking load of 44.2 kN showed a decrease of 8% compared to the reference specimen. The interfacial-crack at the joint- precast slab interface was observed at a lower load, with an average value of 20 kN. This crack continued propagating upward along the interface. Flexural cracks continued to propagate on the bottom surface and extended vertically on the slab sides. Diagonal cracks appeared on the slab sides at the shear span at nearly 80% of the ultimate load. Both of interfacial and flexural cracks widths increased as the applied load increased. For specimen G-100-15-B, a wide interfacial-crack was observed close to the ultimate load causing a sudden pull-out failure due to bars slippage at load of 254 kN, as shown in Figure 5.10(a). Specimens G-150-15-B and G-200-15-B behaved similar to the reference specimen G-R-15- B, the diagonal cracks extended along the sides within the shear span region causing a sudden diagonal tension failure. The ultimate loads were 264 and 286 kN for G-150-15-B, G-200-15-B, respectively. In specimens G-100-15-B and G-150-15-B, no significant effect on the

ultimate capacity was observed compared to the reference specimen. Conversely, the specimen G-200-15-B exhibited 9% increase in the ultimate capacity compared to the reference specimen. No visible cracks were observed in the closure joint due to the very high tensile strength of UHPFRC. Nevertheless, in specimen G-200-15-B, fine hair-like cracks were observed on the bottom surface of the UHPFRC closure joint at about 70% of the failure load.

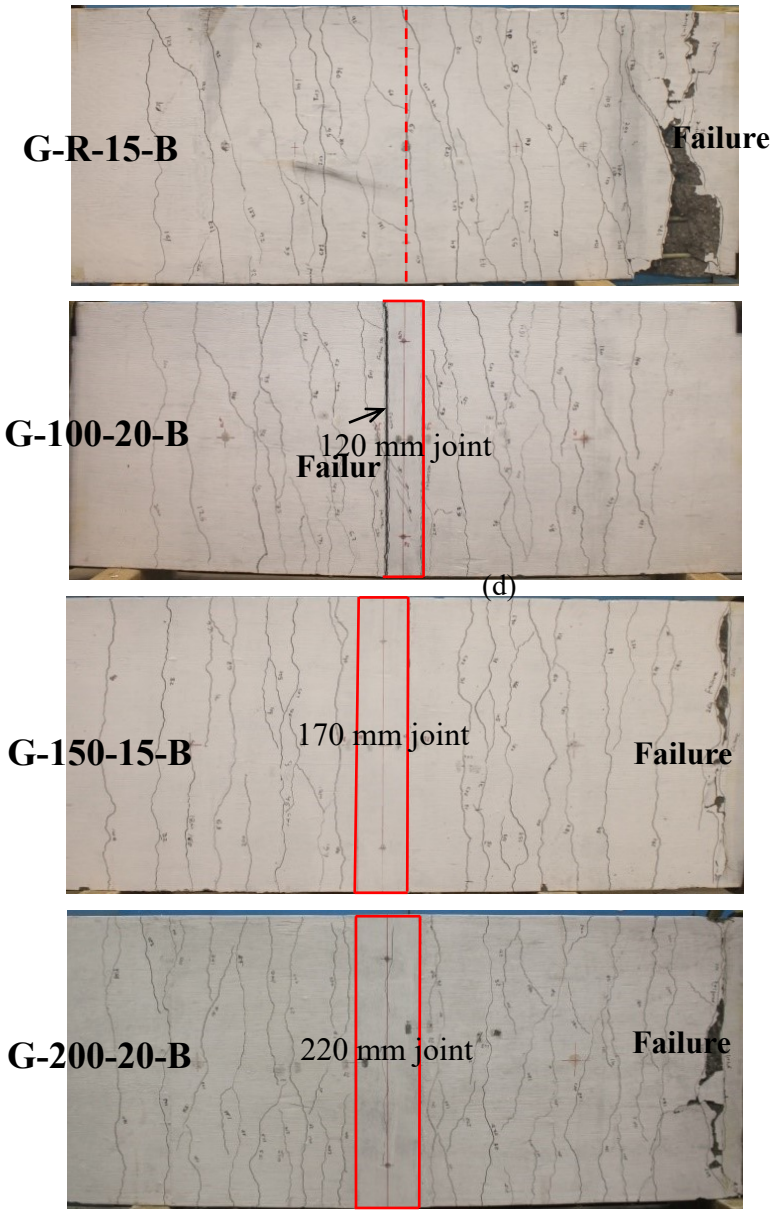

Figure 5.9 - Bottom view of the typical crack pattern

The jointed specimens reinforced with No. 20 GFRP bars (G-100-20-B, G-150-20-B, and G-200-20-B) behaved similarly to those with No. 15 GFRP bars. The cracking loads were 58.2, 57.1, and 52.8 kN at distance 320, 350, and 330 mm from the joint centerline, respectively. The cracking load ranged from 16 to 23 % of the ultimate load. The interfacial-crack started to widen at an average load of 25 kN, with an increase of 25% compared to No. 15 GFRP bars specimens. Other flexural cracks appeared as the load increased over the bottom surface and extended upward through the slab thickness. Subsequently, inclined shear cracks appeared on the sides at shear span at an average load about 75% of the failure load. Specimens G-150-20-B and G-200-20-B exhibited a diagonal tension failure at a load of 327 and 326, respectively. In contrast, Specimen G-100-20-B exhibited a sudden pull-out failure due to bars slippage from the joint, causing a wide crack at the joint-precast slab interface (Figure 5.10(b)). Unlike in specimens G-100-20-B and G-150-20-B, which there were no cracks observed on the closure joint, fine hair-like cracks appeared on the bottom surface of the closure joint of specimen G-200-20-B at about 68% of the failure load.

Increasing the reinforcement ratio by 44%, by a comparison between the specimens reinforced with No. 15 and No. 20 GFRP bars, showed that G-150-20-B and G-200-20-B provided an increase of 23, 14% compared to G-150-15-B, and G-200-15-B, respectively. In contrast, no significant effect in the ultimate capacity was found between G-100-20-B and G-100-15-B. The average cracking load increased by 27% due to increasing the reinforcement ratio by 44%.

Splice length of 100 mm was not long enough and insufficient to maintain the continuity between the precast slabs, which led to a sudden pull-out failure at the joint-precast slab interface. Correspondingly, both of 150 and 200 mm splice lengths were able to transfer tension between the precast slabs, which resulting in the specimens behaved equivalently to the reference specimen despite the presence of two interfacial-cracks.

(a) G-100-15-B

(b) G-100-20-B

Figure 5.10 - Typical bar slippage from the UHPFRC closure joint

5.5.2. Effect of Test Parameters on Load-Deflection Response

Figure 5.11 provides the applied load versus the maximum deflection at the mid-span for all tested specimens. Table 5.3 lists the deflection at the first crack and at the failure, the deflection values represent the average of the two potentiometers (Δ_A, Δ_B), shown in Figure 5.6(c). The load-deflection relationships were in good agreement for all specimens, the reference and jointed specimens behaved similarly showing typical bilinear relationships. The initial line of the relationships was governed by the pre-cracking stiffness, in which all the specimens had almost the same pre-cracking stiffness regardless

the reinforcement ratio, as the stiffness was governed by the gross concrete section. After onset of the first crack, the post-cracking stiffness decreased as cross-section cracked. Accordingly, the axial reinforcement stiffness significantly affected the post-cracking response until failure. Despite rigidity of the UHPFRC closure joint, its small size did not affect the specimen stiffness, accordingly, there was no significant effect on the deflection behavior.

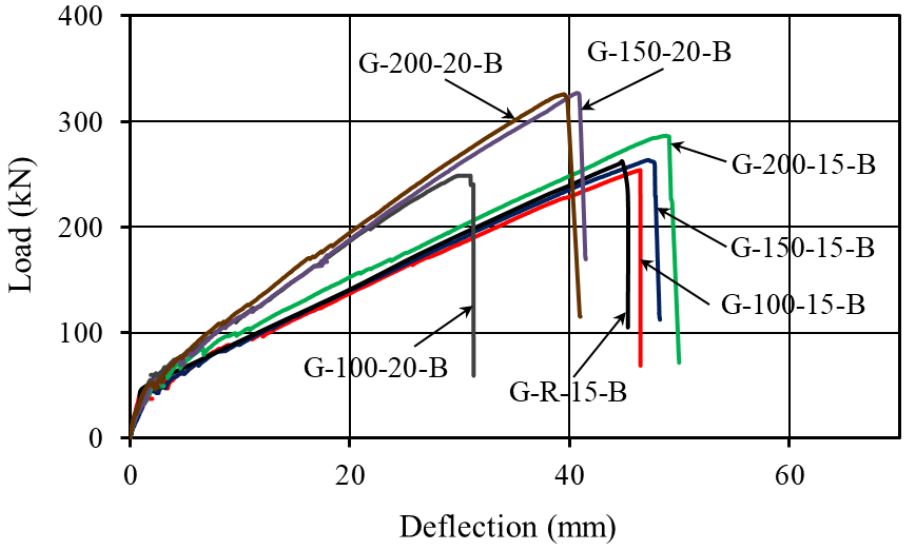

Figure 5.11 - Typical load-deflection relationships

The deflections at cracking load of all specimens (Δ_{cr}) are listed in Table 5.3. The reference specimen G-R-15-B exhibited 1.4 mm deflection at the cracking load of 48 kN, whereas the average deflection of the jointed specimens reinforced with No. 15 GFRP bars was 1.6 mm at an average cracking load of 43.7 kN.

Specimens G-R-15-B, G-100-15-B, G-150-15-B, and G-200-15-B exhibited a maximum deflection at failure of 44.8, 46.4, 47.2 and 48.8 mm, respectively. In addition, the deflection values and the same the load-deflection responses confirm that the joints maintained continuity and the jointed specimens behaved like the reference specimen until failure. Moreover, no significant effect of the splice length of No.15 GFRP bars on the deflection behavior of the specimens.

In the specimens reinforced with No. 20 GFRP bars (G-100-20-B, G-150-20-B, and G-200-20-B), the average deflection of 2.3 mm was monitored at an average cracking load of 56 kN, providing about 44% more than the cracking deflection in No.15 GFRP specimens. This is because the cracking load increased and subsequently the deflection increased. No.20 GFRP specimens showed lower deflection values at failure compared against that of the specimens reinforced with No. 15 GFRP bars. The ultimate deflection was 31.1, 40.7, and 39.5 mm, respectively. For the three splices tested herein 100, 150, and 200 mm, increasing the reinforcement ratio by 44% (from GFRP bars No. 15, area 199 mm^2 to GFRP bars No. 20, area of 284 mm^2) decreased the ultimate deflection by 49, 16, and 24%, respectively. On the other hand, at the same load, the deflection decreased by about 30% due to 44% increase in the reinforcement ratio. For the specimens reinforced with No. 20 GFRP bars, at the same load, the splice length had no significant effect on the deflection value. The small ultimate deflection of specimen G-100-20-B (31.1 mm) resulted from the early low load of pull-out failure. The deflection of G-150-20-B and G-200-20-B was almost the same until failure. It is worth mentioning that using the splice length of 150 or 200 mm accompanied with higher reinforcement ratio enhanced the post-cracking stiffness, accordingly, resulted in lower deflection at the same load level up to failure.

The service-load was set to 30% of the ultimate capacity of each specimen (0.30 P_{exp}). This value was considered by many researchers as a service-load (Mota at al., 2006, Bischoff, 2009, and El-Nemr et al. 2013, Lee and Lee, 2015, Elgabbas et al. 2016, Youssef et al. 2018a). The service load values (P_{ser}) and the corresponding deflections (Δ_{ser}) of the test specimens are listed in Table 5.3. The service-load ranged from 83 to 109 kN, and the corresponding deflection ranged from 5.9 to 9.5 mm. Since the deflection is not a design criterion in the bridge-deck slab in the CHBDC (CAN/CSA S6, 2014), the mid-span deflection at the service-load was compared to the serviceability requirements of AASHTO LRFD (2009, 2012). The deflection at service-load should not exceed L/800, where L is the span length from center-to-center of supports which was equal to 2600 mm (Deflection limit = 2600/800 = 3.25 mm). All the test specimens including the reference specimen exhibited deflections at the service-load larger than the specified limit of AASHTO LRFD (2009, 2012). It is worth mentioning that the deflections in the actual bridge deck are

expected to be less than what were measured in the laboratory at the same load level due to continuity of the slab over girders. Consequently, the deflection limit of AASHTO LRFD (2009, 2012) may be used as a service limit for such jointed bridge-deck slabs when the deflection is of concern.

5.5.3. Crack Width

During the test, cracks appeared within the flexural span then propagated to the shear span on the bottom surface of the specimen. The first two flexural cracks (CR1 and CR2) and the two interfacial cracks were recorded. For the reference specimen (G-R-15-B), the crack widths were not recorded due to a system error and the LVDTs malfunctioned. Table 5.4 lists the first flexural-crack width (CR1) and the average interfacial-crack width (ICR) at both the service-load and failure load. Figure 5.12 shows the variation of the measured crack widths (CR1, CR2, and ICR) versus the applied load for the tested specimens. The crack width varies linearly with the applied load up to failure and the coefficient of determination (R^2) ranged from 0.95 to 1. Thus, the load-crack width relationships were not significantly influenced by the splice length or the reinforcement ratio. These findings are in good agreement with past work conducted with GFRP (Arafa et al. 2016; Youssef et al. 2018a), and with steel (Lee and Lee, 2015).

Table 5.4 - Crack width at service and failure-load

Specimen ID	Flexural crack width (mm)		interfacial crack width (mm)	
	P_{ser}	P_{exp}	P_{ser}	P_{exp}
G-R-15-B	---[a]	---[a]	N/A	N/A
G-100-15-B	0.53	1.59	0.32	1.86
G-150-15-B	0.56	1.97	0.59	2.42
G-200-15-B	0.44	1.98	0.45	1.45
G-100-20-B	0.35	1.1	0.27	1.54
G-150-20-B	0.46	1.28	0.4	1.6
G-200-20-B	0.42	1.5	0.3	1.22

Notes: P_{ser}: at service load level; P_{exp}: at failure load; [a] the LVDT malfunctioned.

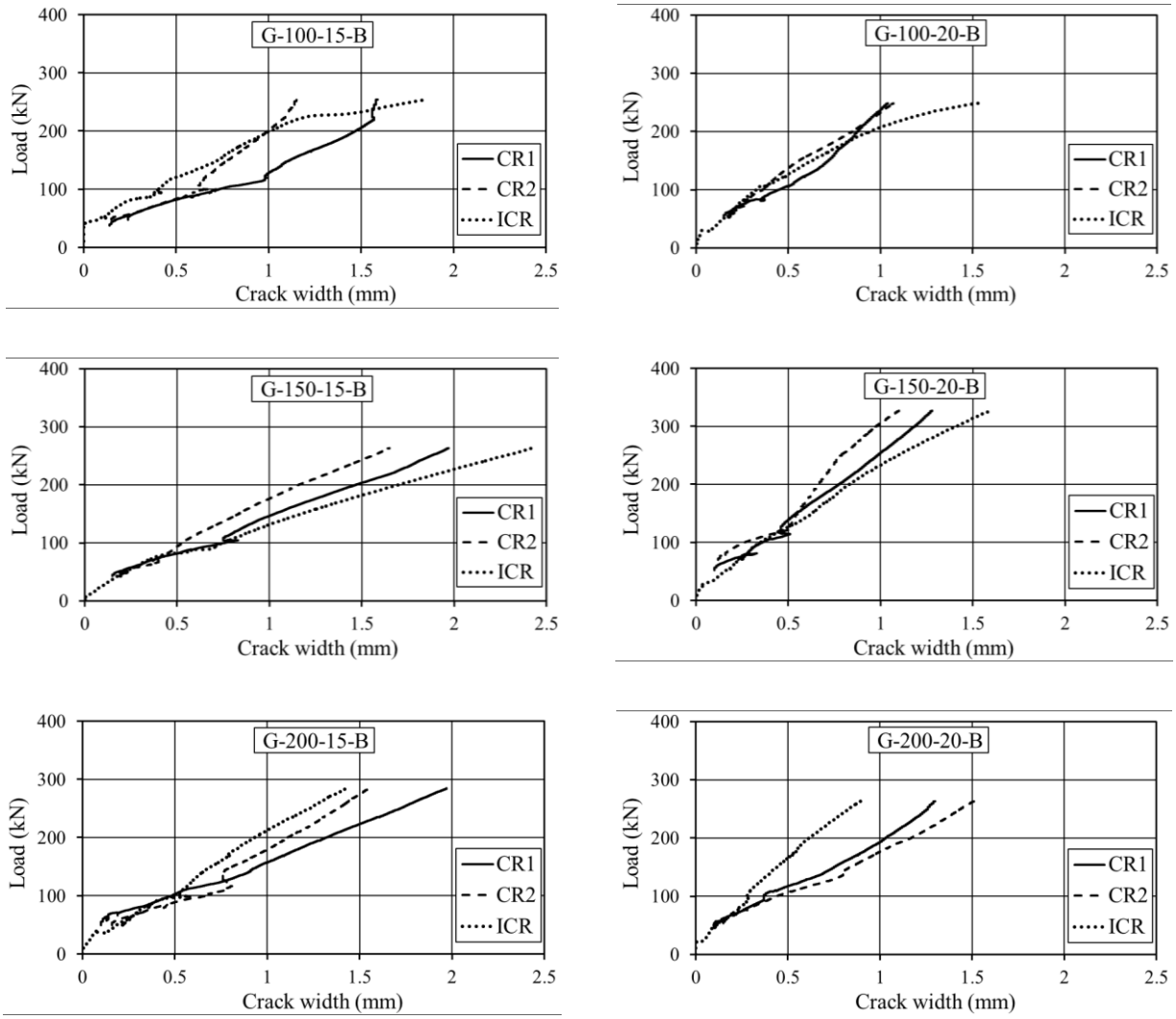

Figure 5.12 - Load-crack width relationships

The specimens G-100-15-B, G-150-15-B, and G-200-15-B exhibited flexural-crack widths of 1.59, 1.97, and 1.98 mm, respectively, at failure. Accordingly, increasing the splice length from 100 mm to 150 and 200 mm increased the flexural-crack width by 24% and 0.5%, respectively. In addition, increasing the reinforcement ratio by 44% in No. 20 GFRP specimens (G-100-20-B, G-150-20-B, and G-200-20-B decreased the flexural-crack width at failure by about 40%, compared to No.15 GFRP specimens. This can be attributed to the fact that the higher reinforcement ratio reduces the stress in the GFRP bars and consequently yields smaller crack widths. Furthermore, In No.20 GFRP specimens, the

flexural-crack width increased by 16% and 36% when the splice length increased from 100 mm to 150 and 200 mm, respectively, at the failure load.

Interfacial-cracks are inherent in the UHPFRC closure joint and should be considered as a representative parameter of the serviceability of closure joint (Lee and Lee, 2015). For specimens G-100-15-B, G-150-15-B, and G-200-15-B, the interfacial-crack widths at failure were 1.86, 2.42, and 1.45 mm, respectively, with an average value of 1.90 mm. Specimens G-100-20-B, G-150-20-B, and G-200-20-B exhibited interfacial-crack widths at failure of 1.54, 1.60, and 1.22 mm, respectively, with an average value of 1.45 mm. Accordingly, 44% increase in the reinforcement ratio decreased the interfacial-crack width by an average value of 24 %. By increasing the reinforcement ratio, the interfacial-crack width decreased as a result of reduction in the strain of the GFRP splices. Increasing the splice length was expected to decrease the interfacial-crack width, this tendency was not observed in the test results. This could be attributed to the range of splice length used in this work (100 to 200 mm), further investigation may be needed with wide range of splice length.

At the service-load (0.30 P_{exp}), the flexural-crack width of the test specimens ranged from 0.42 to 0.56 while the interfacial-crack width ranged from 0.3 to 0.59. The flexural and interfacial-crack widths were compared to the crack width limit at the service-load for members subjected to aggressive environments, which is 0.5 mm, (AASHTO LRFD, 2009 and CAN/CSA S6, 2014). The measured crack widths for the test specimens were well below the allowable code limit of 0.5 mm except in G-100-15-B and G-150-15-B, which had a bit higher crack width, but still in the acceptable range.

5.5.4. Strains in GFRP-reinforcement and concrete

Using the strain gauges described earlier, reinforcement strains were monitored along the splice length for the jointed specimens. In the reference specimen G-R-15-B, the strains were not recorded due to a system error and the two strain gauges malfunctioned. Also, strain in UHPFRC and NSC were measured. Figure 5.13(a) shows the applied load versus the maximum measured strains in GFRP splices as well as in the top surface of the NSC

for selected specimens. The load–strain relationships were typically bilinear, the strains in the GFRP and concrete varied linearly with increasing the load after the cracking up to failure (Youssef et al. 2018a). The observations prove that the GFRP splices transferred the loads between the precast segments for all specimens until failure. Bond-strength degradation was only observed in the specimens of short splice length of 100 mm close to the failure load, which resulted in pull-out failure.

The jointed specimens exhibited maximum measured tensile strains in FRP at failure ranged between 5348 and 9800 με, which represent 31% to 53% of the ultimate strain (Pultrall, 2016). The NSC compressive strains ranged from 1970 to 2768 με, these values are less than the ultimate concrete compressive specified by CAN/CSA S6 (2014) and AASHTO LRFD (2009). The tensile strain in the GFRP splices increased as the joint width decreased (Figure 5.13(a)). Increasing the splice length from 100 to 150 and 200 mm (comparing G-100-15-B to G-150-15-B and G-200-15-B, respectively) decreased the maximum strain in the FRP splices by 10 and 30%, respectively, at the same load level. This can be attributed to an increase in the bonding stresses as the splice length decreased to transfer the same magnitude of tension.

Figures 5.13(b and c) present the strain distributions along the GFRP splices at service and failure-load levels for specimens G-150-15-B and G-150-20-B. It can be noted that the test specimens maintained the same strain distribution along both sides of the joint centerline. Consequently, this also confirms a successful load transfer between the precast slabs through the closure joint. The measured strains in both GFRP bars and concrete decreased with an increase in the GFRP reinforcement ratio. For the specimens reinforced with No.20 GFRP bars, 44% increase in the reinforcement ratio decreased the GFRP strain with an average value of about 37%, at the same load level.

For serviceability requirements of the CHBDC (CAN/CSA S6, 2014), the tensile stress under service load should not exceed 25% of the guaranteed tensile strength of the GFRP bars. For the jointed specimens, the monitored tensile stresses in the GFRP bars ranged between 152 and 223 MPa, at service-load (0.30 P_{exp}). This range of tensile stresses, however, is less than 25% of the guaranteed tensile strength (0.25 × 1185 = 296 MPa).

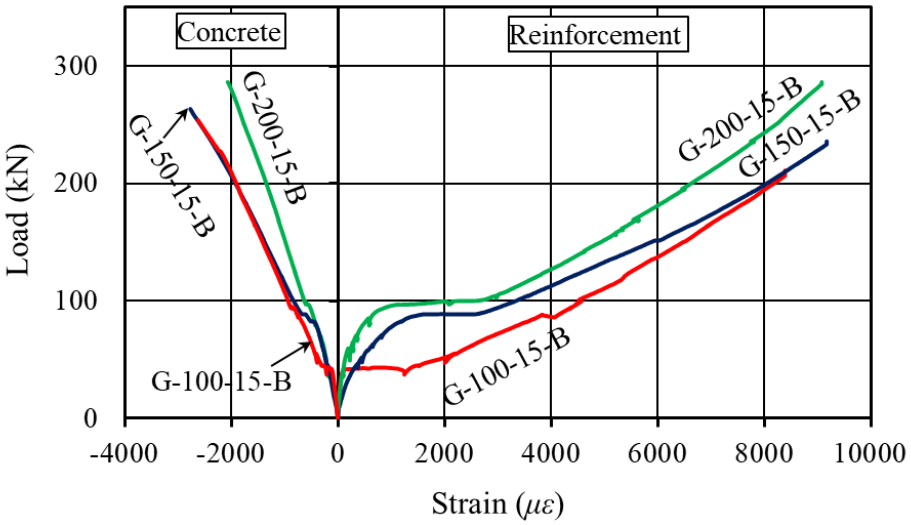

(a) Representative load-strain relationships for FRP and concrete

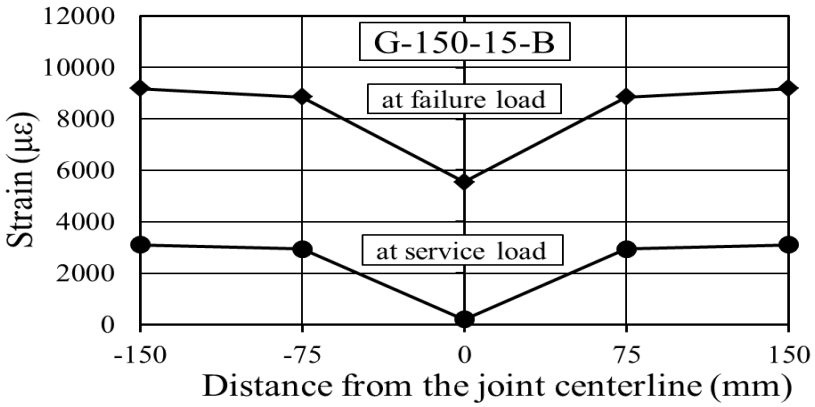

(b) Strain distribution of G-150-15-B

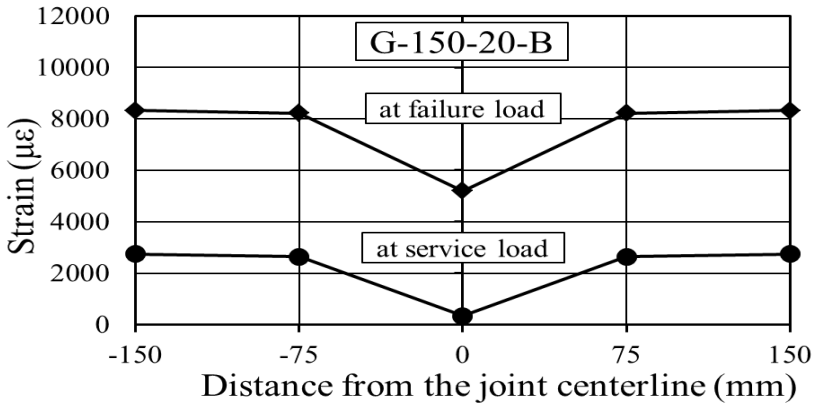

(c) Strain distribution of G-150-20-B

Figure 5.13 - Load- GFRP strain relationships

5.5.5. Curvature and Deformability

Figure 5.14 shows the experimental curvature (Ψ) at mid-span versus the applied load for the jointed specimens. Curvatures were calculated at the service and ultimate load levels based on the measured strains of UHPFRC and GFRP splices at the mid-span. Table 5.5 lists the measured strains of FRP and UHPRFC at the middle of the joint, these values were not the maximum strains. Neutral axis-to-depth ratio (*c/d*) is calculated at the middle of the joint for each specimen at failure load according to Eq. 5.1. The curvature of an uncracked cross-section is determined using Eq. 5.2.

$$\frac{c}{d} = \frac{\varepsilon_c}{\varepsilon_c + \varepsilon_t} \tag{5.1}$$

$$\psi = \frac{M}{EI} = \frac{\varepsilon_c}{c} \tag{5.2}$$

Where c is the neutral axis depth (mm), d is distance from the extreme compression fiber to the centroid of tension force (mm), ε_c is the concrete compressive strain, ε_t is the FRP tensile strain, Ψ is the curvature (mm^{-1}), M is the applied moment, EI is the bending stiffness of the cross-section.

The specimens exhibited typical bilinear load-curvature relationships, the relationships were not significantly influenced by the splice length or the reinforcement ratio. It was observed that as the joint width increased, the experimental curvature decreased.

Specimens G-100-15-B, G-150-15-B, and G-200-15-B exhibited a curvature at failure of 3.7, 3.42, and 2.81 x 10^{-2} m^{-1}, respectively, with an average value of 3.32 x 10^{-2} m^{-1}. Increasing the splice length from 100 to 150 and 200 mm decreased the curvature by 9 and 32%, respectively. The specimens reinforced with No.20 GFRP bars exhibited an average curvature of 3.1 x $10^{-2}m^{-1}$. Accordingly, 44% increase in the reinforcement ratio decreased the curvature at failure by 7%.

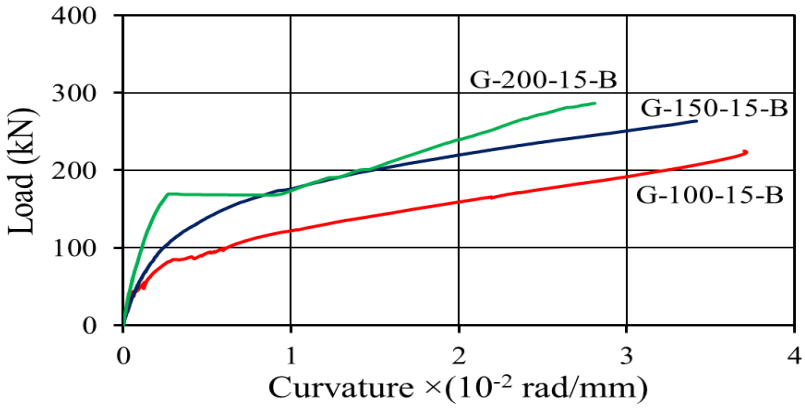

(a) No.15 GFRP specimens

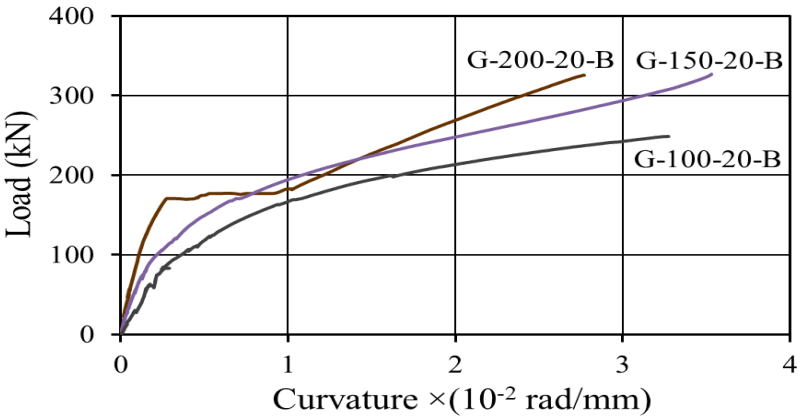

(b) No.20 GFRP specimens

Figure 5.14 - Load-curvature relationships for the jointed specimens

Deformability of FRP reinforced concrete elements can be defined as the capacity of the structural element to absorb energy without suffering failure, and is generally related to the amount of inelastic deformation that takes place before a complete failure (Jaeger et al. 1997). Deformability factor *J* can be determined using Eq. 5.3 according to CAN/CSA S6 (2014). The *J*-factor is calculated as the ratio of the value of the ultimate moment M_u and its corresponding curvature ψ_u to the service moment M_s and its corresponding curvature ψ_s. The service moment is set as 30% of the ultimate moment (M_s = 0.30 M_u)

$$J = \frac{M_u}{M_s} \times \frac{\psi_u}{\psi_s} \tag{5.3}$$

Table 5.5 - Curvature and Deformability of the Test Specimens

Specimen ID	FRP strain ($\mu\varepsilon$)		UHPFRC strain ($\mu\varepsilon$)		(c/d)	Ψ x 10^{-2}, m^{-1}		J
	P_{ser}	P_{exp}	P_{ser}	P_{exp}	P_{exp}	P_{ser}	P_{exp}	
G-100-15-B	346	5965	179	585	0.09	0.30	3.70	4.11
G-150-15-B	206	5548	131	499	0.08	0.19	3.42	6.00
G-200-15-B	150	4256	110	717	0.14	0.10	2.81	9.37
G-100-20-B	340	5142	175	602	0.11	0.29	3.27	3.76
G-150-20-B	332	5506	131	685	0.11	0.26	3.53	4.53
G-200-20-B	94	4058	118	800	0.17	0.12	2.77	7.69

Notes:
(c/d): neutral axis-to-depth ratio; P_{ser}: at service load; P_{exp}: at failure load; Ψ: experimental curvature; J: deformability factor.

The CHBDC (CAN/CSA S6, 2014) requires that the deformability factor (J) shall be at least 4 for rectangular sections reinforced with FRP. Table 5.5 lists the value of J-factor using the above approach, which ranged from 3.76 to 9.37. Except specimen G-100-20-B, the tested specimens exhibited J-factor well above the code limit. The J-factor increased as the splice length increased. Increasing the splice length from 100 to 150 and 200 mm (comparing specimen G-100-15-B to G-150-15-B and G-200-15-B) increased the J-factor by 46 and 128%, respectively. 44% increase in the reinforcement ratio decreased the J-factor by 22%, comparing No.20 GFRP specimens to No.15 ones. The J-factor indicates the amount of cracks and deflections of the FRP-reinforced concrete member can exhibit from service to ultimate conditions (El-Salakawy and Benmokrane, 2004). Besides, the higher value of J-factor indicates the more broad warning the FRP-reinforced concrete member gives before failure.

5.6. Comparison of Predicted and Experimental Capacities

Based on the design provisions of the available bridge codes AASHTO LRFD (2009) and CAN/CSA S6 (2014), the ultimate shear capacities of the specimens failed in shear were predicted. The predicted shear values were compared to the experimental results to identify

the accuracy of the available code provisions. Since the shear failure occurred in the precast slabs, the prediction was executed using the properties of the NSC. Table 5.6 provides the ratios of the measured to the predicted shear capacities (V_{exp}/V_{pred}) according to AASHTO LRFD (2009) and CAN/CSA S6 (2014). Figure 5.15 - presents a comparison of the ratios V_{exp}/V_{pred} for the test specimens.

Table 5.6 - Prediction of Ultimate Shear Capacity

Specimen ID	V_{exp}[a] (kN)	AASHTO LRFD (2009)		CAN/CSA S6 (2014)	
		V_{pred}[b] (kN)	V_{exp}/V_{pred}	V_{pred}[b] (kN)	V_{exp}/V_{pred}
G-R-15-B	131	82	1.60	86	1.52
G-150-15-B	132	86	1.53	92	1.43
G-200-15-B	143	86	1.66	92	1.55
G-150-20-B	164	101	1.62	105	1.56
G-200-20-B	163	101	1.61	105	1.55
Mean			1.60		1.52
Standard Deviation (SD)			4.72%		5.36%
Coefficient of variation (COV)			2.94%		3.52%

Notes:
[a] V_{exp}: experimental shear strength = P_{exp} / 2.
[b] V_{pred}: predicted shear strength at failure.

Generally, the provisions underestimated the shear strength with different degrees of conservatism. AASHTO LRFD (2009) yielded very conservative predictions with an average V_{exp}/V_{pred} value of 1.60, with a standard deviation of 8.27%. CAN/CSA S6 (2014), however, provided reasonable yet conservative predictions compared to AASHTO LRFD (2009), with an average V_{exp}/V_{pred} of 1.52 and a standard deviation of 5.36%. Moreover, these findings are in agreement with past work conducted by Youssef et al. (2018a) and Arafa et al. (2016) for bridge-deck slabs spliced with UHPFRC joints.

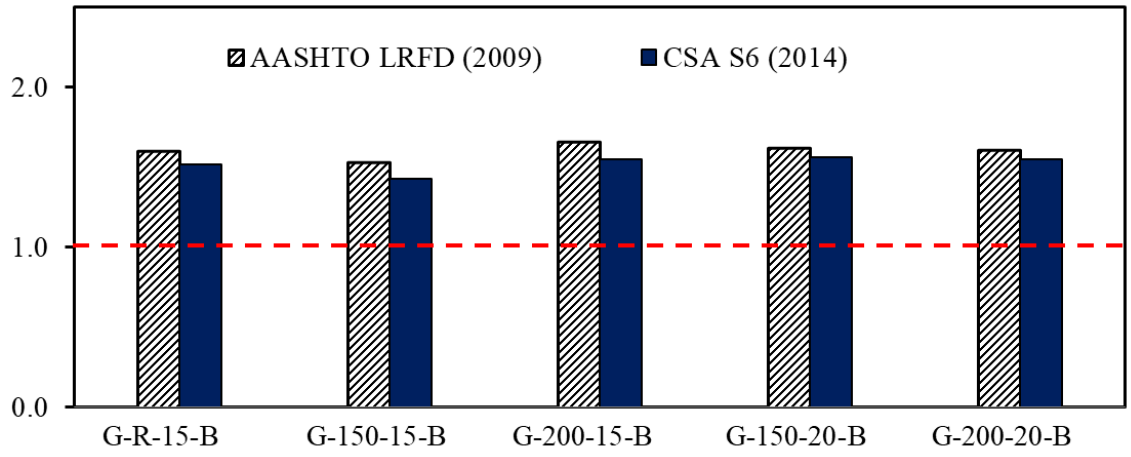

Figure 5.15 - Comparison of V_{exp}/V_{pred} for the test specimens

5.7. Conclusions

This paper was carried out to investigate the flexural performance of the UHPFRC closure joint between precast bridge-deck slabs reinforced with GFRP bars. A total of seven full-size one-way concrete slab specimens of dimensions 3000 mm long × 1000 mm wide × 225 mm thick, including a reference specimen and six jointed specimens, were constructed and tested. Three splice lengths (100, 150, and 200 mm) and two GFRP reinforcement ratios (0.79 and 1.14%) were considered in this study. The specimens were tested to failure in a four-point bending scheme, with the UHPFRC closure joint subjected to pure flexural stresses. Based on the experimental test results and discussions, the main conclusions are as follows:

- The presence of the UHPFRC closure joint connecting the GFRP-RC precast slabs had no degradation effect on the ultimate capacity or mid-span deflection compared to the reference specimen, with negligible difference.
- The mode of failure was significantly affected by the splice length. The specimens of 100-mm splice length exhibited a sudden pull-out failure due to bond-strength degradation between the GFRP splices and the UHPFRC occurred close to the failure load. Increasing the splice length to 150 and 200 mm changed the failure

mode into diagonal tension failure within the shear span, thereafter, the specimen capacity was dominated by the strength of the NSC precast slabs.

- For the jointed specimens with 150 and 200-mm splice length, increasing the GFRP reinforcement ratio by 44% increased both cracking and ultimate capacities by about 25%.
- All the test specimens showed a typical bilinear load-deflection relationship up to failure. The splice length had no significant effect on the deflection value at the same load. For a given load, It was observed that the deflection decreased by about 30% due to 44% increase in the reinforcement ratio.
- The test observations showed initial cracks at the joint-precast slab interfaces. These interfacial-cracks are inherent and appeared at earlier loading stages compared to the other flexural-cracks. Unlike expected, no clear effect of the splice length was observed in this study (100 to 200 mm) on the interfacial crack-width.
- At failure, the tensile strains in the GFRP splices ranged between 31 and 53% of the ultimate strain. The tensile strain in the GFRP splices was observed to increase as the splice length decreased. Increasing the reinforcement from by 44% (from GFRP No. 15 to No. 20) decreased the bar tensile strain by about 37%.
- For all tested specimens except G-100-20-B, The values of the deformability factor ($J > 4$) were well above the limit required by the Canadian Highway Bridge Design Code CHBDC (CAN/CSA S6, 2014). The *J*-factor increased as the splice length increased. Increasing the GFRP reinforcement ratio from No.15 to No.20 decreased the J-factor by about 22%.
- At the assumed service load of 0.30 V_{exp} , The tested specimens satisfactorily meet the serviceability allowable limits in terms of crack width and stresses in the GFRP bars.
- The current shear provisions in AASHTO LRFD (2009) provided conservative predictions for the shear capacity of GFRP-RC deck slabs with an average V_{exp}/V_{pred} of 1.60. On the other hand, the CHBDC (CAN/CSA S6, 2014) showed reasonable yet conservative predictions with an average V_{exp}/V_{pred} of 1.52.

- A GFRP splice length of 150-mm or 9.5 d_b, whichever is greater, embedded in UHPFRC closure joint, is sufficient to guarantee adequate continuity and transfer the loads between the precast slabs to behave equivalent to monolithic concrete specimen. Accordingly, no slippage or bond-strength degradation was observed and the failure occurred within the shear span away from the joint. Moreover the joint remained intact up to failure without visible damage. More investigations are needed to assess the performance of 150-mm splice length under cyclic and fatigue tests.

CHAPTER 6 GENERAL CONCLUSIONS AND RECOMMENDATIONS

6.1. Summary

This thesis presents the results of a detailed experimental investigation including fourteen full-scale one-way GFRP reinforced concrete slab specimens. The main objective of this study was to provide a better understanding of the structural behavior of the UHPFRC closure joints between GFRP-RC bridge-deck slabs, as a common technique of accelerated bridge construction (ABC). The splice length was 100, 150, and 200 mm in a joint width of 120, 170, and 220 mm, respectively. Two GFRP reinforcement ratios (0.79 and 1.14%) were considered in this study. The specimens were classified into two phases according to the loading case, at which the closure joints were subjected to either combined flexural and shear stresses or pure flexural stresses. Each phase contained seven specimens; one reference specimen without closure joint and six jointed specimens. The jointed specimen consisted of two precast slabs connected with a closure joint.

For the first phase (Phase I), the specimens were tested up to failure in a cantilever –panel setup under quasi-static line loading. The closure joints were located at the zone of maximum negative moment and subjected to flexural and shear stresses. In the second phase (Phase II), the specimens were loaded to failure using a four-point bending scheme, the closure joints were positioned in the middle of the constant moment region and subjected to pure flexural stresses. The test results were discussed and analyzed in terms of crack pattern, load–deflection response, crack width, and GFRP-reinforcement and concrete strains. Moreover, the experimental failure loads were compared to the current Bridge design codes and guidelines.

6.2. Conclusions

Based on the experimental testing and the analysis conducted in this research program, the following conclusions are drawn:

6.2.1. Closure Joints Subjected to Combined Shear and Flexural Stresses

1. The observed mode of failure for all test specimens was diagonal tension failure within the cantilever zone (NSC slabs). The use of GFRP reinforcement with a splice length of 100 mm to 200 mm in the UHPFRC joint enabled the slabs to achieve their shear capacity when the same GFRP reinforcement as in the reference slab was used. Increasing the GFRP-reinforcement ratio slightly increased the shear capacity of the jointed slabs; the failure also occurred due to diagonal tension in the NSC slabs.
2. The high rigidity of the UHPFRC closure joint shifted the location of the first flexural crack from the zone of maximum negative moment (over the centerline of the support). Accordingly, the cracking capacity of the jointed specimens increased by an average of 54% compared to the reference specimen.
3. The ultimate capacity was dominated by the strength of the NSC precast segments, not by that of the UHPFRC closure joint. Thus, the GFRP-bar splice length did not significantly affect the ultimate capacity. Increasing the GFRP reinforcement from No. 15 to No. 20 (44%) increased the ultimate shear capacity of the test specimens by an average ratio of 9%.
4. The reference and jointed specimens experienced the typical bilinear deflection response up to failure. At the same load, the deflection decreased with increasing bar splice length (closure-joint width), while the reinforcement ratio remained the same. The UHPFRC joint maintained the uncracked inertia at this location as the UHPFRC did not have any visible cracks. Consequently, the jointed slabs showed lower deflection than the reference specimen at the same load. Moreover, for a given load, increasing the GFRP-reinforcement ratio decreased deflection by about 22%.

5. The interfacial cracks initiated at earlier loading stages than the other flexural cracks, but no slippage of GFRP bars was observed and the joints remained intact until the slabs failed in shear away from the UHPFRC joints. Due to the UHPFRC having very high tensile strength, no cracks were observed within the closure joint and the joints allowed the specimens to maintain continuity.

6. The maximum measured tensile strains in the GFRP bars along the splice length ranged between 35% and 47% of bar ultimate strain. The maximum strain in the GFRP bars decreased with increasing splice length (closure-joint width). Increasing the reinforcement from No. 15 to No. 20 (44%) significantly decreased the strain in the GFRP bars by about 22%.

7. At 30% of the failure load (0.30 V_{exp}, assumed service load of the specimens), the stresses in the GFRP bars were less than 0.25 of the guaranteed tensile strength and the flexural and interfacial crack widths of the joints were less than 0.50 mm, even with 100 mm splices (120 mm joints).

8. AASHTO LRFD (2009) yielded conservative shear predictions with an average V_{exp}/V_{pred} of 1.69. The CHBDC (CAN/CSA S6, 2014) had reasonable yet conservative predictions with an average V_{exp}/V_{pred} of 1.60. CAN/CSA S806 (2012), however, provided the most accurate yet conservative predictions with an average V_{exp}/V_{pred} of 1.13.

9. In UHPFRC closure joint, A GFRP splice length of 100 mm or 6.5 d_b, whichever is greater, performed adequately and achieved continuity of the jointed slabs. No slippage or bond-strength degradation was observed. Moreover, the jointed slabs evidenced less deflection and strain than the reference specimen at the same load level.

6.2.2. Closure Joints Subjected to Pure Flexural Stresses

10. The presence of the UHPFRC closure joint connecting the GFRP-RC precast slabs had no degradation effect on the ultimate capacity or mid-span deflection compared to the reference specimen, with negligible difference.

11. The mode of failure was significantly affected by the splice length. The specimens of 100-mm splice length exhibited a sudden pull-out failure due to bond-strength degradation between the GFRP splices and the UHPFRC occurred close to the failure load. Increasing the splice length to 150 and 200 mm changed the failure mode into diagonal tension failure within the shear span, thereafter, the specimen capacity was dominated by the strength of the NSC precast slabs.

12. For the jointed specimens with 150 and 200-mm splice length, increasing the GFRP reinforcement ratio by 44% increased both cracking and ultimate capacities by about 25%.

13. All the test specimens showed a typical bilinear load-deflection relationship up to failure. The splice length had no significant effect on the deflection value at the same load. For a given load, It was observed that the deflection decreased by about 30% due to 44% increase in the reinforcement ratio.

14. The test observations showed initial cracks at the joint-precast slab interfaces. These interfacial-cracks are inherent and appeared at earlier loading stages compared to the other flexural-cracks. Unlike expected, no clear effect of the splice length (100 to 200 mm) was observed in this study on the interfacial crack-width.

15. At failure, the tensile strains in the GFRP splices ranged between 31 and 53% of the ultimate strain. The tensile strain in the GFRP splices was observed to increase as the splice length decreased. Increasing the reinforcement from by 44% (from GFRP No. 15 to No. 20) decreased the bar tensile strain by about 37%.

16. At the assumed service load of 0.30 V_{exp} , The tested specimens satisfactorily meet the serviceability allowable limits in terms of crack width and stresses in the GFRP bars.

17. The current shear provisions in AASHTO LRFD (2009) provided conservative predictions for the shear capacity of GFRP-RC deck slabs with an average V_{exp}/V_{pred} of 1.60. On the other hand, the CHBDC (CAN/CSA S6, 2014) showed reasonable yet conservative predictions with an average V_{exp}/V_{pred} of 1.52.
18. A GFRP splice length of 150 mm or 9.5 d_b, whichever is greater, embedded in UHPFRC closure joint is sufficient to guarantee adequate continuity and transfer the loads between the precast slabs to behave equivalent to monolithic concrete specimen. Accordingly, no slippage or bond-strength degradation was observed and the failure occurred within the shear span away from the joint. Moreover the joint remained intact up to failure without visible damage.

6.3. Recommendations for Future Work

The current research demonstrated the adequacy of connecting GFRP-RC bridge deck slabs with short splices embedded in narrow field-cast UHPFRC closure joints. It provided an understanding of the behavior of these closure joints and the variables that affect their performance. The scope of this investigation was limited to the test conditions and parameters studied herein. Consequently, further research investigations should be conducted in this promising field, some suggested recommendations for future work are as follows:

- Conduct series of testing to investigate efficiency of the reinforcement configuration embedded in the closure joints, such as GFRP headed bars and L shaped bars.
- Perform series of tests considering low modulus GFRP bars to validate the findings of the current study.
- Develop an analytical finite element model (FEM) simulating the GFRP-RC slabs jointed by UHPFRC closure joints to conduct an extended parametric study on a wide range of the affecting parameters.
- More experimental works are needed to investigate the performance of the jointed slabs under cyclic and fatigue loading.

6.4. Conclusions

Sur la base des essais expérimentaux et des analyses effectuées dans le cadre de ce programme de recherche, les conclusions suivantes ont été tirées:

6.4.1. Joints de Clavage Soumis à une Combinaison de Contraintes de Cisaillement et de Flexion

1. Le mode de rupture observé pour tous les spécimens était une rupture de traction diagonale dans la zone de porte-à-faux (dalles en béton de résistance normale). L'utilisation d'armatures en PRFV avec une longueur de recouvrement comprise entre 100 mm et 200 mm dans le joint de clavage en BFUP a permis aux dalles d'atteindre leur capacité de cisaillement avec le même renforcement en PRFV que celui de la dalle de référence. L'augmentation du taux d'armature des barres en PRFV a permis d'augmenter légèrement la capacité de cisaillement des dalles jointées. La rupture des dalles en béton de résistance normale était due également à la traction diagonale.
2. La grande rigidité du joint de clavage en BFUP a entraîné le déplacement de l'emplacement de la première fissure de flexion de la zone de moment négatif maximal (sur l'axe du support). Par conséquent, la résistance à la fissuration des spécimens jointés a augmenté en moyenne de 54% par rapport au spécimen de référence.
3. La résistance à la rupture des spécimens était gouvernée par la résistance des segments préfabriqués en béton de résistance normale et non par celle du joint de clavage en BFUP. Ainsi, la longueur de recouvrement des barres en PRFV n'a pas eu d'effet significatif sur la résistance à la rupture. L'augmentation du taux d'armature des barres de PRFV en remplaçant les barres n° 15 par les barres n° 20 (44%) a permis d'augmenter la résistance à la rupture par cisaillement des spécimens d'un rapport moyen de 9%.
4. Les spécimens de référence ainsi que les spécimens jointés ont présenté un comportement typique bilinéaire de la flèche jusqu'à la rupture. Pour un même niveau de charge, la flèche diminuait à mesure que la longueur de recouvrement des barres

augmentait (largeur du joint clavage), tandis que le taux d'armature demeurait constant. La grande largeur du joint en BFUP de rigidité élevée a permis d'augmenter l'inertie de la dalle à cet endroit, de sorte que les dalles jointées présentaient une flèche inférieure à celle des dalles de référence pour le même niveau de charge. De plus, pour un niveau de charge donné, l'augmentation du taux d'armature de PRFV a permis de réduire la flèche de 22% environ.

5. Les fissures à l'interface sont apparues plus tôt que les autres fissures de flexion pendant le chargement, mais aucun glissement des barres en PRFV n'a été observé et les joints sont restés intacts jusqu'à ce que les dalles aient une rupture en cisaillement loin des joints en BFUP. En raison de la très haute résistance en traction du BFUP, aucune fissure n'a été observée dans le joint de clavage et les joints ont permis aux spécimens d'assurer la continuité.

6. Les déformations de traction maximales mesurées dans les barres en PRFV le long du recouvrement se situaient entre 35% et 47% de la déformation ultime de la barre. La déformation maximale dans les barres en PRFV diminuait avec l'augmentation de la longueur de recouvrement (largeur du joint de clavage). En augmentant le taux d'armature par replacement des barres n ° 15 par les barres n ° 20 (44%), la déformation des barres en PRFV a été réduite de manière significative d'environ 22%.

7. À 30% de la charge de rupture (0,30 V_{exp}, charge de service supposée des spécimens), les contraintes dans les barres en PRFV étaient inférieures à 25% de la résistance à la traction garantie et les largeurs de fissure en flexion et à l'interface des joints étaient inférieures à 0,50 mm, même avec des recouvrements de 100 mm (joints de 120 mm).

8. Les prévisions de l'AASHTO LRFD (2009) pour le cisaillement sont conservatrices avec une moyenne du rapport $V_{exp}/V_{prév}$ de 1,69. La norme CSA (2014) avait des prévisions raisonnables mais conservatrices avec une moyenne du rapport $V_{exp}/V_{prév}$ de 1,60. La norme CSA (2012) a toutefois fourni les prévisions les plus précises, mais conservatrices avec une moyenne du rapport $V_{exp}/V_{prév}$ de 1,13.

9. L'utilisation d'une courte longueur de recouvrement de 100 mm dans des joints en BFUP de 120 mm avec des barres en PRFV n° 15 et n° 20 a démontré une performance

adéquate et a permis d'assurer une continuité des dalles jointées. Aucun glissement n'a été observé. La rupture des dalles jointées était régie par la résistance de la dalle. Les dalles jointées présentaient des flèches et des déformations moins élevées que l'échantillon de référence pour un même niveau de charge. Néanmoins, le comportement de ce court recouvrement sous charge cyclique et en fatigue devrait être étudié.

6.4.2. Joints de Clavage Soumis à des Efforts de Flexion Simple

10. La présence du joint de clavage en BFUP reliant les dalles préfabriquées en béton armé de PRFV n'a pas eu d'effet de dégradation sur la capacité ultime ou sur la flèche à mi-portée comparé au spécimen de référence, et ce avec une différence négligeable.
11. Le mode de rupture était significativement affecté par la longueur de recouvrement. Les spécimens ayant une longueur de recouvrement de 100 mm présentaient une rupture soudaine par pullout due à la dégradation de l'adhérence entre le recouvrement des barres de PRFV et le BFUP, survenue à l'approche de la charge de rupture. L'augmentation de la longueur de recouvrement à 150 et 200 mm a permis de changer le mode de rupture en rupture de traction diagonale dans la travée de cisaillement. La capacité de l'échantillon a par la suite été régie par la résistance des dalles préfabriquées en béton de résistance normale.
12. Pour les spécimens jointés avec une longueur de recouvrement de 150 et 200 mm, l'augmentation du taux d'armature de PRFV de 44% a permis d'augmenter les résistances à la fissuration et à la rupture d'environ 25%.
13. Tous les spécimens ont montré une relation bilinéaire charge-flèche typique jusqu'à la rupture. La longueur de recouvrement n'a eu aucun effet significatif sur la valeur de la flèche à la même charge. Pour une charge donnée, il a été observé que la flèche diminuait d'environ 30% pour une augmentation de 44% du taux d'armature.
14. Les essais ont montré des fissures initiales aux interfaces joint-dalles préfabriquées. Ces fissures à l'interface sont inhérentes et sont apparues à des étapes de chargement plus tôt comparées aux autres fissures de flexion. Contrairement aux attentes, la

longueur de recouvrement (100 à 200 mm) n'a pas eu d'effet évident sur la largeur de la fissure à l'interface dans la présente étude.

15. À la rupture, les déformations en traction dans les barres de PRFV avec recouvrement étaient comprises entre 31 et 53% de leur déformation ultime. Il a été observé une augmentation de la déformation en traction dans les barres en PRFV avec jonction à mesure que la longueur de recouvrement diminuait. En augmentant le taux d'armature de 44% (remplacement des barres de PRFV n° 15 par les barres n° 20), les déformations de traction des barres ont été réduites d'environ 37%.
16. Pour une charge de service supposée de 0,30 V_{exp}, les spécimens testés respectent de manière satisfaisante les limites admissibles en termes de largeurs de fissures et de contraintes dans les barres en PRFV.
17. Les dispositions actuelles relatives au cisaillement dans l'AASHTO LRFD (2009) fournissent des prévisions conservatrices concernant la capacité de cisaillement des dalles de pont en béton armé de PRFV avec une moyenne du rapport V_{exp} / $V_{prév}$ de 1,60. Par ailleurs, la norme CSA (2014) a démontré des prévisions raisonnables mais conservatrices avec une moyenne du rapport Vexp / Vpred de 1,52.
18. Une longueur de recouvrement des barres en PRFV de 150 mm ou 9,5 d_b, selon la valeur la plus grande, au niveau du joint de clavage en BFUP est suffisante pour garantir une continuité adéquate et transférer les charges entre les dalles préfabriquées pour qu'elles se comportent comme des spécimens de béton monolithiques. Par conséquent, aucun glissement ou dégradation de l'adhérence n'a été observé et la rupture s'est produite dans la travée de cisaillement à l'extérieur du joint. De plus, le joint est resté intact jusqu'à la rupture, sans dommage visible. Des recherches supplémentaires sont nécessaires pour évaluer la performance du recouvrement de 150 mm de long à l'aide d'essais cycliques et de fatigue.

6.5. Recommandations pour des Travaux Futurs

Le présent projet de recherche a démontré la pertinence de relier les dalles de tablier de pont en béton armé de PRFV à l'aide de joint de clavage en BFUP coulé sur place. Il a

permis de comprendre le comportement des joints de clavage et les paramètres qui influencent leurs performances. La portée de cette étude était limitée aux conditions et paramètres d'essais. Par conséquent, des études plus approfondies devraient être menées dans ce champ de recherche prometteur. Voici quelques recommandations pour les travaux futurs :

- Réaliser une série d'essais pour examiner l'efficacité de la configuration des armatures incorporées dans les joints de clavage, telles que les barres à tête en PRFV et les barres en forme de L.

- Réaliser une série d'essais sur les barres en PRFV à faible module afin de valider les résultats de la présente étude.
- Développer un modèle analytique par éléments finis (FEM) simulant le comportement des dalles en béton armé de PRFV jointées à l'aide d'un joint de clavage en BFUP afin de mener une étude paramétrique étendue sur un large éventail de paramètres.
- Des travaux expérimentaux supplémentaires sont nécessaires pour étudier les performances des dalles jointées sous des sollicitations cycliques et en fatigue.

REFERENCES

AASHTO. (1996), "Standard Specifications for Highway Bridges." *AASHTO LRFD*, 16th Ed., Washington, D.C.

AASHTO. (2009), "Bridge Design Guide Specifications for GFRP-Reinforced Concrete Bridge Decks and Traffic Railings." *AASHTO LRFD*, 1st Ed., Washington, DC.

AASHTO. (2010), "Bridge Design Specifications." *AASHTO LRFD*, 5rd Ed., Washington, DC.

AASHTO. (2012), "Bridge Design Specifications." *AASHTO LRFD*, 6th Ed., Washington, DC.

ACI Committee 318. (1995), "Building Code Requirements for Reinforced Concrete." *ACI 318-95*, Farmington Hills, Michigan, USA.

ACI Committee 318. (2014), "Building Code Requirements for Structural Concrete and Commentary." *ACI 318R-14*, Farmington Hills, Michigan, USA.

Ahmed, E. A., Settecasi, F., and Benmokrane, B. (2014), "Construction and testing of GFRP steel hybrid reinforced-concrete bridge-deck slabs of the Sainte-Catherine overpass bridges." *ASCE Journal of Bridge Engineering*, 19(6), 04014011.

Ahmed, E. A., and Benmokrane, B. (2014), "DESIGN OF BRIDGE DECK SLABS USING GLASS FIBERREINFORCED POLYMER (GFRP) BARS OF DIFFERENT GRADES." *Proceedings of the 9th International Conference on Short and Medium Span Bridges (CSCE)*, Calgary, Alberta, Canada.

Arafa, A., Farghaly, A. S., Ahmed, E. A., and Benmokrane, B. (2016), "Laboratory Testing of GFRP-RC Panels with UHPFRC Joints of the Nipigon River Cable-Stayed Bridge in Northwest Ontario, Canada." *ASCE Journal of Bridge Engineering,* 21(11), 05016006.

ASTM. (1997), "Standard Test Method for Flexural Toughness and First-Crack Strength of Fiber-Reinforced Concrete (Using Beam With Third-Point Loading)." *ASTM C1080-97*, West Conshohocken, PA

ASTM. (2002), "Standard Test Method for Static Modulus of Elasticity and Poisson's Ratio of Concrete in Compression." *ASTM C469-02*, West Conshohocken, PA.

ASTM. (2005), "Standard Test Method for Compressive Strength of Cylindrical Concrete Specimens." *ASTM C39/C39M-05*, West Conshohocken, PA.

ASTM. (2006), "Standard Test Method for Length Change of Hardened Hydraulic-Cement Mortar and Concrete." *ASTM C157/C157M-06*, West Conshohocken, PA

ASTM. (2008), "Standard Test Method for Resistance of Concrete to Rapid Freezing and Thawing." *ASTM C666/C666M-8*, West Conshohocken, PA.

ASTM. (2011), "Standard Test Method for Splitting Tensile Strength of Cylindrical Concrete Specimens." *ASTM C496/C496M-11*, West Conshohocken, PA.

ASTM. (2011), "Standard test methods for tensile properties of fiber-reinforced polymer matrix composite bars." *ASTM D7205-11*, West Conshohocken, PA.

ASTM. (2014), "Standard Test Method for Flow Table for Use in Tests of Hydraulic Cement." *ASTM C230/C230M-14*, West Conshohocken, PA.

ASTM. (2017), "Standard practice for fabricating and Testing specimens of ultra-high performance concrete." *ASTM C1856/C1856M-17*, West Conshohocken, PA.

ASTM. (2018), "Standard Test Method for Compressive Strength of Cylindrical Concrete Specimens." *ASTM C39/C39M-18*, West Conshohocken, PA.

Au, A., and Lam, C. (2011), "Laboratory Testing of Closure Strip Models for Prefabricated Bridge Deck System–Part II." *Technical Report No. BRO-053*, Ontario Ministry of Transportation, Bridge Office, Toronto.

Au, A., Lam, C., and Tharmabala, B. (2011), "Investigation of Closure Strip Details for Connecting Prefabricated Deck Systems." *PCI Journal*, 56(3), 75–93.

Azizinamini, A., Power, E. H., Myers, G. F., Ozyildirim, H. C., Kline, E. S., Whitmore, D. W., and Dennis R. Mertz, D. R. (2013), "Design Guide for Bridges for Service Life." *SHRP 2 Renewal Project R19A*, National Academies of Sciences, Engineering, and Medicine, Washington, DC.

Bank, Lawrence C., (2006), "Composites for construction: structural design with FRP materials." John Wiley & Sons.

Bischoff, P., Gross, S., and Ospina, C. (2009), "The Story behind Proposed Changes to the ACI 440 Deflection Requirements for FRP-Reinforced Concrete." *ACI Special Publication*, SP 264, 53–76.

Blais, P. Y. and Couture. M. (1999), "Precast, Prestressed Pedestrian Bridge—World's First Reactive Powder Concrete Structure." *PCI Journal*, 44 (5), pp. 60–71.

Carbonell, M. A., Harris, D. H., Shann, S. V., and Ahlborn, T. M., (2012), "Bond Strength Between UHPC and Normal Strength Concrete (NSC) in Accordance with Split Prism and Freeze-Thaw Cycling Tests." *3rd International Symposium on UHPC and Nanotechnology for High Performance Construction Materials*, Germany, pp. 377–384.

CSA Canadian Standards Association. (2010), "Specification for fiber-reinforced polymers." *CAN/CSA S807-10*, ON, Canada.

CSA Canadian Standards Association. (2012), "Design and Construction of Building Structures with Fiber Reinforced Polymers." *CAN/CSA S806-12*, ON, Canada.

CSA Canadian Standards Association. (2014), "Canadian Highway Bridge Design Code." *CAN/CSA S6-14*, ON, Canada.

Culmo, M. P. (2011), "Accelerated Bridge Construction - Experience in Design, Fabrication and Erection of Prefabricated Bridge Elements and Systems." *Report No. FHWA-HIF-12-013*, Federal Highway Administration (FHWA), Washington, DC.

Ductal. (2016), https://www.ductal.com/en/engineering/hawk-lake-bridge, February 8, 2016.

Elgabbas, F., Vincent, P., Ahmed, E., and Benmokrane, B. (2016), "Experimental Testing of Basalt-Fiber-Reinforced Polymer Bars in Concrete Beams." *Composites Part B*: Engineering, 91, 205-218.

El-Nemr, A., Ahmed, E. A, and Benmokrane, B. (2013), "Flexural Behavior and Serviceability of Normal- and High-Strength Concrete Beams Reinforced with Glass Fiber-Reinforced Polymer Bars." *ACI structural journal*, 110(6), 1077–1088.

El-Salakawy, E. F., and Benmokrane, B. (2004), "Serviceability of Concrete Bridge Deck Slabs Reinforced with Fiber-Reinforced Polymer Composite Bars." *ACI structural journal*, 101(5), 727-736.

Federal Highway Administration, FHWA. (2019), "Accelerate Bridge Construction." Website https://www.fhwa.dot.gov/bridge/abc/, accessed on Jan. 16, 2019.

French, C. E., Shield, C. K., Klaseus, D., Smith, M., Eriksson, W., Ma, Z. J., Zhu, P., Lewis, S., and Chapman, C. E. (2011), "Cast-in-place concrete connections for precast deck systems." *NCHRP Project 10-71*, Transportation Research Board, Washington, DC.

fib TG 9.3, (2007), "Design and use of fibre reinforced polymer reinforcement (FRP) for reinforced concrete structures." Technical Report, jib Task Group 9.3 FRP (Fiber Reinforced Polymer) reinforcement for concrete structures, 157pp.

Graybeal, B. A. (2006a), "Material Property Characterization of Ultra-High Performance Concrete." *Report No. FHWA-HRT-06-103*, Federal Highway Administration, Washington, DC.

Graybeal, B. A. (2006b), "Structural Behavior of Ultra-High Performance Concrete Prestressed I Girders." *Report No. FHWA-HRT-06-115,* Federal Highway Administration, Washington, DC.

Graybeal, B. A. (2007), "Compressive Behavior of an Ultra-High-Performance Fiber-Reinforced Concrete." *ACI Materials Journal,* 104 (2), 146-152.

Graybeal, B., Perry, V., and Royce, M. (2010), "UHPC Ultra-High Performance Concrete." NHI Innovations Webinar.

Graybeal, B. A. (2010), "Behavior of Field-Cast Ultra-High Performance Concrete Bridge Deck Connections under Cyclic and Static Structural Loading." *Report No. FHWA-HRT-11-023*, Federal Highway Administration, Washington, DC.

Graybeal, B., A. (2011), "Fatigue Response of an Ultra-High Performance Concrete Field-Cast Bridge Deck Connection." *Proceedings of International Conference on Transportation Research Board Systems Engineering,* Washington, DC.

Graybeal, B. and Baby, F. (2013), “Development of a Direct Tension Test Method for UHPFRC.” *ACI Materials Journal*, Vol. 110(2).

Graybeal, B. A. (2014), “Design and construction of field-cast UHPC connections.” *Report No. FHWA-HRT-14-084*, Federal Highway Administration, Washington, DC.

Haber, Z. B., De la Varga, I., Graybeal, B. A., Nakashoji, B., and El-Helou, R. (2018), “Properties and Behavior of UHPC-Class Materials.” *Report No. FHWA-HRT-18-036*, Federal Highway Administration, McLean, VA, USA, 153 p.

Haber, Z. B., and Graybeal, B. A. (2018), “Lap-Spliced Rebar Connections with UHPC Closures.” *ASCE Journal of Bridge Engineering*, 23(6), 04018028.

Harryson, Peter, (2003), "High performance joints for concrete bridge applications." Structural Engineering International, 13(1), pp. 69-75.

Honarvar, E., Sritharan, S., Matthews Rouse, J., and Aaleti, S., (2015), “Bridge Decks with Precast UHPC Waffle Panels: A Field Evaluation and Design Optimization.” *ASCE Journal of Bridge Engineering*, 21(1), 04015030.

Hwang, H., and Park, S. Y. (2014), “A study on the flexural behavior of lap-spliced cast-in-place joints under static loading in ultra-high performance concrete bridge deck slabs.” *Canadian Journal of Civil Engineering, NRC*, 41(7), 615-623.

ISIS Canada, (2006), “Specifications for Product Certification on Fibers Reinforced Polymer (FRPs) as Internal Reinforcement in Concrete Structures.” Product Certification of FRP Materials, the Canadian Network of Centers of Excellent on Intelligent Sensing for Innovation Structures, University of Manitoba, Winnipeg, Canada.

ISIS Canada, (2007), “Reinforcing Concrete Structures with Fiber Reinforced Polymers.” Design Manual No. 3 (ISIS-M03), The Canadian Network of Centers of Excellence on

Intelligent Sensing for Innovative Structures, University of Manitoba, Winnipeg, Canada.

Issa, M. A., Anderson, R., Domagalski, T., Asfour, S., and Islam, M. S., (2007), "Full-scale testing of prefabricated full-depth precast concrete bridge deck panel system." *ACI structural journal*, 104(3), 324 p.

Jaeger, L. G., Mufti, A. A., and Tadros, G. (1997), "The Concept of the Overall Performance Factor in Rectangular-Section Reinforced Concrete Members." *Proceedings of the 3rd International Symposium on Non-Metallic (FRP) Reinforcement for Concrete Structures (FRPRCS-3)*, Sapporo, Japan, Vol. 2, 551–559.

JSCE. (2006), "Recommendations for Design and Construction of Ultra High Strength Fiber Reinforced Concrete Structures." (Draft), Japan Society of Civil Engineers, JSCE Guidelines for Concrete No. 9.

Khalafalla, I. E. and Sennah, K. (2013), "Development of Prefabricated Bridge Girder System with Closure Strips Incorporating Sand-Coated GFRP Bars with Headed Ends." *Proceedings of General Conference (CSCE)*, Montreal, Quebec, Canada, 1-10.

Lafarge. (2009), "Ductal Product Data Sheet – JS1000." Lafarge-Holcim Canada Inc., Calgary, Alberta, Canada.

Lee, J. K., and Lee, S. H. (2015), "Flexural Behavior of Ultra-High-Performance Fiber-Reinforced Concrete Moment Connection for Precast Concrete Decks." *ACI Structural Journal,* 112(4), 451-462.

Li, L., Ma, Z., Griffey, M. E., and Oesterle, R. G. (2010), "Improved longitudinal joint details in decked bulb tees for accelerated bridge construction: Concept development." *ASCE Journal of Bridge Engineering*, 15(3), 327-336.

Li, L., Ma Z. J., Griffey, M. E., and Oesterle, R. G., (2009-a), "Improved longitudinal joint details in decked bulb tees for accelerated bridge construction: Concept development." *ASCE Journal of Bridge Engineering*, 15(3), pp. 327-336.

Li, L., Ma Z. J., and Oesterle, R. G., (2009-b), "Improved longitudinal joint details in decked bulb tees for accelerated bridge construction: Fatigue evaluation." *ASCE Journal of Bridge Engineering*, 15(5), pp. 511-522.

Ma, Z. J., Lewis, S., Cao, Q., He, Z., Burdette, E. G., and French, C. E., (2011), "Transverse joint details with tight bend diameter U-bars for accelerated bridge construction." *ASCE Journal of Structural Engineering*, 138(6), pp. 697-707.

Ma, Z. J., Cao, Q., Chapman, C. E., Burdette, E. G., and French, C. E. (2012), "Longitudinal joint details with tight bend diameter U-bars." *ACI Structural Journal,* 109(6), 815-824.

Mota, C., Alminar, S., and Svecova, D. (2006), "Critical Review of Deflection Formulas for FRPRC Members." *ASCE Journal of Composites for Construction*, 3 (10), 183–194.

Perry, V., and Royce, M. (2010), "Innovative Field Cast UHPC Joints for Precast Bridge Decks (Side-By-Side Deck-Tees) Village of Lyons, NY." *Proceedings of the 3rd International fib conference on Bridges.* Washington, USA.

Pirayeh Gar, S., Head, M., Hurlebaus, S., and Mander, J. B., (2013), "Experimental performance of AFRP concrete bridge deck slab with full-depth precast prestressed panels." *ASCE Journal of Bridge Engineering*, 19(4), 04013018.

Pultrall Inc. (2016), "Composite Reinforcing Rods Technical Data Sheet." Pultrall Canada Inc., Thetford Mines, Canada.

Richard, P., (1996), "Reactive Powder Concrete: A New-Ultra High Strength Cementitious

Material." *Proceedings of the Fourth International Symposium on the Utilization of High-Strength/High-Performance Concrete*, Paris, France, Ed., de Larrard, F. and Lacroix, R., Vol. 3, pp. 1,343–1,357.

Richard, P., and Cheyrezy, M., (1995), "Composition of reactive powder concretes." Cement and Concrete Research, 25(7), 1501–1511.

Russell, H. G. and Graybeal, B. A. (2013), "Ultra-High Performance Concrete: A State-of-the-Art Report for the Bridge Community." *Report No. FHWA-HRT-13-060*, Federal Highway Administration, Washington, DC.

Sayed-Ahmed, M., and Sennah, K. (2015), "Ultimate and fatigue strength of GFRP-reinforced, full-depth, precast bridge deck panels with zigzag-shape transverse joints filled with UHPFRC." *Proceedings of the 5th international/11th Construction Specialty Conference (CSCE)*, Vancouver, British Columbia, 10pp.

Sayed-Ahmed, M. (2016), "Development and Study of Closure Strip between Precast Deck Panels in Accelerated Bridge Construction." *Ph.D. Thesis,* Ryerson University, Toronto, Ontario, Canada.

Sherif, M., and Sennah, K. (2017), "Strength of the GFRP-reinforced precast concrete deck panels with closure strips filled with ultra-high performance fiber-reinforced concrete." *Proceedings of the 5th International Conference on Durability of Fiber Reinforced Polymer (FRP) Composites For Construction and Rehabilitation of Structures (CDCC)*, Sherbrooke, Quebec, Canada, 457-464.

Vella, J. P., Vollum, R. L., and Jackson, A. (2017), "Flexural Behaviour of Headed Bar Connections between Precast Concrete Panels*." Journal of Construction and Building Materials*, 154, 236-250.

Virmani, P., and Hooks, J. M. (2013), "Mitigation of Corrosion in Concrete Bridges." Baidu Library, Professional Profile, Engineering technology, Construction / civil engineering, Nov., 8 p. https://wenku.baidu.com/view/303f955ba417866fb84a8e44.html.

Youssef, M. H., Ahmed, E. A., and Benmokrane, B. (2018a), "Structural behavior of GFRP-RC bridge deck slabs connected with UHPFRC joints under flexure and shear." *ASCE Journal of Bridge Engineering.* (Submitted).

Youssef, M. H., Ahmed, E. A., and Benmokrane, B. (2018b), "Development and testing of UHPFRC closure joints between precast bridge deck slabs reinforced with GFRP bars." *Proceedings of the 10th International Conference on Short and Medium Span Bridges (CSCE)*, Quebec City, Quebec, Canada, 9 pp.

Yuan, J., and Graybeal, B. (2015), "Bond of reinforcement in ultra-high-performance concrete." *ACI Structural Journal*, 112(6), 851–860.

Yuguang, Y., Walraven, J., and Uiji, J. D. (2008), "Study on bending behavior of an UHPC overlay on a steel orthotropic deck." *Proceedings of the 2nd international symposium on ultra-high performance concrete*, Kassel, Germany, 8pp.

Zhu, P., Ma, Z. J., Cao, Q., and French, C. E, (2011-a), "Fatigue evaluation of longitudinal U-bar joint details for accelerated bridge construction." *ASCE Journal of Bridge Engineering*, 17(2), pp. 201-210.

Zhu, P., Ma, Z. J., Cao, Q., and French, C. E, (2011-b), "Fatigue evaluation of transverse U-bar joint details for accelerated bridge construction." *ASCE Journal of Bridge Engineering*, 17(2), pp. 191-200.